Particle Motion Analysis in Pancreatic Islets Isolation using a Quadrupole Magnetic Flow Sorter

by

Venkata Sunil Kumar Sajja

A dissertation submitted to the Graduate Faculty of
Auburn University
in partial fulfillment of the
requirements for the Degree of
Doctor of Philosophy

Auburn, Alabama
May 09, 2011

Keywords: Islet Isolation, Diabetes, Quadrupole Magnetic Sorter, Particle Tracking Velocimetry

Copyright 2010 by Venkata Sunil Kumar Sajja

Approved by

Thomas R. Hanley, Chair, Professor of Chemical Engineering
Paul W. Todd, Chief Scientist, Techshot Inc.
James F. Leary, Professor of Biomedical Engineering, Purdue University
Robert P. Chambers, Professor of Chemical Engineering
Elizabeth Lipke, Assistant Professor of Chemical Engineering

Abstract

Pancreatic islet transplantation offers a viable option to achieve permanent metabolic control in Type 1 diabetes patients. However, large quantities of pure viable donor islet cells are necessary for transplantation. Using currently available islet isolation methods multiple donor organs are required to achieve successful transplantation, and there is a demand for an isolation method with high islet yield and viability. Additionally, with porcine xeno-islet cell transplantation providing much hope, improving the porcine islet isolation process has become a worthwhile endeavor. This dissertation is the summery of the work aimed to develop a Quadrupole Magnetic Sorter to isolate pancreatic islets from exocrine tissue.

Computational Fluid Dynamics (CFD) simulations were used (Chapter 2) to predict the flow patterns, pressure drop and nonspecific crossover in a newly designed QMS flow channel for the isolation of pancreatic islets of Langerhans. Simulation results were compared with the theoretically and experimentally determined results to validate the CFD model. CFD simulations were employed to compare performance of two models of QMS flow channels with differing splitter positions. Results of the simulations were used to show that one design gives up to 10% less nonspecific crossover than another and this model can be used to optimize the flow channel design to achieve maximum purity of magnetic particles.

Magnetic isolation is a promising method for separating and concentrating pancreatic islets for transplantation in Type 1 Diabetes patients. Continuous magnetic islet sorter was designed to overcome the restrictions of current purification methods that result in limited yield, viability and purity of the isolated islets. The performance of the islet sorter depends on the

resulting speed of the islets in an applied magnetic field, a property known as magnetophoretic mobility. Essential to the design and operation of the magnetic sorter is a method to measure the magnetophoretic mobilities of magnetically infused islets. Magnetic particle tracking velocimeter (MPTV) was developed to measure (Chapter 3) the magnetophoretic mobility of particles up to 1000 microns in diameter. Velocity measurements are performed in a well-characterized isokinetic magnetic energy gradient using video imaging followed by analysis of the video images using a computer algorithm that produces histogram of absolute mobilities. Mobility distributions obtained indicated that magnetized islets have sufficient mobility to be captured by the proposed sorting method, with this result confirmed in test isolations of magnetized islets.

To achieve islet isolation with high purity and yield Quadrupole Magnetic Sorting (QMS), a single cell separation method, is being modified for the isolation of pancreatic islets (Chapter 4). Islets are infused with 4.6µm Dynabeads® and separated continuously with QMS. Results from 10 porcine pancreas isolations indicated possibility of infusing islets with magnetic beads and isolating them continuously by reducing the exposure time of islets to enzymes. QMS isolated islets showed good morphology compared to standard COBE isolated islets and the Oxygen Consumption Rate (OCR) per DNA measurements confirmed the viability of the islets after isolation. QMS isolation can save the culture time and help to eliminate the mechanical stress due to centrifugation on the islets. Nude mice transplantation results confirmed Dynabeads do not affect the functionality of the islets.

Acknowledgements

I would like to express my sincere gratitude towards Dr. Thomas R. Hanley for giving me an opportunity to work with him on this research. I also would like to sincerely thank him for his consistent support, warm encouragement I would like to extend my thanks to Dr. Paul W. Todd for his support, guidance, thoughtful ideas, and also for serving on my committee. I would like to acknowledge Dr. James F. Leary, Dr. Robert P. Chambers and Dr. Elizabeth Lipke for serving on my committee and university reader Dr. Christopher J. Easley.

I would like to express my sincere thanks to David J. Kennedy and Byron Guernsey from IKOTECH, LLC for their help and support. I would like to thank Mark Deuser and John Vellinger for giving me opportunity to work at Techshot, IN. I express my earnest appreciation toward the members of Techshot for their kind help, especially Alan Constance and Bill Johnson.

I also want to thank Dr. Klearchos Papas and his group from University of Minnesota, MN, Mike Taylor and his group at Cell Tissue Systems and Robert McCarthy and his group at Vitacyte, IN group for providing facilities and help with isolations.

I would like to express deep gratitude and gratefulness to my father Mr. Seshagiri Rao Sajja for being a constant source of inspiration and motivation, mother Mrs. Nagamani Sajja for her enduring love and immense moral support and family members Sunanda, Picheswara Rao and Sai Sreeja. My most special thanks belong to my wife Saroja for her love, sacrifice and subject discussions.

Table of Contents

List of Figures

List of Tables

1. Introduction

1.1 Diabetes and Transplantation

Diabetes is a group of metabolic diseases that cause hyperglycemia. The consequences of diabetes include retinopathy (loss of vision), nephropathy (renal failure) and peripheral neuropathy with risk of amputation. The majority of diabetes cases fall into two categories: In type 1 diabetes, the cause is deficiency of insulin secretion. Type 1 diabetes accounts for 5 to 10 per cent of diagnosed diabetes. In type 2 diabetes the cause is combination of resistance to insulin action and deficit insulin secretion (Gavin et al., 2003).

According to the reports presented by CDC in 2008, 24 million Americans, 8 per cent of the population, are diabetic (CDC, 2008). Diabetes costs the US economy $132 billion per year, $92 billion in direct medical costs (CDC, 2002; Paul et al., 2003). It has been suggested that insulin independence can be achieved in diabetes with islet transplantation (Markmann et al., 2003).

Since the discovery of insulin in 1921, insulin therapy has saved many lives of type 1 diabetics. Insulin treatment cannot fully prevent chronic complications, and intensive insulin treatment to improve metabolic control has paralleled an increased risk of severe hypoglycemia (Berney et al., 2001; Oberholzer et al., 1999). The English surgeon Watson Williams was the first to attempt transplantation of pancreatic fragments in 1893 from a sheep to a boy. The first rodent pancreas transplantation was performed in 1966 along with kidney transplantation at the University of Minnesota (Ballinger et al., 1972). The International Pancreas Transplant Registry reports 17,000 whole pancreas transplants performed in the US up to 2004. Success after one

year varied from 72 to 84 per cent. Although whole pancreas transplantation is the most reliable means of restoring full metabolic control, it involves complex surgery. With only 5,000 cadaver organs available in any given year, transplantation is not available to treat all diabetes patients (Markmann et al., 2003). Islet transplantation offers a viable option to insulin therapy for improved metabolic control and to full organ transplantation with lower cost and risk.

Successful islet transplantation can result in insulin independence (Berney et al., 2001). The recent dramatic improvement in the success rate of the islet transplantation in humans has prompted considerable interest for more widespread application of this methodology (Shapiro et al., 2000). The first clinical islet transplantation in humans was attempted in 1985 at Washington University Medical School in St. Louis (Ricordi et al., 1988). The process involved maceration of the organ into cell fragment broth, from which islets were purified by a density gradient method as islets are slightly less dense than acinar tissue. Islets constitute only 1-2 % of the pancreas volume and their isolation and purification are stressful mechanical and enzymatic procedures that can inflict significant damage, which may be further amplified by prolonged times of warm and cold ischemia with human islets (London et al., 1994; Robertson et al., 1998). One limiting factor to the islet transplantation is the need for the large numbers of islets, obtained from more than one donor pancreas per recipient.

1.2 Recordi Method

The most important development for islet isolation was the automated method introduced by Dr. Camillo Ricordi. Ricordi's method utilized a refined mixture of enzymes (collagenase) produced by the bacterium *Clostridium hystoliticum*. Ricordi disconnected the organ from the duodenum, and a canula was inserted into the main pancreatic duct which serves as the outlet for digestive enzymes produced by the pancreatic exocrine. With all the accessory ducts clamped,

the organ was distended by collagenase injected into the main duct. The dilated organ was placed in a conical chamber, the "Ricordi Chamber (Figure 1.1)", through which the heated enzyme solution was circulated. A ball mill using either glass or ceramic marbles was used to liberate islets from the tissue (Ricordi et al., 1988). Flow diagram of the Ricordi digestion process is shown in figure 1.2.

The output from the Ricardi Chamber contains islets with some exocrine tissue. Large volumes of contaminated acinar tissue within islet auto grafts have been associated with portal hypertension, hepatic infarction, splenic bleeding and death. Therefore, it is necessary to purify islets before transplantation (Sulaiman et al., 2006). A diagram of the steps involved in the isolation and transplantation of pancreatic islets is shown in figure 1.3.

1.3 Purification of Islets

Insulin independence can be achieved in type 1 diabetes by transplanting 10,000 Islet Equivalents (IEQ) per kilogram recipient weight of purified islets (Sakuma et al., 2008). To achieve high yields with required purities, many islet purification techniques have been developed for isolation of islets from exocrine tissue either by targeting islets or by targeting exocrine tissue, e.g. hand picking of islets, fluorescence-activated sorting by staining islets with neutral red (Gray et al., 1989; Jindal et al., 1994), or destruction of non-islet tissue by laser energy (Brunicardi et al., 1994). All these techniques were successfully employed to purify rat islets but failed to scale up to the human tissue digest volume.

Islets or acinar tissue has been labeled with magnetic beads coated with monoclonal antibodies and then isolated with bar magnet (Muller-Ruchhoiltz et al., 1987; Winoto-Morbach et al., 1989; Winoto-Morbach et al., 1989a; Soon-Shiong et al., 1990; Winoto-Morbach et al., 1994; Davies et al., 1994; Davies et al., 1996). Since islets make up only one to two per cent of

Figure 1.1: Ricordi chamber used for islet isolation (www.biorep.com).

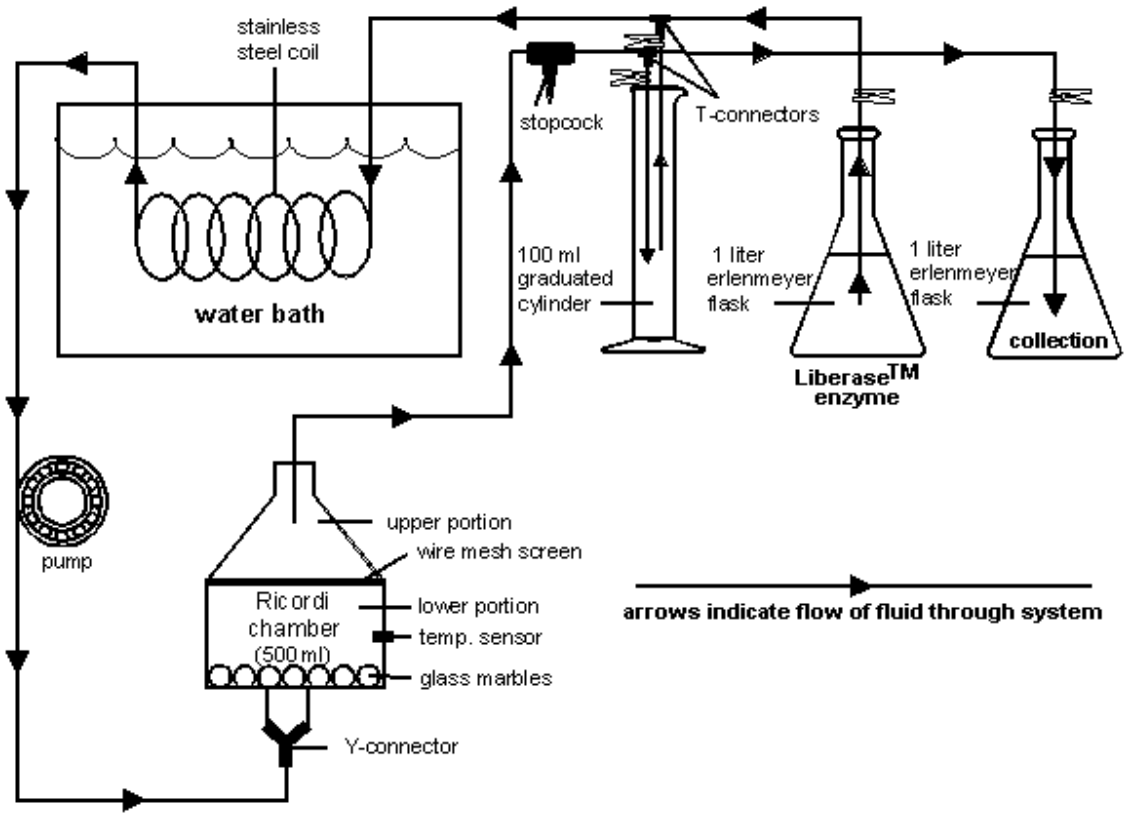

Figure 1.2: Flow diagram of the islets isolation process (Ricordi, 1992).

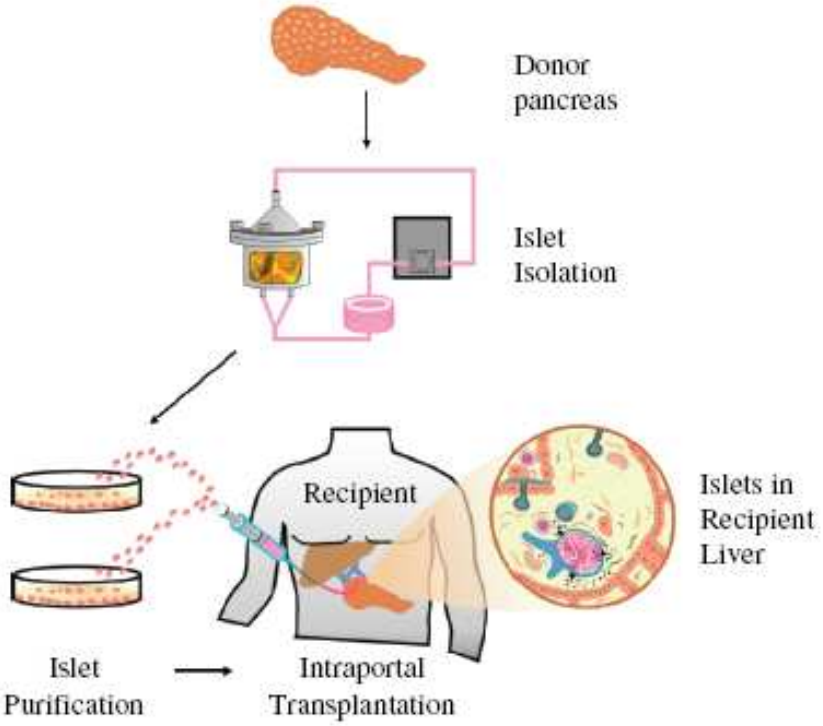

Figure 1.3: Steps involved in Islet Transplantation (Sulaiman et al., 2006).

pancreas, negative selection is difficult, requiring effective labeling of 98 per cent of the tissue. In addition, negative selection removes only the acinar cells, leaving ductal and other unidentified cell types remaining after pancreatic digestion. Positive selection of the islets offers the advantage over negative selection and the presence of beads in islets does not alter islet functionality (Nandigala et al., 1997).

1.4 Density Gradient Method

While several methods of the islet isolation have been developed, the most successful method is density gradient centrifugation. In this method, tissue digestate is centrifuged and re-suspended in a dense medium. Less dense media are layered on top and the gradient is fed to a COBE 2991 cell processor. After several minutes of centrifugation, islets are separated from the interface between two discontinuous gradient layers (Samejima et al., 1998).

The current clinical practice using on density gradient centrifugation does not achieve the necessary yield and purity of islets as this process relies on the small density difference between islets and acinar tissue. Density gradient cannot be standardized because tissue density and size distribution vary with each pancreas isolation. Tissue size is a function of the degree of enzymatic digestion, over which there is no direct control. In addition, density gradients have a limited ineffectiveness for digests in which islets have not been completely disconnected from the surrounding acinar tissue (London et al., 1998; Soon-Shiong et al., 1989).

Exocrine tissue present in purified islets, such as lymph nodes, vascular tissue and ductal fragments, are major stimuli for induction of the immune response that results in acute rejection (Mitsukazu et al., 1986). Although some studies indicate that islets should be transplanted unpurified, transplantation of purified islets should be preferred to achieve appropriate revascularization of transplants (Heuser et al., 2000).

1.5 Magnetic Separations

There is a major disparity between the number of available organ donors and recipients in need. Using current protocols 1 to 4 pancreas may be required to restore normal blood sugars in a single recipient. This is in large part due to variations in islet recovery and potency and the substantial losses in islet yield during organ procurement and storage as well as islet isolation and purification (Hering et al., 2002). Additionally, with porcine xeno-islet cell transplantation providing much hope (Hering et al., 2006), improving the porcine islet isolation process has become a worthwhile endeavor. Figure 1.4 shows the insulin independence achived in the patients who received islets transplantation in last decade (Michael et al., 2009). Immunomagnetic cell separation provides a highly attractive alternative to density–dependent methods for islet purification. The versatility of magnetic fields makes them a useful candidate for biological separations. Magnetic separations were initially developed to isolate glomuruli from murine kidneys by infusing iron oxide particles (Joyce Gauthier et al., 1988). Since islets of Langerhans have a similar angioarchitecture to mouse glumeruli, islets can be purified using magnetic force (Pinkse et al., 2004).

The use of Dynabeads for islet purification was first reported in 1989. Magnetic particles coated with antibodies impart mobility to selected cells and allow separation by a magnetic field. Magnetic fields have been used to select islets and separate them from the acinar tissue (Winoto-Morbach et al., 1989b; Davies et al., 1995). The degree of purification achieved in rats nearly reached hand selection quality (Muller-Ruchholtz et al., 1987). By positive selection, many unwanted tissue elements, such as lymph nodes, arteries and other ductal fragments, would not contaminate the purified islets. Unlike the density gradient method, magnetic separation subjects islets to little mechanical stress and requires less time for separation. Magnetic separations are

effective in any medium and are easily scalable. The use of quadrupole magnetic separation increases the purity and yield of islets compared to use of simple magnet (Davies et al., 1994).

1.6 - Quadrupole Magnetic Sorting

The QMS technology is based on a process known as split-flow lateral transport thin separation, also referred to by the acronym SPLITT, which is a subset of Field Flow Fractionation (FFF) technology. SPLITT was introduced by J.C. Giddings (Giddings et al., 1985) to extend the capabilities of FFF to the separation of colloids, macromolecules, and particulate materials (Martin et al., 1992). Quadrupole magnetic sorting (QMS) has been extensively modeled and tested and proved successful for single cell separation. QMS is a high-throughput, high-gradient, continuous magnetic cell separation system. QMS was initially designed for the positive separation of immunomagnetically labeled single cells from nonmagnetic cell population. Figure 1.5 provides a diagrammatic view of the QMS sorting mechanism. QMS employs three subsystems for operation: a fluid flow channel, a magnetic field for particle separation and pumps to regulate flow into and out of the flow channel. A sample containing labeled and unlabeled cells enters the flow channel (a') with carrier buffer (b'). Separated labeled cells (b) and unlabeled cells (a) leave the flow channel at the bottom. Separation is a function of many factors including the entering flow rates, the total flow rate and the degree of magnetization of cells. Cell labeling may be quantified by the magnetophoretic mobility (Sun et al., 1998; Williams et al., 1999; Hoyos et al., 2000; McCloskey et al., 2003; McCloskey et al., 2003a; Moore et al., 2004; Tong et al., 2007; Jing et al., 2007).

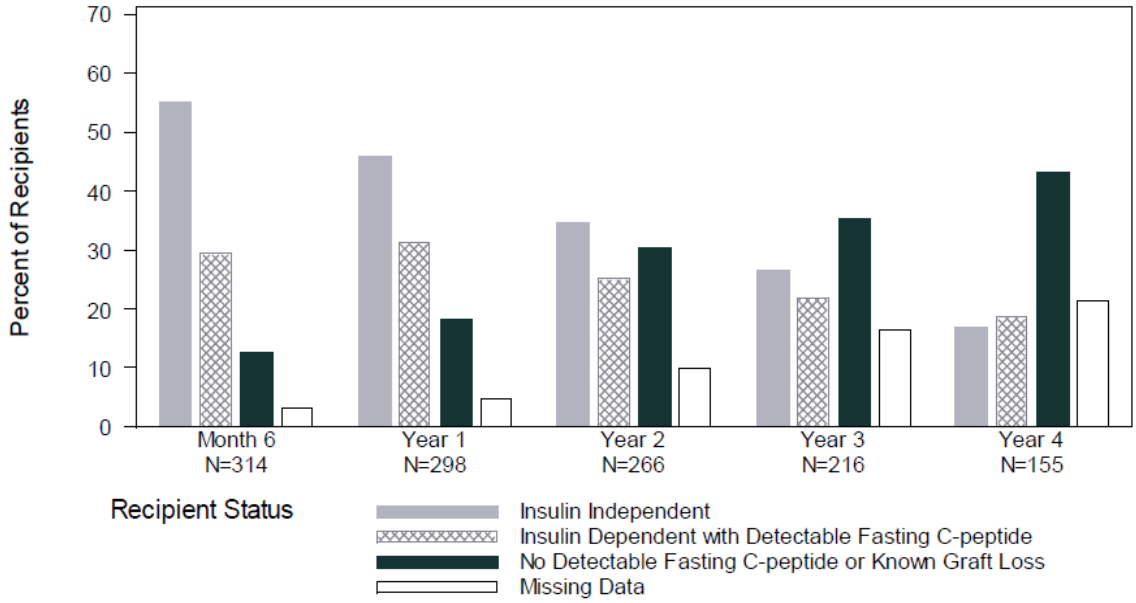

Figure 1.4: Insulin independence, insulin dependence or absence of Fasting C-peptide post last infusion of islets alone recipients (Michael et al., 2009).

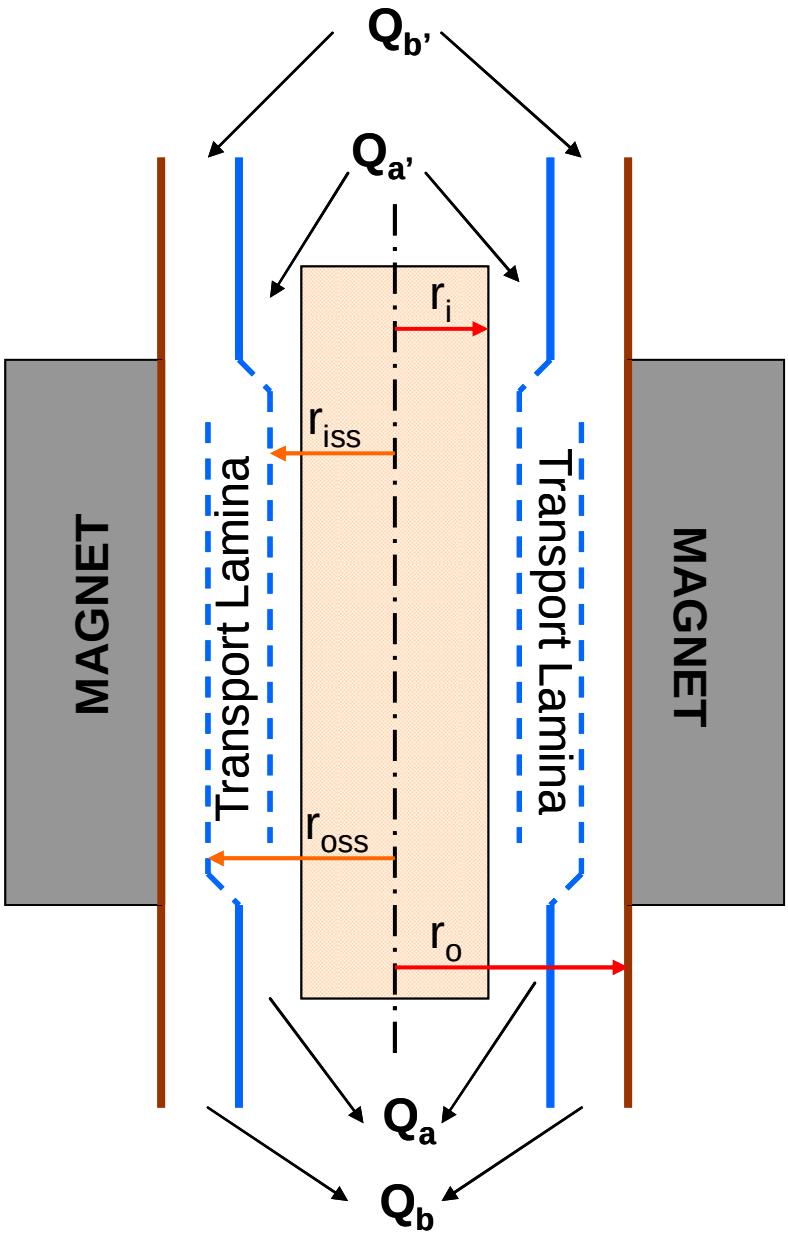

Figure 1.5: Schematic diagram of the quadrupole magnetic cell sorter (QMS).

1.7 – Magnetic Particle Tracking Velocimetry

Magnetophoretic mobility of magnetically labeled cells can be measured by a Magnetic Particle tracking velocimetry (MPTV). Figure 1.6 illustrates the MPTV system MPTV leverages current technologies in video microscopy, computer processing speed and finite element analysis for magnetic fields to measure the induced motion of cells and particles in the highly characterized magnetic and gravity field. The motion of the particles in the known field is then translated into a characteristic parameter called magnetophoretic mobility in a magnetic field and sedimentation rate in a gravity field. MPTV measurements involve videotaping the movement of immunomagnetically labeled particles through a known viscosity medium and magnetic susceptibility in a well-defined magnetic energy density gradient. The velocity of each particle along with its location within the magnetic energy gradient is recorded. From this information, magnetophoretic mobility of each particle is calculated. A significant advantage of this method over other techniques is that larger numbers of cells can be processed in very little time (Moore et al., 2004; Chalmers et al., 1999; Zhang et al., 2002; Chalmers et al., 1999a).

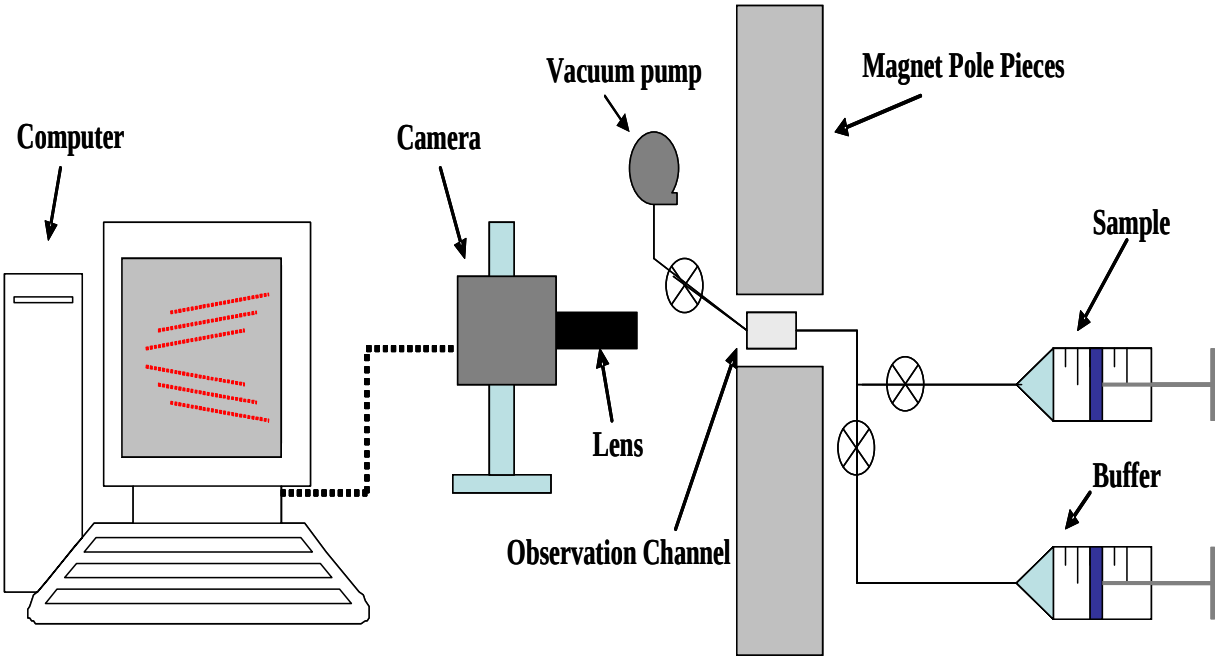

Figure 1.6: Magnetic Particle Tracking Velocimeter (MPTV) showing coordinate orientation.

1.8 Magnetic Beads

Several manufactures like Spherotech™, Miltenyi™, Invotrogen™ produce magnetic beads from 50 nm to 10 µm in size for biological separation applications. Some of the magnetic beads available for separations are tested for their magnetophoretic mobility. After considering the differences in the vasculature of the islets and acinar tissue Dynabeads® were selected to use for pancreas infusion to isolate islets from acinar tissue. Figure 1.7 shows the histograms of the magnetophoretic mobilities of different magnetic beads from 50nm to 10µm in size and Dynabeads shows the highest mobility among the all beads tested.

1.9 Research Objectives

The application of the QMS system for isolation of islets can lead to greater efficiencies and lower costs in the islet transplantation for Type 1 diabetics. The overall objective of this research is to design and characterize a flow channel and develop optimized conditions for islet isolation using QMS. The specific objectives are as follows:

- To develop a reliable QMS process for isolation of human islets from acinar tissue for transplantation.
- To design and operate an improved MPTV to determine magnetophoretic mobilities of islets.
- To optimize flow channel operation using computational fluid dynamics to simulate the QMS flow channel to study the flow patterns and pressure variations.

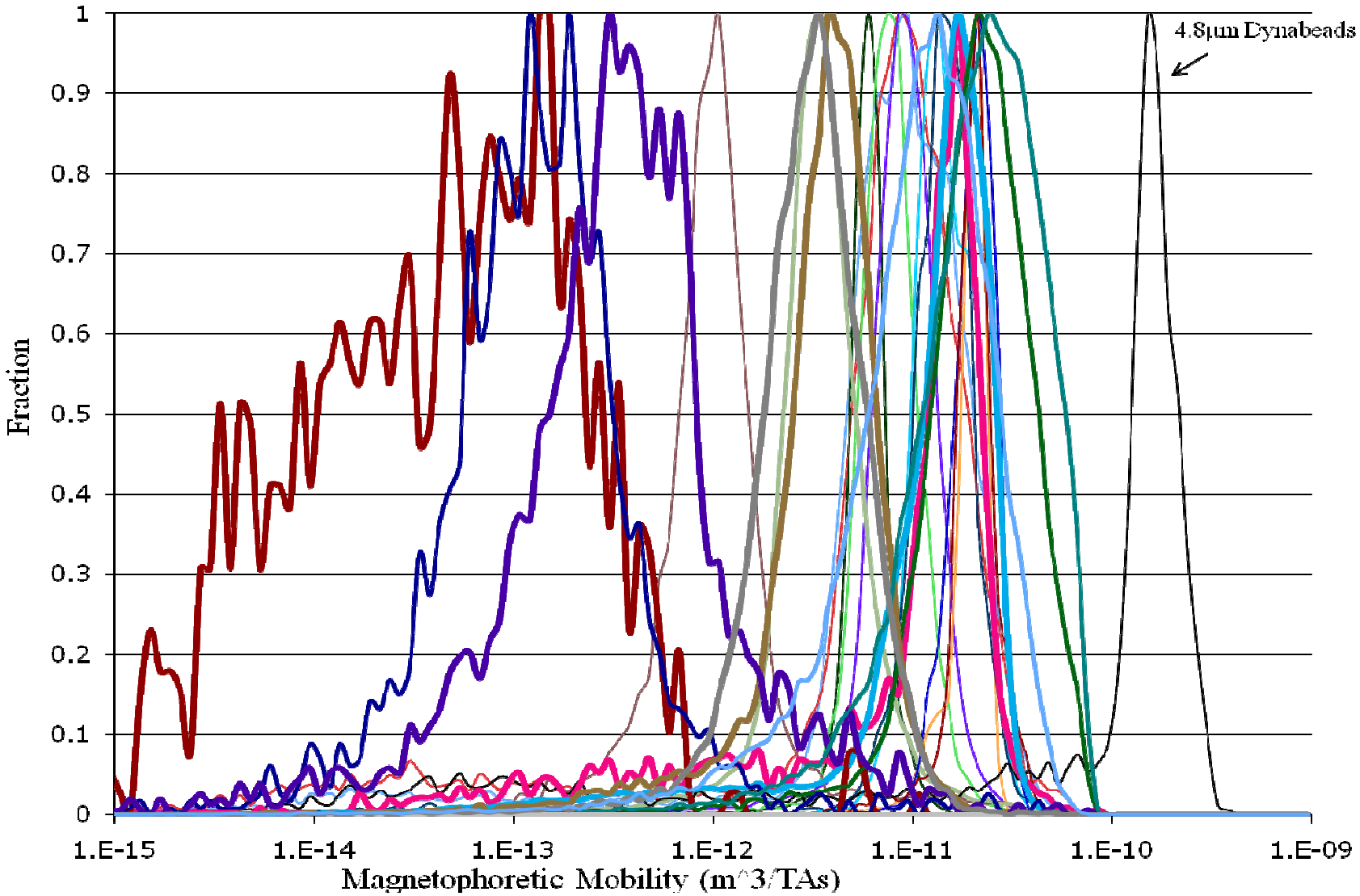

Figure 1.7: Magnetophoretic Mobility Histograms for selected microbeads, 50nm – 10µm (data provided by David J. Kennedy of IKOTECH, LLC)

1.10 References

Ballinger WF, Lacy PE. 1972. Transplantation of intact pancreatic islets in rats. Surgery 72:175-186.

Berney T, Buhler L, Caulfield A, Oberholzer J, Toso CH, Alejandro R, Cooper DKC, Ricordi C, Morel PH. 2001. Transplantation of islets of Langerhans New developments. Swiss Med Wkly 47-48:671-680.

Brunicardi FC, Oh Y, Shevlin L, Suh E, Kleinman R, Stein E, Lipaz G, Plant DV, Imagawa D, Fetterman HR. 1994. Laser destruction of human nonislet pancreatic tissue. Transplant Proc 26(6):3354-3355.

CDC. 2008. Number of people with diabetes increases to 24 million, in Press Release, D.o.h.a.h. services, Editor, Center for Disease Control.

CDC. 2002. National Health Interview Survey. Centers for Disease Control and Prevention, National Center for Chronic Disease Prevention and Health Promotion, Division of Diabetes Translation.

Chalmers JJ, Zhao Y, Nakamura M, Melnik K, Lasky L, Moore L, Zborowski M. 1999. An Instrument to Determine the Magnetophoretic Mobility of Labeled, Biological Cells and Paramagnetic Particles. Journal of Magnetism and Magnetic Materials 194:231-241.

Chalmers JJ, Haam S, Zhao Y, McCloskey K, Moore L, Zborowski M, Williams PS. 1999a. Quantification of Cellular Properties from External Fields and Resulting Induced Velocity: Cellular Hydrodynamic Diameter. Biotechnology and Bioengineering 64:509-518.

Davies JE, Robertson GS, Swift S, Chamberlain J, Bell PR, James RF, London NJ. 1994. Use of a quadripole magnet significantly improves immunomagnetic islet purification. Transplant Proc 26(2):649-650.

Davies JE, Winoto-Morbach S, Ulrichs K, James RF, Robertson GS. 1996. A comparison of the use of two immunomagnetic microspheres for secondary purification of pancreatic islets. Transpntation 62(9):1301-1306.

Davies JE, James RF, London NJ, Robertson GS. 1995. Optimization of the magnetic field used for immunomagnetic islet purification. Transplantation 59(5):767-771.

Gavin JR, Alberti K, Davidson M, DeFronzo R, Drash A, Gabbe S, Genuth S, Harris M, Kahn R, Keen H, Knowler W, Lebovitz H, Maclaren N, Palmer J, Raskin P, Rizza R, Stern M. 2003. Report of the expert committee on the diagnosis and classification of diabetes mellitus: Committee Report. Diabetes Care 26(S1):S5-S20.

Giddings JC. 1985. A System Based on Split-Flow Lateral-Transport Thin (SPLITT) Separation Cells for Rapid and Continuous Particle Fractionation. Sep Sci Technol 20:749-768.

Gray DW, Göhde W, Carter N, Heiden T, Morris PJ. 1989. Separation of Pancreatic islets by Fluorescence-Activated Sorting, Diabetes 38(suppl 1):133-135.

Hering BJ, Matsumoto I, Sawada T, Nakano M, Sakai T, Kandaswamy M, Sutherland DER. 2002. Impact of two-layer pancreas preservation on islet isolation and transplantation. Transplantation 74:1813-1816.

Hering BJ, Wijkstrom M, Graham ML, et al. Prolonged diabetes reversal after intraportal xenotransplantation of wild-type porcine islets in immunosuppressed nonhuman primates. Nat Med 2006; 12 (3): 301.

Heuser M, Wolf B, Vollmar B, Menger MD. 2000. Exocrine contamination of isolated islets of Langerhans deteriorates the process of revascularization after free transplantation. Transplantation 69(5):756-761.

Hoyos M, Moore LR, McCloskey KE, Margel S, Zuberi M, Chalmers JJ, Zborowski M. 2000. Study of magnetic particles pulsed-injected into an annular SPLITT-like channel inside a quadrupole magnetic field. J Chromatogr A 903(1-2):99-116.

http://www.biorep.com/RicordiChamber-1#images/ptos/diabetes/ricordi-chamber-gal2.jpg (09/17/2010).

Jindal RM, McShane P, Gray DWR, Morris PJ. Isolation and Purification of Pancreatic 1994. Islets by Fluorescence Activates Islet Sorter, Transplantation Proceedings 26(2):653.

Jing Y, Chalmers JJ, Zborowski M. 2007. Blood progenitor cell separation from linical leukapheresis product by magnetic nanoparticle binding and agnetophoresis. Biotechnol Bioeng 96(6):1139-1154.

Joyce Gauthier V, Mart Mannik. 1988. A method for isolation of mouse glomeruli for quantitation of immune deposits. Kidney International 33:897-899.

London NJM, Swift SM, Clayton HA. 1998. Isolation, culture and functional evaluation of islets of Langerhans. Diabetes & Metabolism 23:200-207.

London NJ, Robertson GS, Chadwick DR, Johnson PR James RF, Bell PR. 1994. Human pancreatic islet isolation and transplantation. Clin Transplant 8(5):421-459.

Markmann JF, Deng SP, Huang X, Desai NM, Velidedeoglu EH, Lui CY, Frank A, Markmann E, Palanjian M, Brayman K, Wolf B, Bell E, Vitamaniuk M, Doliba N, Matschinsky F, Barker CF, Naji A. 2003. Insulin independence following isolated islet transplantation and single islet infusions. Annals of Surgery 237(6):741-751.

Martin M, Williams PS. 1992. Theoretical Advancement in Chromatography and Related Separation Techniques; Dondi, F., Guiochon, G., Eds.; Kluwer Academic Publishers: Dordrecht, The Netherlands 51:513- 580.

McCloskey KE, Chalmers JJ, Zborowski M. 2003. Magnetic cell separation: Characterization of magnetophoretic mobility. Analytical Chemistry 75(24):6868-6874.

McCloskey KM, Moore LR, Hoyos M, Rodrigues A, Chalmers JJ, Zborowski M. 2003a. Magnetic cell separation is a function of antibody binding capacity (ABC). Biotechnol Prog 19(3):899-907.

Michael A, Hering B. 2009. CITR annual report.

Mitsukazu Gotoh, Takashi Maki, Susumu Satomi, Janis Porter, Anthany P Monaco. 1986. Immunological characteristics of purified pancreatic islet grafts, Transplantation 42(4):387-390.

Moore LR, Milliron S, Williams PS, Chalmers JJ, Margel S, Zborowski M. 2004. Control of Magnetophoretic Mobility by Susceptibility-Modified Solutions as Evaluated by Cell Tracking Velocimetry and Continuous Magnetic Sorting. Analytical Chemistry 76:3899-3907.

Muller-Ruchholtz W, Leyhausen G, Petersen P, Schubert G, Ulrichs K. 1987. A simple methodological principle for large scale extraction and purification of collagenase-digested islets. Transplant Proc 19(1):911-915.

Nandigala P, Chen TH, Yang C, Hsu WH, Heath C. 1997. Immunomagnetic isolation of islets from rat pancreas. Biotechnol Prog 13:844-848.

Oberholzer J, Triponez F, Lou J, Morel P. 1999. Clinical islet transplantation: A review. Annals of the New York Academy of Sciences 875:189-199.

Paul H, Tim D, Plamen N. 2003. Economic costs of Diabetes in the U.S. in 2002, Diabetes Care 26:917-932.

Pinkse GGM, Steenvoorde E, Hogendoorn S, Noteborn M, Terpstra OT, Bruitin JA, De Heer E. 2004. Stable transplantation results of magnetically retracted islets: a novel method. Diabetologia 47:55-61.

Ricordi C, SCHARP dw, Lacy PE. 1988. Reversal of diabetes in nude mice after transplantation of fresh and 7 days cultures (24^{o}C) human pancreatic islets. Transplantation 45: 994-996.

Ricordi C, Lacy PE, Finke EH, Olack BJ, Scharp DW. 1988. Automated method for isolation of human pancreatic islets. Diabetes 37:413-420.

Ricordi C. The automated method for islet isolation. In Pancreatic Islet Cell Transplantation 1892-1991: One Century of Transplantation for Diabetes. Ricordi C, Ed. Austin, TX, R.G. Landes Company 1992, p.99-112.

Robertson GS, Dennison AR, Johnson PR, London NJ. 1998. A review of pancreatic islet autotransplantation. hepatogastroenterology 45(19):226-235.

Sakuma Y, Ricordi C, Miki A, Yamamoto T, Pileggi A, Khan A, Alejandro R, Inverardi L, Ichii H. 2008. Factors That Affect Human Islet Isolation, Transplantation Proc 40:343-345.

Samejima T, Yamaguchi K, Iwata H, Morkawa N, Ikada Y. 1998. Gelatin density gradient for isolation of islets of Langerhans. Cell Transplant 7(1):37-45.

Shapiro AM, Lakey JR, Ryan EA, Korbutt GS, Toth E, Warnock GL, Kneteman NM, Rajotte RV. 2000. islet transplantation in seven patients with type 1 diabetes mellitus using glucocorticoid-free immunosuppressive regimen. N Engl J Meg 343(4) 289-290.

Soon-Shiong P, Heintz R, Terasaki P. 1989. Identification of novel blood groupreactive monoclonal antibodies cytotoxic to human acinar cells but not islets. Transplantation Proceedings 21(1):2622-2623.

Soon-Shiong P, Fujioka T, Terasaki P, Heintz R, Lanza RP. 1990. Islet purification by a novel immunomicrosphere cell depletion technique. Transplant Proc 22(2):780-781.

Sulaiman AN, James Shapiro AM. 2006. Advances in pancreatic islet transplantation in humans, Diabetes, Obesity and Metabolism 8:15-25.

Sun L, Zborowski M, Moore L, Chalmers JJ. 1998. Continuous, Flow-Through Immunomagnetic Cell Separation in a Quadrupole Field. Cytometry 33:469-475.

Tong X, Xiong Y, Zborowski M, Farag SS, Chalmers JJ. 2007. A Novel High Throughput Immunomagnetic Cell Sorting System for Potential Clinical Scale Depletion of T Cells for Allogeneic Stem Cell Transplantation. Exp Hematol 35(10)1613-1622.

Williams PS, Zborowski M, Chalmers JJ. 1999. Flow Rate optimization for the Quadrupole Magnetic Cell Sorter. Anal Chem 71:3799-3807.

Winoto-Morbach S, Ulrichs K, Leyhausen G, Muller-Ruchholtz W. 1989. New principle for large-scale preparation of purified human pancreas islets. Diabetes 38(Supp 1):146-149.

Winoto-Morbach S, Leyhausen G, Schunke M, Ulrichs K, Muller-Ruchholtz W. 1989a. Magnetic microspheres (MMS) coupled to selective lectins: a new tool for large-scale extraction and purification of human pancreatic islets. Transplant Proc 21(1):2628-2630.

Winoto-Morbach S, Krout OS, Heiser A, Ulrichs K, Muller-Ruchholtz W. 1994. Lectin binding to acinar tissue for complete magnetophoretic purification of porcine pancreatic islets depends on the composition and pH of the incubation medium. Transplant Proc 26(2):646-648.

Winoto-Morbach, Ulrichs K, Hering BJ, Leyhausen G, Muller-Ruchholtz W. 1989b. Methods in Islet transplantation research, Hormone and Metabolic Research, Supplement 25:51-54.

Zhang H, Nakamura M, Comella K, Moore L, Zborowski M, Chalmers J. 2002. Characterization/Quantification of the Factors Involved in the Imparting a Magnetophoretic Mobility on Cells and Particles. European Cells and Materials 3(2):34-36.

2. Computational Fluid Dynamics Simulation of a Quadrupole Magnetic Sorter Flow Channel: Effect of Splitter Position on Nonspecific Crossover

2.1 Abstract

In the Quadrupole Magnetic Sorter (QMS) magnetic particles enter a vertical flow annulus and are separated from non-magnetic particles by radial deflection into an outer annulus where the purified magnetic particles are collected via a flow splitter. The purity of magnetically isolated particles in QMS is affected by the migration of nonmagnetic particles across transport lamina in the annular flow channel. Computational Fluid Dynamics (CFD) simulations were used to predict the flow patterns, pressure drop and nonspecific crossover in a newly designed QMS flow channel for the isolation of pancreatic islets of Langerhans. Simulation results were compared with the theoretically and experimentally determined results to validate the CFD model. CFD simulations were employed to compare performance of two models of QMS flow channels with differing splitter positions. Results of the simulations were used to show that one design gives up to 10% less nonspecific crossover than another and this model can be used to optimize the flow channel design to achieve maximum purity of magnetic particles.

Keywords: Quadrupole Magnetic Sorter, Computational Fluid Dynamics, Annulus Flow, Nonspecific Crossover

2.2 Introduction

Insulin independence can be achieved in type 1 diabetes patients by transplanting purified pancreatic islets of Langerhans (Sakuma et al., 2008). Isolation of the islets is the important step in preparing the islets for the transplantation. To achieve high yields with required purities, various islet purification techniques have been developed for isolation of islets from exocrine pancreas tissue either by targeting islets or by targeting exocrine tissue (Soon-Shiong et al., 1990; Winoto-Morbach et al., 1989), e.g. hand picking of islets, fluorescence-activated sorting by staining islets with neutral red (Gray et al., 1989; Jindal et al., 1994), or destruction of non-islet tissue by laser energy (Brunicardi et al., 1994). All of these techniques were successfully employed to purify rat islets but failed to scale up to the human tissue digest volume. Present human islet isolation processes rely on the density gradient centrifugation method which depends on small density difference between islets and acinar tissue. The density gradient centrifugation process, however, has been identified as a potential source of islet mass loss and islet damage due to mechanical stress associated with centrifugation and prolonged exposure to proteolytic enzymes (Samejima et al., 1998; Pinkse et al., 2004).

Quadrupole magnetic sorting (QMS) is a well-designed and tested technology for magnetic separations of single cells, e.g., stem cells (Moore et al., 2001; Nakamura et al., 2001; Lara et al., 2002) and has been successfully applied to several cell separations and purifications (Sun et al., 1998; Tong et al., 2007; Jing et al., 2007). When QMS, developed for single cell separation, was used for isolation of islets, very low purity was achieved with good yields. Low purity is due to the size difference between single cells and islets (Shenkman et al., 2009). Islet diameters are distributed between 50 to 500 microns whereas single cell size is around 1 to 10 microns. It has been observed that the mechanical stress applied in QMS does not affect islet

functionality after isolation (Shenkman et al., 2009). To overcome limitations associated with the commonly used density gradient method and to develop a technique that yields sufficient number of islets to reduce the donor to recipient ratio to 1:1, we redesigned (Kennedy et al., 2007) and tested high capacity QMS to isolate porcine islets of Langerhans.

In QMS isolation procedures particles of interest labeled with magnetic micro particles are isolated from unlabeled particles in a magnetic field while flowing through an annular flow channel. Labeled particles migrate radially outward in a quadrupole magnetic field and leave the channel on its outer periphery as a purified fraction. The presence of any unlabeled particles in isolated magnetically labeled particles is known as nonspecific crossover. The occurrence of nonspecific crossover is of particular importance in the isolation of islets as the islets constitute only one to two percent of the entire pancreas. Thus, even one percent of nonspecific crossover could reduce the purity of islets by 50 percent. There are many factors that contribute to nonspecific crossover in QMS, such as hydrodynamic forces, particle concentration in the sample, total flow rate, flow ratios, splitter imperfections (Williams et al., 2003; Williams et al., 2003a; Williams et al., 2008) and splitter position. The effects of splitter position, sample concentration, total flow rate and flow ratios were tested in this study. Computational fluid dynamics software was used to predict the fluid flow pattern throughout the flow channel and nonspecific crossover.

2.3 Materials and Methods

2.3.1 QMS and Separation Theory

The QMS technology is based on a process known as split-flow lateral transport thin separation, which is a subset of Field Flow Fractionation (FFF) technology that separates immunomagnetically labeled islets based on their magnetophoretic mobility (m).

Magnetophoretic mobility is defined as the velocity of a particle per unit magnetic energy gradient. A QMS system consists of three essential components: flow channel, magnet and pumps. Separation takes place in the flow channel which consists of a cylindrical core that is concentric with an external cylindrical shell (Figure 2.1). The sample, consisting of magnetically labeled islets along with unlabelled tissue particles, enters at a' close to the core through a specially designed inlet: carrier fluid, enters the channel at b' adjacent to the outer wall. Both flows merge at the end of the inlet splitter and continue to flow at each side of a virtual surface, known as inlet splitting surface (ISS) at distance r_{iss} from the center of the core.

ISS can be seen in the Figure 2.1 close to the core and remaining at the same distance along the fully developed laminar flow in the annulus region of the channel. The outer flow rate $Q_{b'}$ is maintained higher than the inner flow rate $Q_{a'}$ to keep the sample flow near the core. A second virtual surface known as the outer splitting surface (OSS) at a distance r_{oss} from the center of the core separates the two outlets which are separated by the outlet splitter. The distance between ISS and OSS, r_{oss}-r_{iss}, is known as the Transport Lamina. Magnetically labeled particles in the sample migrate radially and cross the transport lamina and leave in the positive fraction b. The unlabeled and weakly labeled particles which cannot cross the OSS will exit in the negative fraction a.

For an ideal separation in QMS with laminar flow, the transport lamina thickness should be zero as the unlabeled particles would not be expected to cross the transport lamina. However, magnetically labeled islets are generally not uniform in magnetization. A range of magnetization is exhibited due to variation in the number of magnetic particles that enter the vascular structure of islets. To completely isolate pure labeled particles, it is necessary to create conditions that allow the least mobile particles to migrate across the thickness of the transport lamina. The

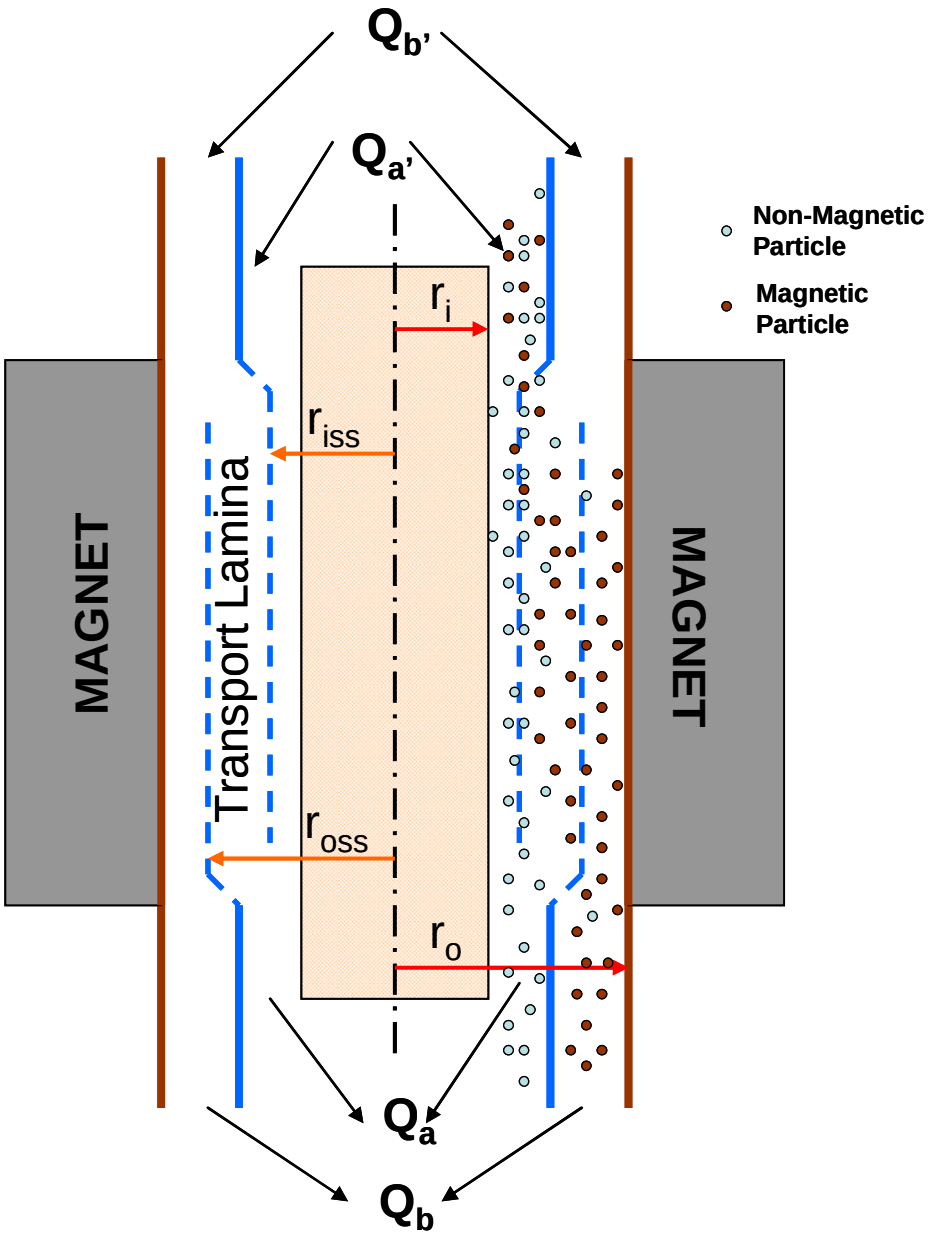

Figure 2.1 : Schematic diagram of the quadrupole magnetic cell sorter (QMS).

thickness of the transport lamina changes with changes in inlet and outlet flow rate ratios and change in splitter position.

The particle trajectory in the annulus is described by the integral equation;

$$\int_0^z dz = \int_{k_1}^{k} \frac{v(k) + v_s}{u_m(k)} dk \qquad (1)$$

where $v(k)$ is the velocity profile of the fluid in the annulus, v_s is the Stokes sedimentation velocity of the particle in the fluid, $u_m(k)$ is the radial magnetophoretic velocity of the particle and k is defined as

$$k = \frac{r}{r_0} \qquad (2)$$

Here r is defined as the radial coordinate from the center of the flow channel core and r_0 is the radius from the center to the wall. Upon the integration of eq. (1) and simplification we can get

$$z = \frac{Q}{2\pi r_0 S_{m0} m_m} \cdot \frac{I_1(k, k_1)}{A_1(1 - k_i^2)} + \frac{r_0 v_s \ln(\frac{k_1}{k})}{m_m S_{m0}} A_1 \qquad (3)$$

where m_m is called the magnetophoretic mobility of the particle, S_{m0} is the magnetic force at the inner surface of the outside wall of the flow channel and v_s is sedimentation velocity of the particle. A_1, A_2 and $I_1(k, k_1)$ are functions used to simplify the calculations and are given by

$$A_1 = (1 + k_i^2 - A_2) \qquad (4)$$

$$A_2 = \frac{1 - k_i^2}{\ln \frac{1}{k_i}} \qquad (5)$$

$$I_1(k, k_1) = [4 \ln k - 2k^2 + 2A_2 (\ln k)^2]_{k_1}^{k} \qquad (6)$$

The radial position of the ISS, K_{ISS} is calculated using the following integration factor (Kennedy et al., 2007):

$$I_2(k_i, k_{ISS}) = [2k^2 - k^4 + 2A_2k^2 \ln k - A_2k^2]_{k_i}^{k_{ISS}} \quad (7)$$

Similarly, the position of the OSS can be calculated using eq. (7) by replacing k_{ISS} with k_{OSS}.

2.3.2 Experimental Measurements

The flow channel used for the experiments was called "prototype I". Nonspecific crossover experiments were performed with nonmagnetic particles, Cultisphers®, macro-porous gelatin-coated micro-carrier beads with diameter range of 200 to 380 µm, similar in size and density to islets and fragments of exocrine tissue in pancreas digests. The sample consisting of cultisphers was introduced into the a' inlet flow stream and carrier buffer was introduced into the b' inlet flow stream by dual head Watson-Marlow peristaltic pumps, and the positive fraction outlet was controlled by a peristaltic pump while leaving the negative fraction outlet to exit at atmospheric pressure to maintain equilibrium of flow in the flow channel.

Experiments were carried out at total flow rates of 250, 300 and 400 ml/min with inlet flow ratio ($Q_{a'}/Q$) of 0.25 and at different outlet flow ratios (Q_a/Q) 0.25, 0.3, 0.5 and 0.7. Experiments were conducted at different sample concentrations to study the effect of particle concentration in the sample on nonspecific crossover. Turbidity sensors are connected to positive and negative fraction outlets to detect absorbance. Nonspecific crossover was calculated from the areas of the absorbance peaks.

2.3.3 Computational Fluid Dynamics

The commercial CFD code, FLUENT, was used for the simulations, and FLUENT's preprocessor, GAMBIT, was used to generate flow-field meshes. An unstructured mesh consisting of tetrahedral volumetric elements in 3D is used in the entire domain. Velocity inlet

boundary conditions with velocities normal to the plane of the channel inlets with fluid properties corresponding to water at 298K are set at the inlets, outflow boundary conditions corresponding to fully developed flow were used at the outlets and the no-slip condition is applied to all walls.

The geometry used for the first case is based on the quadrupole magnetic separation channel for islets, "prototype I". The length of this flow channel is 254 mm with inner diameter of the outer wall of 6.03 mm and core diameter is 5.08 mm. Splitters with radius 5.588 mm and thickness 0.14 mm are used at inlet and outlet. A specially designed flow distributor with diameter 5.96 mm is placed in the b inlet. For the second case (prototype II), the channel length and outer wall diameter are the same as for Prototype I, but the core diameter is 5.08 mm and inlet splitter diameter 5.58 mm with thickness 0.14 mm and outlet splitter diameter 5.84 mm with thickness 0.14 mm. The two QMS separation flow channels analyzed in the study are shown in Figure 2.2.

2.3.4 Governing Equations

For flow in the QMS flow channel, FLUENT, a commercial CFD package, is utilized to solve conservation equations for mass and momentum. FLUENT is based on a set of partial differential equations maintaining conservation of mass and momentum. These equations describe the convective motion of the fluid. The law of conservation of mass applied to an infinitesimal fixed control volume generates the continuity equation in differential conservation form:

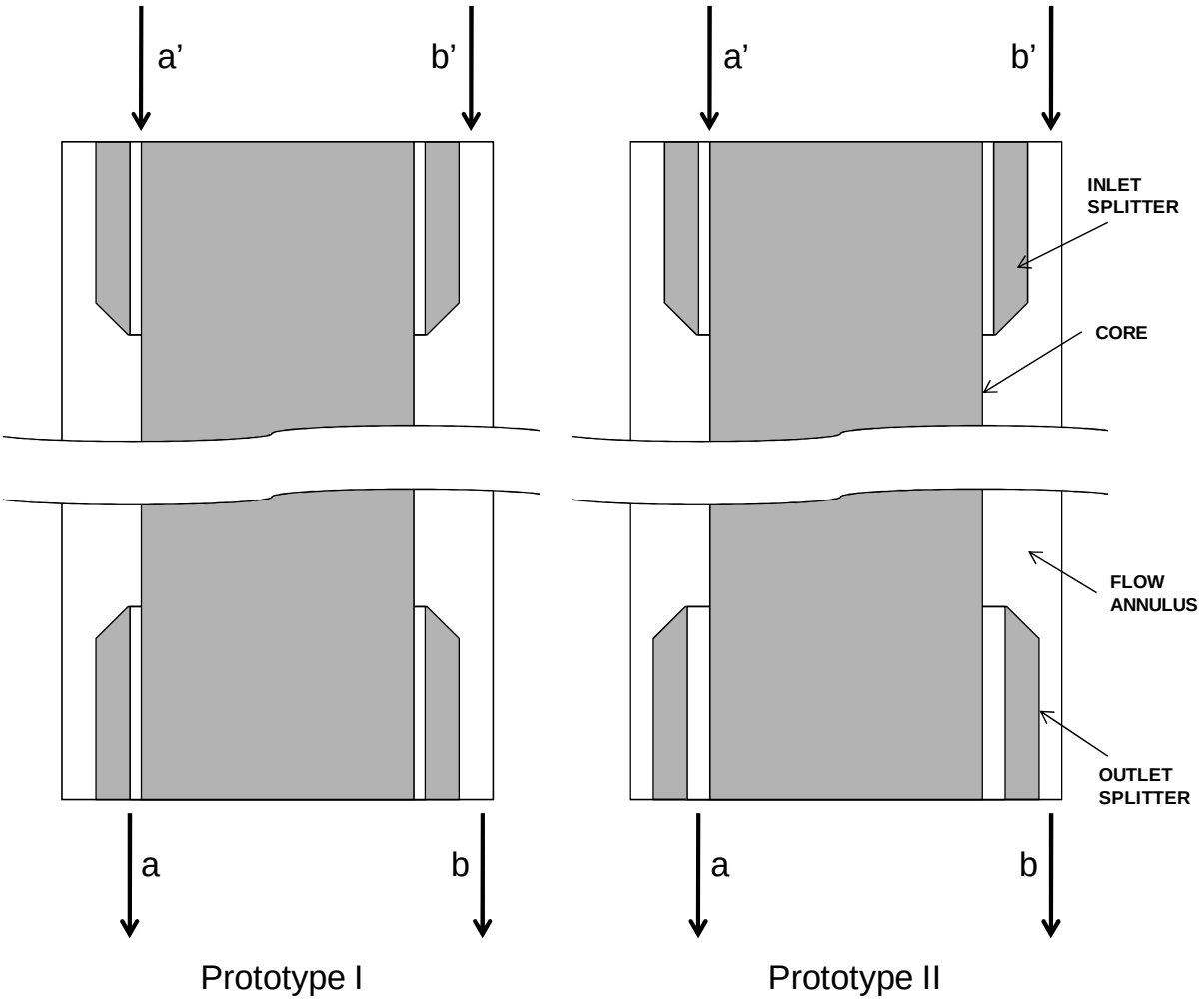

Figure 2.2: Geometry drawings of Prototype I and Prototype II flow channels.

$$\frac{\partial \rho}{\partial t} + \nabla . \rho \vec{V} = 0 \tag{10}$$

The first term in the Equation 10 represents the rate of increase in the density and the second term represents the rate of mass flux passing out of the control volume. For a steady incompressible flow, ρ = constant and $\frac{\partial \rho}{\partial t} = 0$ which reduces Equation 10 to

$$\nabla . \vec{V} = 0 or \frac{\partial u}{\partial x} + \frac{\partial u}{\partial y} + \frac{\partial u}{\partial z} = 0 \tag{11}$$

Newton's second law applied to a fluid passing through an infinitesimal control volume yields the momentum equation:

$$\frac{\partial}{\partial t}(\rho \vec{V}) + \nabla . (\rho \vec{V} \vec{V}) = \nabla . \pi_{ij} \tag{12}$$

The first term in the Equation 12 represents the rate of increase of momentum per unit volume in the control volume. The second term represents the rate of momentum lost by convection through control surface. The forces applied by external stresses such as normal and shearing stresses which can be represented by the stress tensor π_{ij}. The stress tensor can be written as

$$\pi_{ij} = -p\delta_{ij} + \mu[(\frac{\partial u_i}{\partial x_j} + \frac{\partial u_j}{\partial x_i}) - \frac{2}{3}\delta_{ij}\frac{\partial u_k}{\partial x_k} \tag{13}$$

Substituting equation 13 into equation 12 and simplifying produces the Navier - Stokes equations:

$$\rho \frac{D\vec{V}}{Dt} = -\delta_{ij}\nabla p + v\frac{\partial}{\partial x_j}\left[\mu(\frac{\partial u_i}{\partial x_j} + \frac{\partial u_j}{\partial x_i}) - \frac{2}{3}\delta_{ij}\frac{\partial u_k}{\partial x_k}\right] \tag{14}$$

For a Cartesian coordinate system, Equation 14 can be separated into three scalar equations. The conservation of momentum in the x-direction is given by

$$\rho \frac{Du}{Dt} = -\frac{\partial p}{\partial x} + \frac{\partial \tau_{xx}}{\partial x} + \frac{\partial \tau_{yx}}{\partial y} + \frac{\partial \tau_{zx}}{\partial z} \tag{15}$$

The conservation of momentum in the y-direction is given by

$$\rho \frac{Dv}{Dt} = -\frac{\partial p}{\partial y} + \frac{\partial \tau_{xy}}{\partial x} + \frac{\partial \tau_{yy}}{\partial y} + \frac{\partial \tau_{zy}}{\partial z} \tag{16}$$

The conservation of momentum in the z-direction is given by

$$\rho \frac{Dw}{Dt} = -\frac{\partial p}{\partial z} + \frac{\partial \tau_{xz}}{\partial x} + \frac{\partial \tau_{yz}}{\partial y} + \frac{\partial \tau_{zz}}{\partial z} \tag{17}$$

The viscous normal stresses are given by

$$\tau_{xx} = \frac{2}{3}\mu\left(2\frac{\partial u}{\partial x} - \frac{\partial v}{\partial y} - \frac{\partial w}{\partial z}\right) \tag{18}$$

$$\tau_{yy} = \frac{2}{3}\mu\left(2\frac{\partial v}{\partial y} - \frac{\partial u}{\partial x} - \frac{\partial w}{\partial z}\right) \tag{19}$$

$$\tau_{zz} = \frac{2}{3}\mu\left(2\frac{\partial w}{\partial z} - \frac{\partial v}{\partial y} - \frac{\partial u}{\partial x}\right) \tag{20}$$

and the viscous shear stresses are given by

$$\tau_{xy} = \tau_{yx} = \mu\left(\frac{\partial v}{\partial x} + \frac{\partial u}{\partial y}\right) \tag{21}$$

$$\tau_{xz} = \tau_{zx} = \mu\left(\frac{\partial w}{\partial x} + \frac{\partial u}{\partial z}\right) \tag{22}$$

$$\tau_{yz} = \tau_{zy} = \mu\left(\frac{\partial w}{\partial y} + \frac{\partial v}{\partial z}\right) \tag{23}$$

The first law of thermodynamics applied to a fluid passing through an infinitesimal, fixed control volume yields the following energy equation:

$$\frac{\partial}{\partial t}(\rho h)+\vec{\nabla}.\left(\rho\vec{V}h\right)=\vec{\nabla}.\left(k\vec{V}T\right)-\frac{\partial}{\partial x}(up)-\frac{\partial}{\partial y}(vp)-\frac{\partial}{\partial z}(wp)$$

$$+\frac{\partial}{\partial x}(u\tau_{xx})+\frac{\partial}{\partial y}(u\tau_{yx})+\frac{\partial}{\partial z}(u\tau_{zx})$$

$$+\frac{\partial}{\partial x}(u\tau_{xy})+\frac{\partial}{\partial y}(u\tau_{yy})+\frac{\partial}{\partial z}(u\tau_{zy})$$

$$+\frac{\partial}{\partial x}(u\tau_{xz})+\frac{\partial}{\partial y}(u\tau_{yz})+\frac{\partial}{\partial z}(u\tau_{zz}) \quad (24)$$

For most problems in gas dynamics, it is possible to assume an ideal gas, defined as a gas whose intermolecular forces are negligible. An ideal gas obeys the ideal gas equation of state:

$$p = \rho RT \quad (25)$$

In this study, the ideal gas equation of state is used to calculate the density for the compressible gas flow with change in pressure.

The continuity, x-momentum, y-momentum, z-momentum and energy equations are solved using FLUENT to simulate incompressible, laminar, steady-state flow.

2.3.5 Discretization

The process of converting partial differential equations into a set of algebraic relations that can be solved using a computer is called discretization (Anderson, 1999). Discretization involves two main steps: (1) converting the continuum partial differential equations into algebraic relations and (2) converting the continuous physical domain into nodes, volumes, or elements where the algebraic equations will be solved. Discretization of partial differential equations can be accomplished in many different ways. Among those, the two types of discretization used to solve problems in fluid mechanics and heat transfer are finite differences (discretization of partial differential form of equations) and finite volumes (discretization of equations in the integral form).

In the finite difference approach, the continuous problem or domain is discretized so that the dependent variables are considered to exist only at discrete points. In the finite volume method, the conservation principles are applied to a fixed region or space known as the control volume. Using the finite volume approach, either control volumes are established first and grid points are placed at the center of the volumes (cell-centered method) or grid points are established first and then the boundaries of the control volume are fixed (vertex-centered method) (Tannehill et al., 2004). The finite volume method using the cell-centered approach is used in this study to convert the governing equations into an algebraic form that is then solved numerically.

A variety of methods are used for discretizing the governing equations using the finite volume method. In this study, first-order and second-order accurate upwind methods are used. The cell-centered method is used, solving the flow properties at the cell centers; the values at the interfaces (used to obtain cell fluxes) are obtained by interpolating the cell-centered values with an upstream direction bias. This method is called an upwinding scheme.

2.3.6 Solvers

FLUENT was used in this study to simulate flows through the QMS flow channel. This section discusses the FLUENT solver options that are used in this study. Governing equations for conservation of mass, momentum, energy, and chemical species are solved using cell-centered control volume based segregated solver.

Using a segregated solver, the governing equations are solved sequentially (i.e., segregated from one another). Several iterations of the solution loop are performed before obtaining a converged solution. The segregated solver basic steps, shown in Figure 2.3, are:

1. Initial guess of pressure, velocity and species transport quantities, such as mass flux, is made.
2. The discretized Navier-Stokes equations (i. e., momentum equations) are solved using the guessed values of P*, u*, v*, etc. In this step coefficient to determine the fluxes through the cell/boundary faces by conduction/convection etc. The flow variables (p, u, v, w, etc.) for the entire domain (for each grid node) are obtained at the end of this step.
3. Once the flow properties are calculated, the continuity equation is next verified. If the continuity equation is not satisfied, pressure and velocity values (u, v, w) are corrected using pressure correction equation. SIMPLE algorithm is used for pressure-velocity coupling.
4. Once the flow properties are obtained, other discretized transport equations are solved. The initial guess for the transport quantities are depicted in step 1. After solving the transport equation, we get the transport properties at each node
5. In this step the flow and transport variables, obtained in step 3 and 4, at each node are compared with values of previous iteration and residuals are calculated using L2 Norm. If the residuals are less than prescribed tolerance limit, the solution is final. If the residual is higher than the tolerance limit, steps 1 through 5 are repeated until the convergence criteria are satisfied. The initial guess values are replaced with values of flow and transport variables obtained from the current iteration.

2.3.7 Pressure-Velocity Coupling Method

A pressure-velocity coupling is used to derive an equation for pressure from the discrete continuity equation. The SIMPLE algorithm is used to obtain a relationship between velocity and pressure corrections to enforce mass conservation and thus obtain the pressure field.

2.3.8 Geometric Modeling

GAMBIT, a commercial pre-processor, is used to generate geometric models used in this study. FLUENT is used to solve the discretized governing equations. For post-processing the results obtained from FLUENT, TECPLOT are used. GAMBIT is used to create a volume mesh in the fluid domain. An unstructured mesh consisting of tetrahedral volumetric elements in three dimensions is used in the entire domain except at the walls, where a boundary layer mesh consisting of prismatic volumetric elements is used.

Figure 2.4 shows a sample mesh consisting of triangular elements on the splitter and sample inlet. Figure 2.5 shows the unstructured mesh on the top inlet face along with the prismatic boundary layer mesh on the inlet pipe faces. The effect of using a boundary layer mesh around the fibers and particles is also examined by considering a case with an unstructured mesh in the entire domain. Pressure drops on the structured and unstructured mesh around the fibers and the particles varied by up to two to eight per cent; moreover, the unstructured mesh results had significantly larger numerical error as estimated by a grid refinement study. The accuracy of the fully tetrahedral mesh results could be increased by refining the mesh, but the additional refinement is expensive in both computation cost and solution time. As a result, a prismatic boundary layer mesh is used around the fibers and the particles to reduce the computation cost and to improve numerical accuracy.

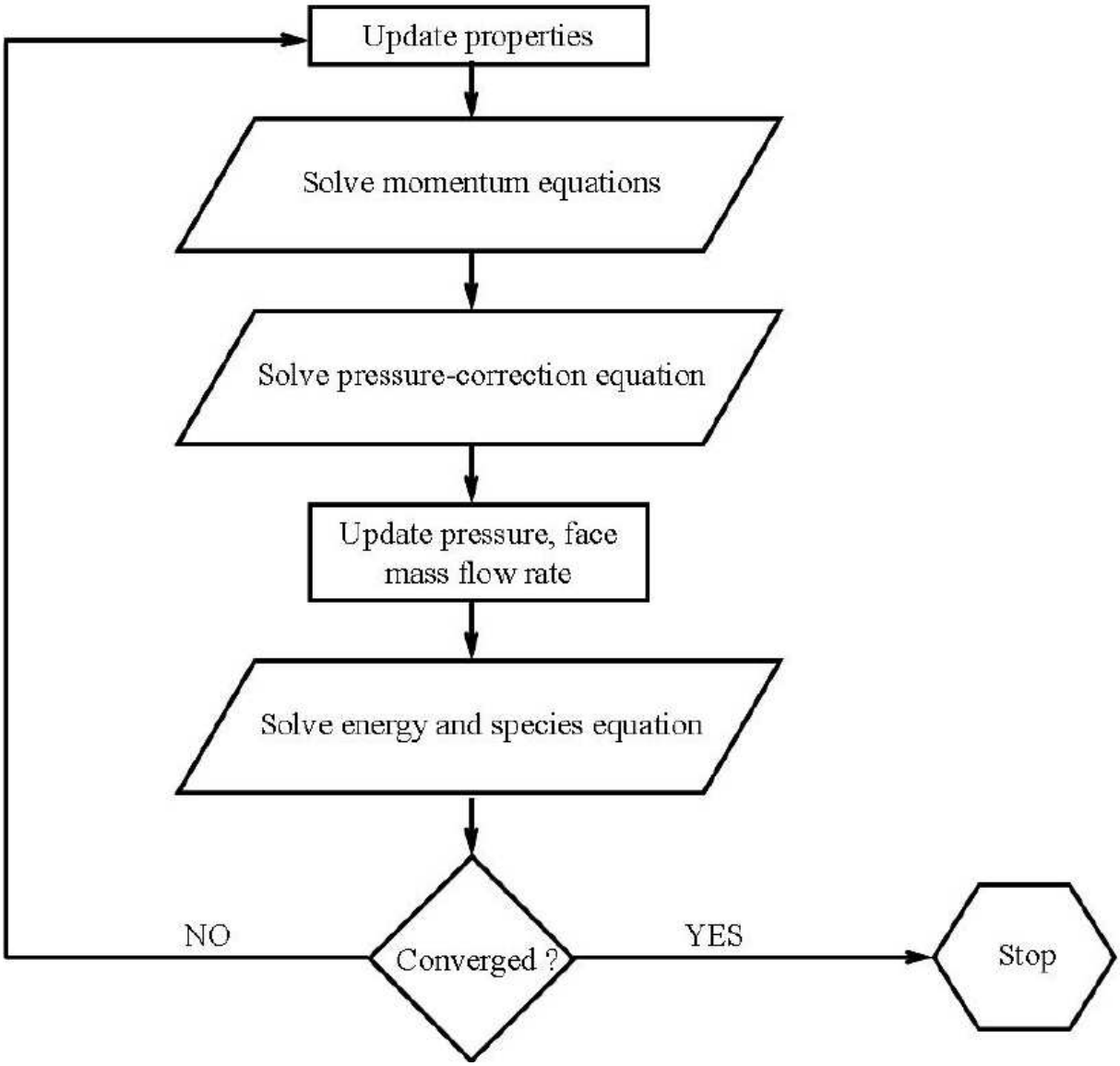

Figure 2.3: Flow chart for segregated solver used in this study.

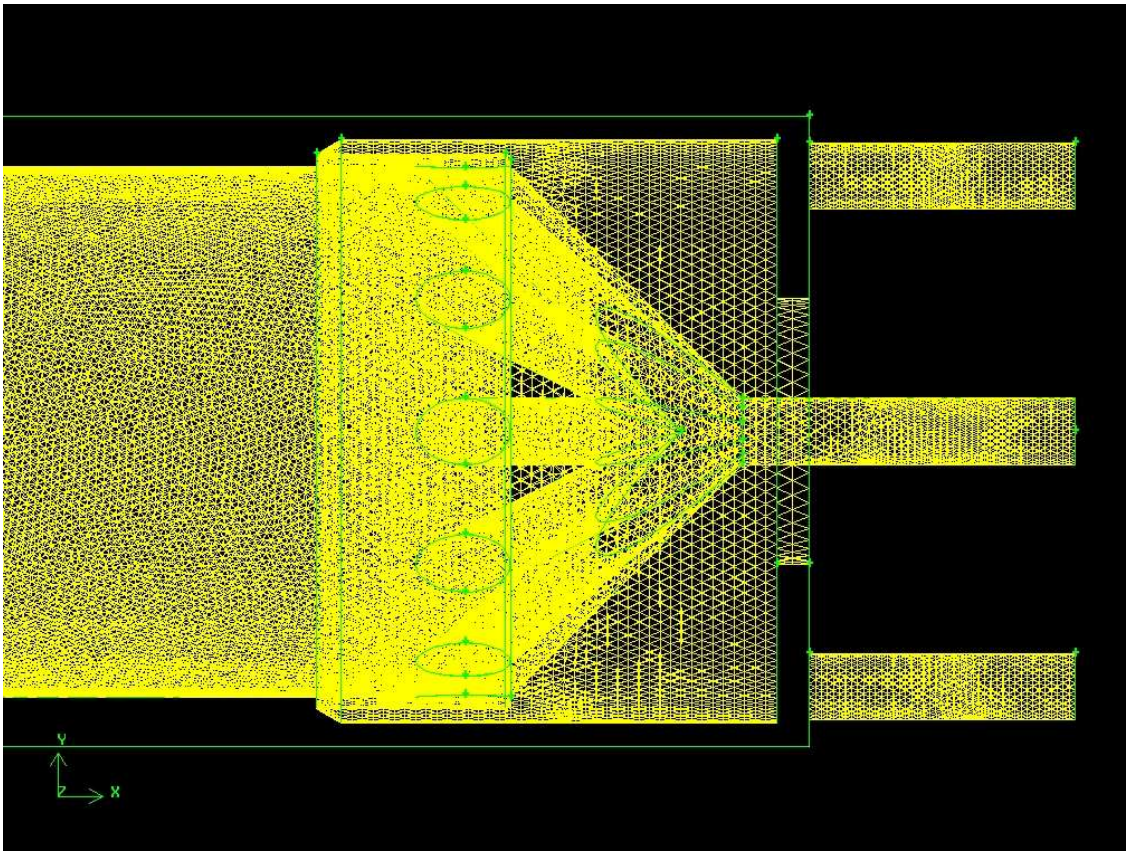

Figure 2.4: Unstructured triangular mesh on the faces of QMS flow channel.

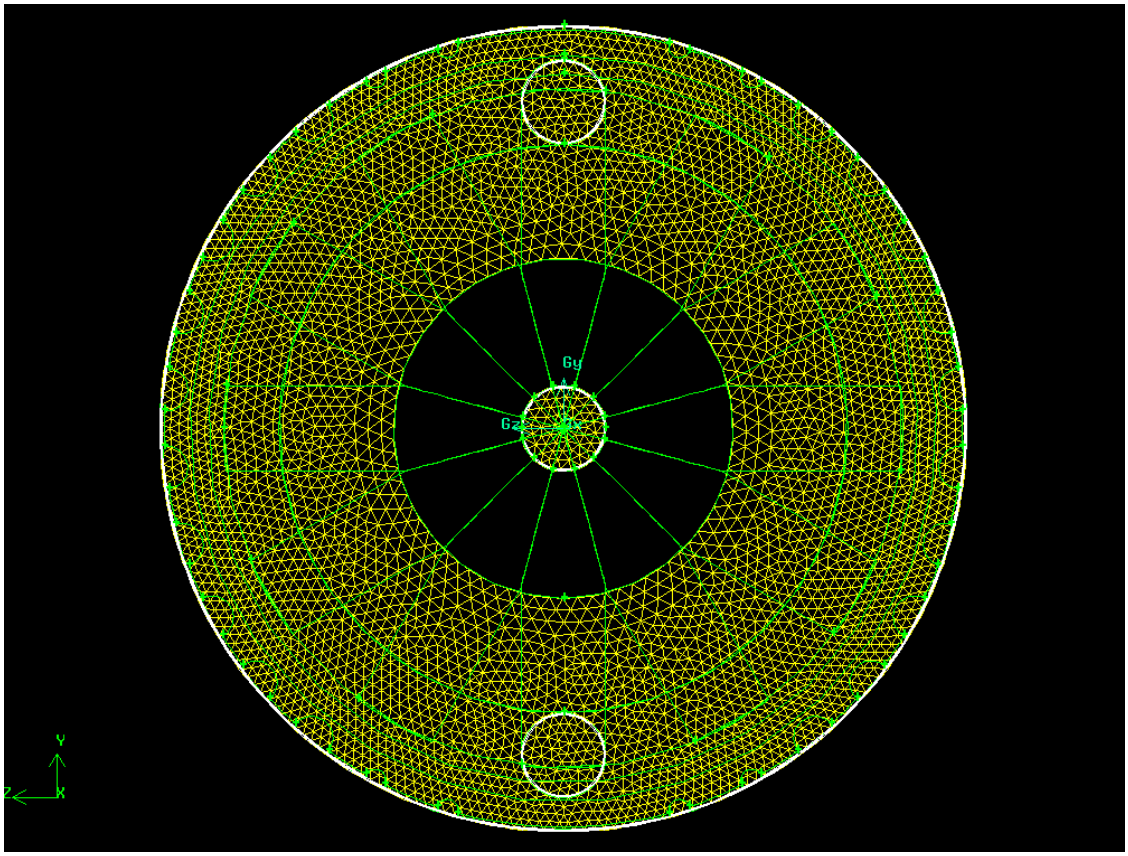

Figure 2.5: Unstructured mesh along with the boundary layer on the inlet pipes and channel face.

2.3.9 Boundary Conditions

Three different boundary conditions used in this study are no-slip, velocity inlet, and outflow. For laminar flows with zero velocity at the wall, the no-slip boundary condition is enforced at the walls. Velocity inlet boundary conditions are used to define the flow velocity along with all flow properties at the inlet and in some cases at outlet. Outflow boundary conditions are used to model flow exits where the details of the flow velocity and pressure are not known prior to solution of the flow problem. At outflow boundaries, all of the necessary boundary information is extrapolated from the interior.

2.3.10 Simulation Procedure

An iterative solution approach is employed where the solution is advanced in pseudo-time until the steady state equations are satisfied to a specified tolerance. At each iteration the governing equations are solved using a segregated solver. A finite volume technique is used to solve the discrete form of the governing equation on the computational grid. The standard SIMPLE algorithm is used in which the momentum equations are first solved for the velocity components. A pressure correction is then determined that drives the velocity field towards satisfying the mass conservation equation. Iterative convergence is assessed by monitoring the L2 norms of the steady-state residuals. The convergence criterion is set to 10^{-7} for all conservation equations.

2.4 Results and Discussion

2.4.1 CFD Simulations: Flow Analysis and Pressure Drop Predictions

One important feature of the flow channel is the design of the flow distributor placed at the carrier buffer inlet (b') to obtain circumferentially uniform flow in the flow channel. Uniform flow around the core is important to maintain laminar flow in the annulus to yield

minimum crossover and maximum isolation. Improvements made to the flow distributor design were verified by CFD analysis. Figure 2.6 shows the flow distributor design with flow profile at different distances downstream from the distributor. Incoming fluid enters the distributor from two branches. Direct flow through the distributor from these branches is prevented by the lack of notches at the two inflow locations. The simulations show the uniform flow developed by the time fluid reaches the splitter end point.

CFD simulations are performed using the generated flow-field meshes in order to predict the pressure drop and analyze the details of the flow in the flow channel. A plane is extracted at the center of the domain (i.e., Z=3.01625 mm) and displayed as a colored ring for the case with total flow rate 400 ml/min with inlet and outlet flow ratio 0.25. The velocity magnitude contours are shown in Figure 2.7a for sample (a') velocity 0.05 m/s and buffer (b') velocity 0.15 m/s. Careful examination of the calculated fluid velocity profiles revealed that the flow was fully developed within a relatively short distance of the splitter edge for every ratio of inlet and outlet flows.

Figure 2.7b shows the velocity profile at the middle of the channel. Pressure magnitude contours are shown in Figure 2.8 along with the pressure gradient found from CFD simulations plotted against total flow rates compared with the theoretically calculated pressure drop using the Haigen-Poiseuille equation for annular pipes. Figure 2.8b shows that the pressure drop predicted using CFD is in good agreement with theoretical calculations with pressure drop increasing with the increase in total flow rate.

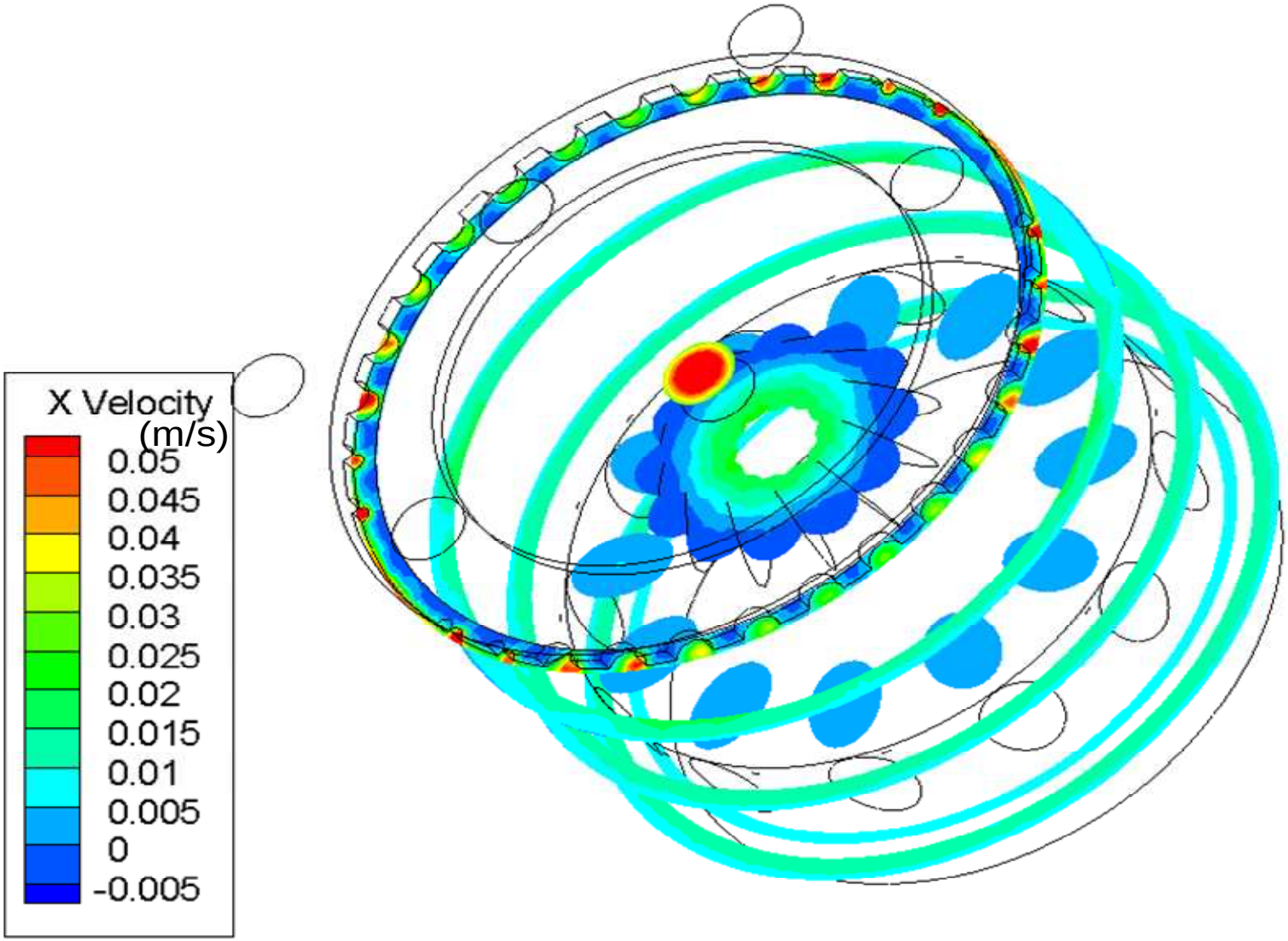

Figure 2.6: Velocity (m/s) contours in x plane at different distance from flow distributor to the end point of the splitter.

2.4.2 Nonspecific Crossover

The new design of the flow channel is tested for nonspecific crossover at different total flow rates ranging from 250 ml/min to 400 ml/min, input flow ratios ($Q_{a'}/Q$), outlet flow ratios (Q_a/Q) ranging from 0.25 to 0.7. When flow rates less than 250ml/min were used, cultisphers settled in the tubing and clogging of the inlet was observed. The effect of the particle concentrations in the sample and total flow rate on the crossover was examined. Some of these experiments were also conducted with pig pancreas (results not presented) and the same results as with cultisphers were observed. CFD simulations were conducted for all of these cases using the discrete phase model and compared with the experimental results. Nonspecific crossover (S_b) is calculated as the ratio of non-magnetic particles leaving in positive collection (N_b) to the particles leaving in both negative (N_a) and positive collection.

$$S_b = \frac{N_b}{N_a + N_b} \tag{26}$$

Figure 2.9 shows the nonspecific crossover of Cultisphers at different outlet flow ratios and at fixed inlet flow ratio of 0.25 and total flow rate of 400ml/min. These experiments were conducted with the flow channel design prototype I, in which the inlet and outlet splitters have the same 5.58mm diameter. A clear decrease in nonspecific crossover with increase in outlet flow ratio is observed because the increase in outlet flow ratio increases the transport lamina thickness. Figure 2.9 also presents the comparison of nonspecific crossover obtained from experiments with prototype I and CFD simulation-predicted crossover for prototype II. Good

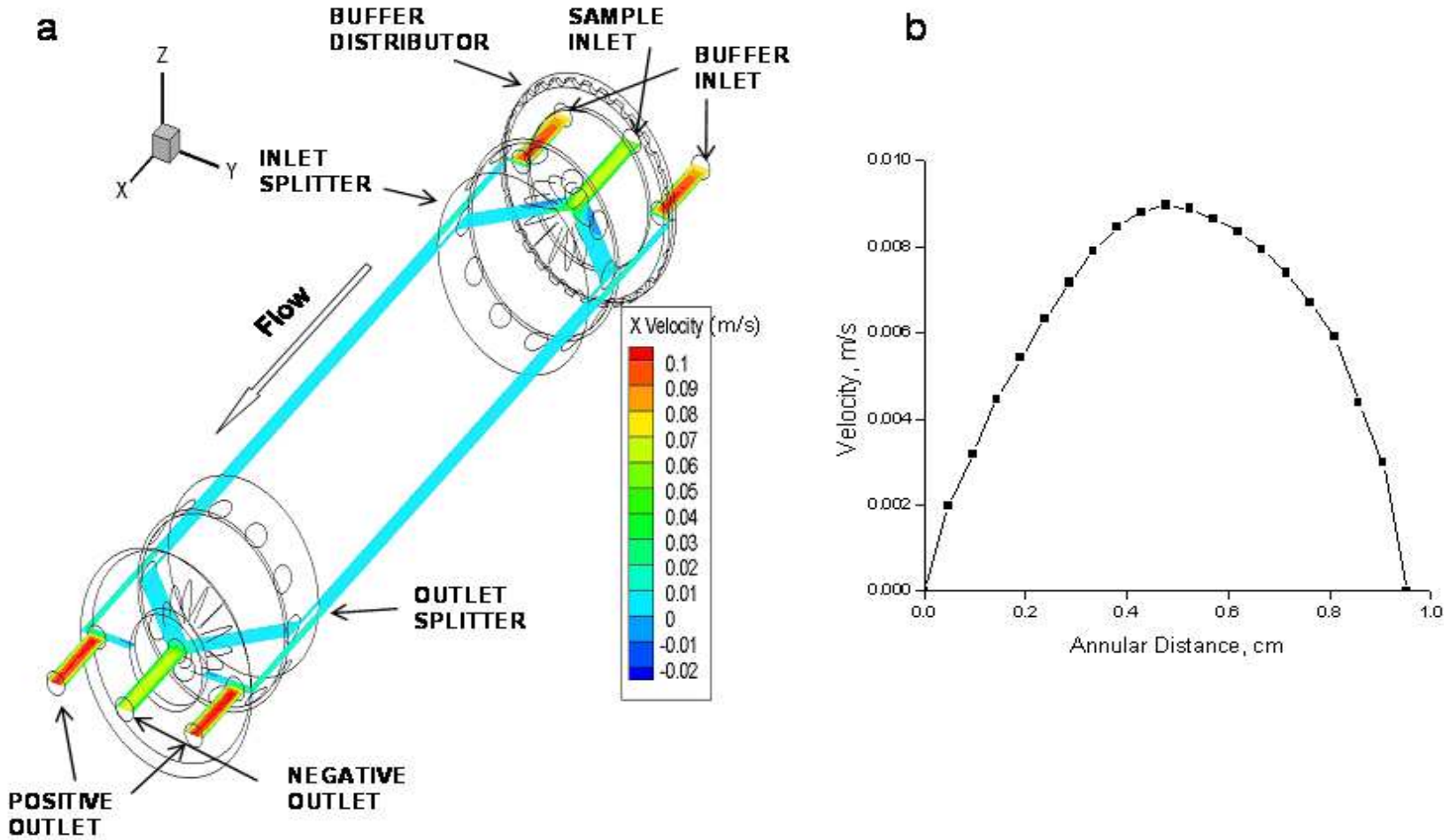

Figure 2.7: a) Velocity (m/s) magnitude contours in the flow channel at z = 1.1875" (flow is in positive x direction. b) Velocity profile of the fluid at the middle point of the channel.

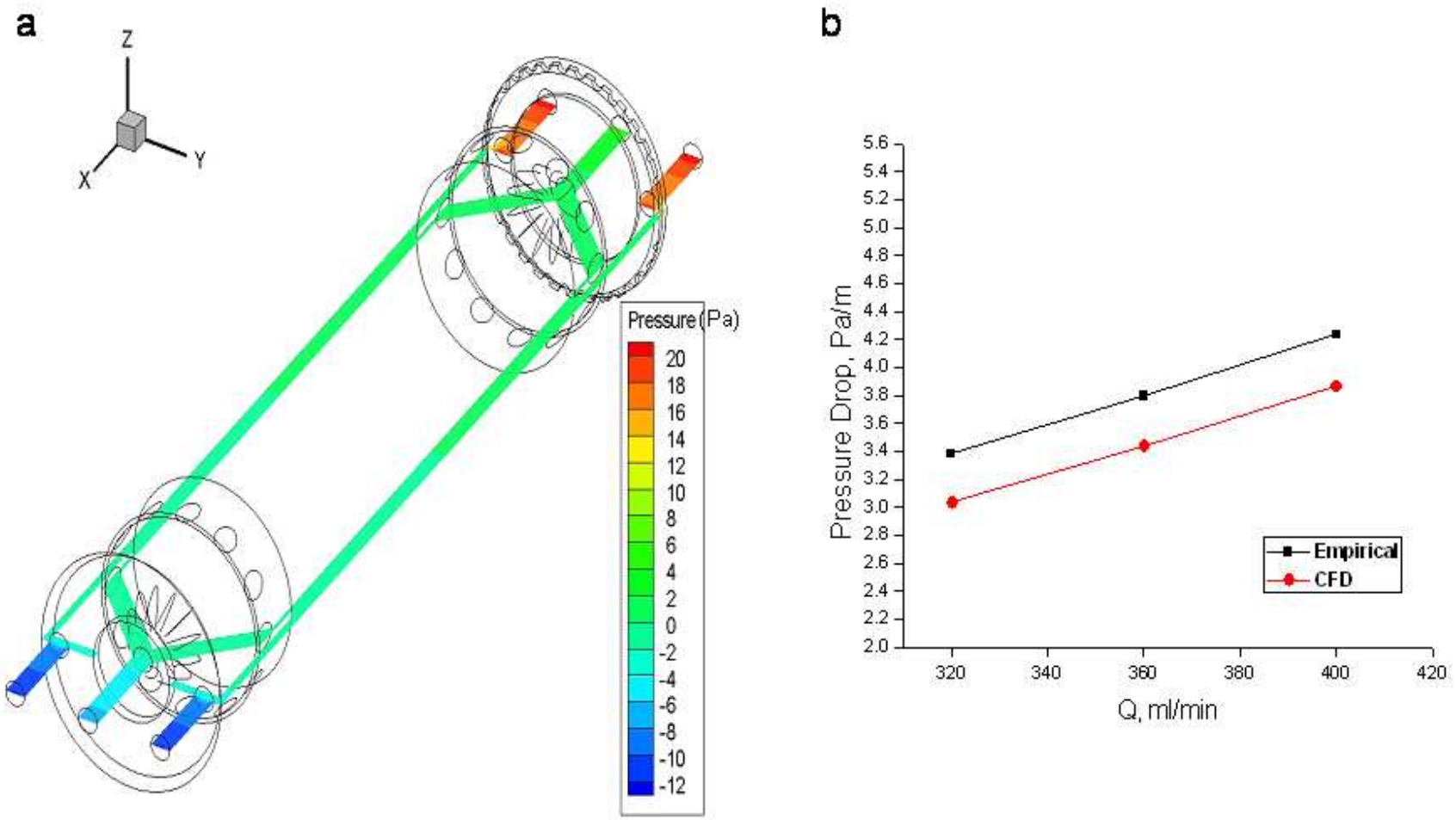

Figure 2.8: a) Pressure (Pa) contours in the flow channel at z = 1.1875" b) Comparison of the pressure drop from CFD simulations and empirical correlations.

agreement is found between experimental results and CFD simulation-predicted values with same prototype flow channel with less than 10% deviation. This deviation might be due to the negligence of particle-particle interaction in CFD modeling. CFD-predicted crossover for prototype II is compared with that of CFD predictions and experimental values with Prototype I. Crossover is slightly less for prototype II when compared to prototype I. The diameter of the outlet splitter is increased in prototype II which increases the transport lamina thickness and reduces the number of nonmagnetic particle that leave in the positive fraction. Straight line in the figure 2.9 represents the ideal flow of the fluid without solid particles.

Figure 2.10 shows the crossover of nonmagnetic particles at different total flow rates in the Prototype I channel at a fixed inlet and outlet flow ratio of 0.25. Experimental crossover values increase with decreasing total flow rates as the hydrodynamic lift forces move the particles away from wall at low flow rates which helps particles to cross the transport lamina and leave in the positive fraction. Crossover obtained from CFD simulations for different total flow rates are under predicted by 5 to 10 percent for prototype I. Comparison of calculated crossover values at different total flow rates for the two prototypes shows a decrease in crossover for prototype II due to the increase in transport lamina thickness resulting from the outlet splitter position.

Figure 2.11 shows crossover values at different sample concentrations at a fixed total flow rate of 400ml/min. Outlet flow ratio is maintained equal to inlet flow ratio at 0.25. Increasing cultisphers concentration increases the particle-particle interaction which results in more nonspecific crossover. Higher concentrations of particles during experiments also clogged the flow paths in the sample inlets. CFD simulations predict decreased crossover with the new design prototype II when compared with the prototype I.

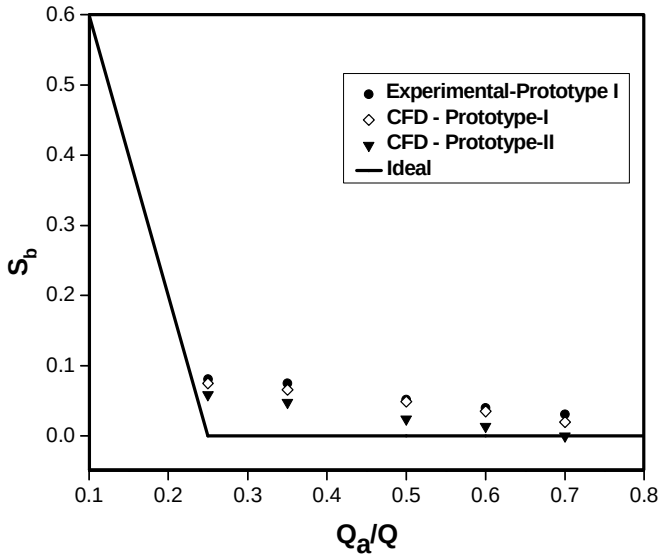

Figure 2.9: Comparison of calculated and observed nonspecific crossover as a function of outlet flow ratio at a total flow rate of 400 ml/min and inlet flow ratio of 0.25.

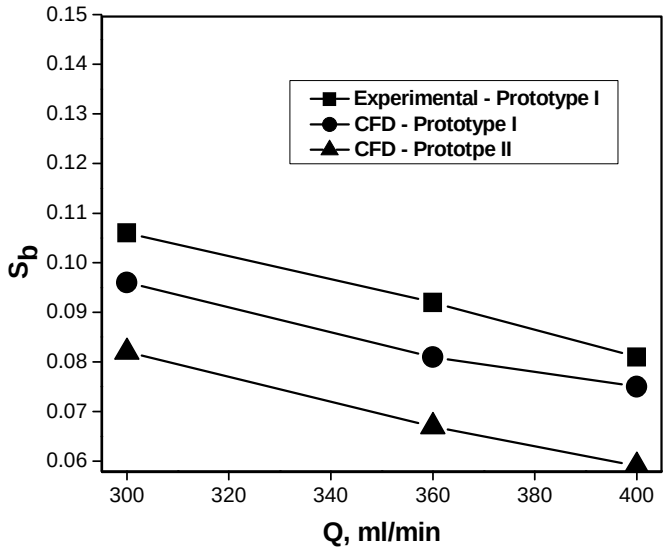

Figure 2.10: Comparison of the nonspecific crossover as a function of total flow rate at an inlet and outlet flow ratio of 0.25.

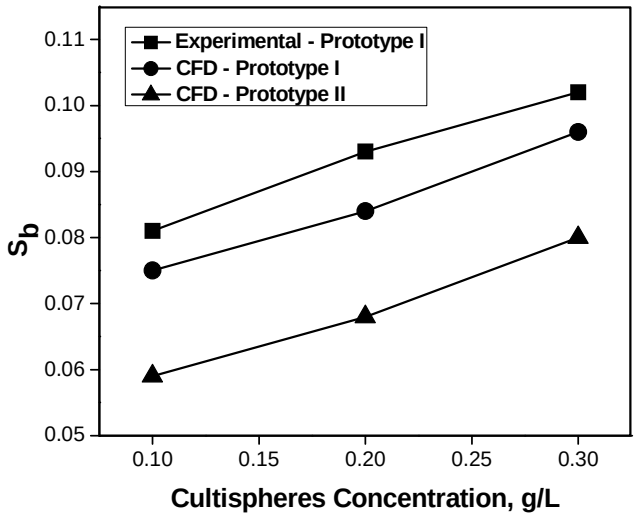

Figure 2.11: Nonspecific crossover as a function of particle concentration in the sample at a total flow rate of 400ml/min, inlet and outlet flow ratio of 0.25.

2.5 Conclusions

CFD simulations of flow pattern performed on the new design of QMS flow channel confirm circumferentially uniform flow development around the annular channel. Quantitative agreement between experimental measurements of nonspecific crossover and prediction based on CFD modeling of the fluid flow was shown. For all flow conditions, crossover predicted by CFD simulations was found to be slightly lower than experimentally observed results. This difference may be due to the contribution of crossover from other factors such as particle lift and particle interactions. Diffusion was not considered in the CFD modeling. The good agreement between experimental and CFD predicted results allowed the performance of simulations with different channel prototype models to develop a design to minimize nonspecific crossover. Though increasing the diameter of the outlet splitter decreases nonspecific crossover the diameter needs to be optimized based on the yield of magnetically labeled particles with change in splitter diameter. Therefore future CFD simulations must include the migration of the magnetic particles.

2.6 Acknowledgements

This research was funded in part by the U.S. Department of Health and Human Services under SBIR grant 5R44DK072647-03 from the National Institute and Digestive and Kidney Research (NIDDK) awarded to Techshot, Inc., Greenville, Indiana, USA.

2.7 References

Anderson JD. Computational Fluid Dynamics: The Basics with Applications. McGraw Hill, Inc., 1995. ISBN 0-07-001685-2.

Brunicardi, FC, Oh Y, Shevlin L, Suh E, Kleinman R, Stein E, Lipaz G, Plant DV, Imagawa D, Fetterman HR. 1994. Laser destruction of human nonislet pancreatic tissue. Transplant Proc 26(6):3354-3355.

Gray DWR, Gohde W, Carter N, Heiden T, Morris PJ. 1989. Separation of Pancreatic islets by Fluorescence-Activated Sorting. Diabetes 38(suppl 1):33-135.

Jindal RM, McShane P, Gray DWR, Morris PJ. 1994. Isolation and Purification of Pancreatic Islets by Fluorescence Activates Islet Sorter. Transplant Proc 26(2):653.

Jing Y, Chalmers JJ, Zborowski M. 2007. Blood progenitor cell separation from clinical leukapheresis product by magnetic nanoparticle binding and magnetophoresis. Biotechnol Bioeng 96(6):1139.

Kennedy DJ, Todd P, Logan S, Becker M, Papas KK, Moore LR. 2007. Engineering quadrupole magnetic flow sorting for the isolation of pancreatic islets. Journal of Magnetism and Magnetic Materials 311:388-395.

Lara O, Nakamura M, Zborowski M and Chalmers JJ. 2002. Negative depletion cell sorting using a quadrupole magnetic cell sorter. Eur. Cells Mater. 3:62-64.

Moore LR, Rodriguez AR, Williams PS, McCloskey K, Bolwell BJ, Nakamura M, Chalmers JJ and Zborowski M. 2001. Progenitor cell isolation with a high capacity quadrupole magnetic flow sorter. J. Magn. Magn. Mater. 225:277-284.

Nakamura M, Decker K, Chosy J, Comella K, Melnik K, Moore LR, Lasky LC, Zborowski M and Chalmers JJ. 2001. Separation of Breast Cancel Cell Line from Human Blood Using a Quadrupole Magnetic Flow Sorter. Biotechnol. Prog. 17:1145-1155.

Pinkse G, Steenvoorde E, Hogendoorn S, Noteborn M, Terpstra OT, Bruijn JA, and De Heer E. 2004. Stable transplantation results of magnetically retracted islets: a novel method. Diabetologia 47:55.

Sakuma Y, Ricordi C, Miki A, Yamamoto T, Pileggi A, Khan A, Alejandro R, Inverardi L, Ichii H. 2008. Factors That Affect Human Islet Isolation. Transplant Proc 40:343-345.

Samejima T, Yamaguchi K, Iwata H, Morkawa N, Ikada Y. 1998. Gelatin density gradient for isolation of islets of Langerhans. Cell Transplant 7(1):37- 45.

Shenkman RM, Chalmers JJ, Hering BJ, Kirchhof N and Papas KK. 2009. Quadrupole Magnetic Sorting of Porcine Islets of langerhans, Tissue Engineering: Part C 15(2):147-156.

Shenkman RM, Godoy-Silva R, Papas KK and Chalmers JJ. 2009. Effects of Energy Dissipation Rate on Islets of Langerhans: Implications for isolation and Transplantation, Biotechnology and Bioengineering 103(2):413-423.

Soon-Shiong P, Fujioka T, Terasaki P, Heintz R, Lanza RP. 1990. Islet purification by a novel immunomicrosphere cell depletion technique. Transplant Proc. 22(2):780-781.

Sun L, Zborowski M, Moore LR, Chalmers JJ. 1998. Continuous, Flow-Through Immunomagnetic Cell Separation in a Quadrupole Field. Cytometry 33:469.

Tannehill JC, Anderson DA, Pletcher RH. 2004. Computational Fluid Mechanics and Heat Transfer. Taylor and Francis, second edition, ISBN 1-56032-046-X.

Tong X, Xiong Y, Zborowski M, Farag SS and Chalmers JJ. 2007. A Novel High Throughput Immunomagnetic Cell Sorting System for Potential Clinical Scale Depletion of T Cells for Allogeneic Stem Cell Transplantation. Exp Hematol 35(10):1613.

Williams PS, Moore LR, Chalmers JJ and Zborowski M. 2003. Splitter Imperfections in Annular Split-Flow Thin Separation Channels: Effect on Nonspecific Crossover. Anal. Chem. 75:1365-1373.

Williams PS, Decker K, Nakamura M, Chalmers JJ, Moore LR and Zborowski M. 2003a. Splitter Imperfections in Annular Split-Flow Thin Separation Channels: Experimental Study of Nonspecific Crossover. Anal. Chem. 75: 6687-6695.

Williams PS, Hoyos M, Kurowski P, Salhi D, Moore LR and Zborowski M. 2008. Characterization of Nonspecific Crossover in Split-Flow Thin Channel fractionation. Anal. Chem. 80:7105-7115.

Winoto-Morbach S, Ulrichs K, Leyhausen G and Muller-Ruchholtz W. 1989. New principle for large-scale preparation of purified human pancreas islets. Diabetes. 38(Supp 1):146-149.

3. Application of Magnetic Particle Tracking Velocimetry to Quadrupole Magnetic Sorting of Porcine Pancreatic Islets

3.1 Abstract

Magnetic isolation is a promising method for separating and concentrating pancreatic islets of Langerhans for transplantation in Type 1 Diabetes patients. We are developing a continuous magnetic islet sorter to overcome the restrictions of current purification methods that result in limited yield, viability and purity of the isolated islets. In Quadrupole Magnetic Sorting (QMS) islets are magnetized by infusing superparamagnetic microbeads into islets' vasculature via arteries that serve the pancreas. The performance of the islet sorter depends on the resulting speed of the islets in an applied magnetic field, a property known as magnetophoretic mobility. Essential to the design and successful operation of the QMS is a method to measure the magnetophoretic mobilities of magnetically infused islets. We have adapted a magnetic particle tracking velocimeter (MPTV) to measure the magnetophoretic mobility of particles up to 1000µm in diameter. Velocity measurements are performed in a well-characterized uniform magnetic energy gradient using video imaging followed by analysis of the video images with a computer algorithm that produces a histogram of absolute mobilities. MPTV was validated using surrogate magnetic agarose beads and subjecting them to QMS. Mobility distributions of labeled porcine islets indicated that magnetized islets have sufficient mobility to be captured by the proposed sorting method, with this result confirmed in test isolations of magnetized islets.

Keywords: Particle tracking velocimetry**,** magnetic flow sorter, pancreatic islets isolation, magnetic particles.

3.2 Introduction

Magnetic isolation of islets is gaining in popularity due to its ease of use, speed and selectivity. Current islet isolation procedures depend on centrifugation in density gradients. They are limited in their throughput and separation efficiency, and they subject islets to potentially detrimental physical stresses (London et al., 1998; Soon-Shiong et al., 1989). To address the problems with throughput and efficiency, a continuous flow quadrupole magnetic islet separator was developed (Kennedy et al., 2007). Essential to the design and operation of such a device is a method to measure the magnetophoretic mobilities of magnetically infused islets.

The magnetophoretic mobility of a particle indicates how responsive the particle is to an applied magnetic field. Paramagnetic particles have positive susceptibility and move toward increasing magnetic field intensity. Islets are rendered paramagnetic by infusing the donor pancreas with paramagnetic microspheres such as Dynabeads®. Beads capture efficiency varies with the age of the donor and pancreas weight and affects the magnetophoretic mobility of the islets.

Several different techniques have been used to measure the magnetophoretic mobility of paramagnetic particles, including the use of visual microscopic observation of the movement of the labeled particle with stopwatch and magneto-cytometry (Gill et al., 1960; Davis et al., 1993). Magnetic Particle Tracking Velocimetry (MPTV) measures cell surface antigen counts through the quantification of antibody binding capacities (ABC) (McCloskey et al., 2001; Melnik et al., 2001; McCloskey et al., 2000; McCloskey et al., 2001a) and can be used to characterizes magnetophoretic mobilities of nano and micro-particles (Haefeli et al., 2002; Zhang et al., 2002; Chalmers et al., 1999) and living cells (Chalmers et al., 1999). Two important features of the

MPTV apparatus set it apart from other magnetic tracking technologies: 1) the use of an isodynamic (i.e. constant-force) magnetic field as indicated by "S_m = constant", and 2) capacity to track a large number of individual particles, up to 10,000, in a fraction of an hour. Both features are essential for high accuracy and precision of the MPTV analysis (Sridhra Redy et al., 1996; Moore et al., 2004; Zborowski et al., 2003). Those features are at the basis of the competitive advantage of the MPTV over other magnetic motion analyzers described in the literature that are based on single-particle analysis in high-gradient magnetic fields which are difficult to measure(Watarai et al., 2001; Wanabe et al., 2004; Suwa et al., 2004).

MPTV leverages current technologies in video microscopy, computer processing speed and finite element analysis for magnetic fields to measure the induced motion of cells and particles in the highly characterized magnetic and gravity field. The motion of the particles in the known field is then translated into a characteristic parameter called magnetophoretic mobility in a magnetic field and sedimentation rate in a gravity field. MPTV measurements involve videotaping the movement of immunomagnetically labeled particles through a known viscosity medium and magnetic susceptibility in a well-defined magnetic energy density gradient. The velocity of each particle along with its location within the magnetic energy gradient is recorded. From this information, the magnetophoretic mobility of each particle is calculated. A significant advantage of this method over other techniques is that large numbers of cells or particles can be processed in a very short time.

Present MPTV devices developed to measure magnetophoretic mobility of cells have problems with flow cells and data analysis software. They also have fixed amount of magnetic field strength and are only able to measure mobilities of single cells. The MPTV described here in measures magnetophoretic mobilities and sedimentation rates of cells and large particles like

islets with reliable software and variable magnetic field strength. The software developed for MPTV also gives the optimum parameters to use with QMS to achieve isolation with maximum purity and yields. This paper explains the features of a refined MPTV system with results obtained with large particles including porcine pancreatic islets of Langerhans.

3.3 Theory

The following analysis applies to the use of MPTV applied to the isolation of magnetically labeled pancreatic islets of Langerhans by quadrupole magnetic sorting**.** The magnetophoretic mobility (μ_m) of a particle is defined as the ratio of the velocity of the particle in the magnetic field, u_f, to the magnetic field energy gradient, S_m.

$$\mu_m = \frac{u_f}{S_m} \qquad (1)$$

Any population of magnetically labeled particles exhibits a statistical distribution of μ_m based on several characteristics. Mobility of the pancreatic islets depends on the number of magnetic Dynabeads® infused into each islet. The following equation relates the Dynabeads and islet properties to the magnetophoretic mobility of an immunomagnetically labeled islet.

$$\mu_m = \frac{n_D \Delta\chi V_i}{3\pi\eta D_i} \qquad (2)$$

Where n_D is the number of Dynabeads, $\Delta\chi$ is the difference in magnetic susceptibility between the medium and the beads, V_i is the volume of a bead, η is the viscosity of the medium, D_i is the diameter of the islet.

The magnetophoretic mobility distribution measured using MPTV is used to predict the QMS output fractions based on the defined flow rate parameters. QMS is a split flow type continuous magnetic sorter developed to separate single cells by labeling specific cells with magnetic beads. QMS was improved to isolate Dynabeads infused islets from exocrine tissue

based on their magnetophoretic mobility (μ_m) (Kennedy et al., 2007). Figure 3.1 describes the basic QMS mechanism for isolation of magnetic cells from nonmagnetic cell populations. QMS can be operated continuously with labeled islets with unlabeled tissue entering at inlet a' (sample) and carrier buffer at inlet b' (buffer) and isolated islets exiting the system at outlet b (positive), unlabeled tissue at outlet a (negative), some of the tissue which are labeled high enough to reach the wall of the flow channel will stick to the wall and can be collected at end of the isolation process and is considered as Wall (W) fraction. The boundary between inlet flows is called as Inner Splitting Surface (ISS) and the boundary between outlet flows is called as Outer Splitting Surface (OSS). Distance between ISS and OSS is called the Transport Lamina. The first critical mobility whereby a particle entering the flow channel at the ISS just reaches the OSS and is eluted into the b (positive) fraction is identified as μ_{m0} and is defined by

$$\mu_{m0} = \frac{Q}{2\pi r_0 L S_{m0}} \frac{I_1(\ell_{ISS}, \ell_{OSS})}{A_1(1-\ell_i^2)} + \frac{r_0 v_s \ln(\ell_{OSS}/\ell_{ISS})}{L S_{m0}} \tag{3}$$

Where ℓ_i is the radial position given by $\ell_i = r/r_i$ and $\ell_o, \ell_{ISS}, \ell_{OSS}$ correspond to wall, ISS and OSS. L is distance between two splitters. A_1, A_2 and $I_1(\ell, \ell_1)$ are functions used to simplify the calculations and are given by

$$A_1 = (1 + \ell_i^2 - A_2) \tag{4}$$

$$A_2 = \frac{1-\ell_i^2}{\ln\frac{1}{\ell_i}} \tag{5}$$

$$I_1(\ell, \ell_1) = [4\ln\ell - 2\ell^2 + 2A_2(\ln\ell)^2]_{\ell_1}^{\ell} \tag{6}$$

The radial position of the ISS, ℓ_{ISS} is calculated using the following integration factor (Kennedy et al., 2007):

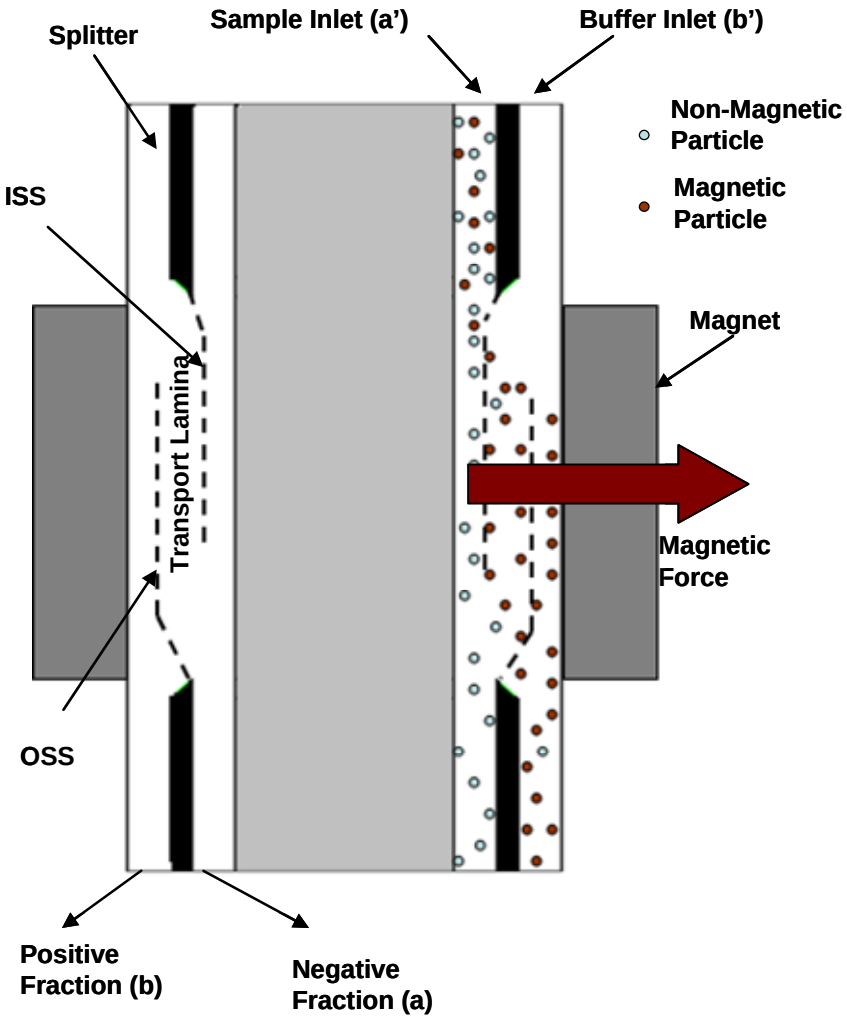

Figure 3.1: Schematic diagram of the Quadrupole Magnetic cell Sorter (QMS)

$$I_2(\ell_i, \ell_{ISS}) = [2\ell^2 - \ell^4 + 2A_2\ell^2 \ln \ell - A_2\ell^2]_{\ell_i}^{\ell_{ISS}} \quad (7)$$

Similarly, the position of the OSS can be calculated using eq. (7) by replacing ℓ_{ISS} with ℓ_{OSS}.

The second critical mobility whereby a particle entering at the wall of the core reaches the OSS and exit with the b fraction is identified as $\mu_{m1}$and is defined by

$$\mu_{m1} = \frac{Q}{2\pi r_0 L S_{m0}} \frac{I_1(\ell_i, \ell_{OSS})}{A_1(1-\ell_i^2)} + \frac{r_0 v_s \ln(\ell_{OSS}/\ell_i)}{LS_{m0}} \quad (8)$$

The third critical mobility whereby a particle entering at the ISS reaches the wall of the shell and may be trapped in the flow channel is identified as μ_{m2} and is defined by

$$\mu_{m2} = \frac{Q}{2\pi r_0 L S_{m0}} \frac{I_1(\ell_{ISS}, \ell_o)}{A_1(1-\ell_i^2)} + \frac{r_0 v_s \ln(\ell_o/\ell_{ISS})}{LS_{m0}} \quad (9)$$

The final critical mobility whereby a particle entering at the core wall reaches the wall of the shell and remains on the wall is identified as μ_{m3} and is defined by

$$\mu_{m3} = \frac{Q}{2\pi r_0 L S_{m0} A_2} + \frac{r_0 v_s \ln(\ell_i/\ell_o)}{LS_{m0}} \quad (10)$$

All the particles with $m<m_0$ exit in a fraction, $\mu_{m0} \leq \mu_m \geq \mu_{m1}$ will exit either in a or b fraction, $\mu_{m1} \leq \mu_m \geq \mu_{m2}$ will exit in b fraction, $\mu_{m2} \leq \mu_m \geq \mu_{m3}$ will exit in b fraction or become trapped on the flow channel wall and $\mu_m \geq \mu_{m3}$ with be trapped on the flow channel wall.

3.4 Materials and Methods

3.4.1 Particles and Viscous Liquid

Three types of magnetic particles with similar size ranges and different magnetization were used for this study. Agarose magnetic beads (Bioscience Beads, RI) with diameters 250-350 µm and magnetite loading of 0.5%, 1% and 6% by volume were used for testing. As the particles used for testing settled very rapidly in the aqueous solution, high-viscosity liquid was

prepared by dissolving Ficoll® (400,000 MW) (Sigma-Aldrich) to maintain the particles in suspension while measuring their mobilities.

3.4.2 QMS System

QMS is a split flow type continuous magnetic sorter developed to separate single cells by labeling specific cells with magnetic beads. QMS was improved to isolate Dynabeads infused islets from exocrine tissue based on their magnetophoretic mobility (μ_m) (Kennedy et al., 2007). Figure 3.1 describes the basic QMS mechanism for isolation of magnetic cells from nonmagnetic cell populations. QMS can be operated continuously with labeled islets with unlabeled tissue entering at inlet a' and carrier buffer at inlet b' and isolated islets exiting the system at outlet b and unlabeled tissue at outlet a.

3.4.3 Magnetic Particle Tracking Velocimetry

The MPTV technology is comprised mainly of four components (Figure 3.2): a sample channel containing the suspension of cells and particles, a magnet capable of providing a constant magnetic force in the sample channel zone, a pump for introducing fluid and sample, a video microscope capable of imaging the sample with various degrees of magnification, and a computer capable of capturing and processing the video images for particle mobility analysis.

3.4.4 Magnet Assembly

The custom designed magnet assembly is comprised of a base plate, two neodymium-iron-boron (NeFeB) magnets and two 1018 carbon steel pole pieces. The pole pieces are shaped to match a very specific modified hyperbolic profile. The magnetic force is perpendicular to the direction of gravitational force so magnetophoretic mobility measurements are independent of sedimentation velocity, which can be used independently to estimate particle dimensions.

3.4.5 Fluid System

The stopped flow channel consists of a borosilicate glass channel with square (2 mm) cross-section. One end of the 6 cm long flow channel is connected by a pair of solenoid pinch valves to a disposable 50 ml syringe for sample injection and a 50ml syringe for priming buffer while the outlet end connects into a waste vessel. The observation channel is positioned within the magnet assembly and is sandwiched between the video lens and the backlight. Vacuum pump and pinch valves were used to control the sample flow into and out of the channel.

3.4.6 Imaging System

The selection of the video microscope system components and their operational settings is critical, as the pixel size, field of view, magnification, and frame capture speed dictate the maximum and minimum velocities and particle sizes that can be accurately analyzed. Particle movement in the flow channel was recorded with a grasshopper 2.0MP B&W, 1394b, and 1/1.8 inch CCD camera (Point Gray, AZ) operating at 30 frames per second with 1x objective (Edmund Optics, NJ) mounted on a ½ inch Manual translation stage (Thor Labs, NJ). Light was supplied by dark field illumination using a white light source (Edmond Optics, NJ).

3.4.7 Analysis of Video Data

Image processing software converts the video data into useful velocity data and corresponding property data such as hydrodynamic radius and magnetophoretic mobility. A program named “Cytotest” first thresholds the images into binary black or white images based on a user-defined gray-level threshold. This eliminates pixels that are below certain brightness, leaving the light-reflecting particles visible in the image records. It then identifies particles or cells in each frame of the video file using a program named “OpenCV” in which cells & particles outside a specific size range are rejected. It then searches successive frames in the video record

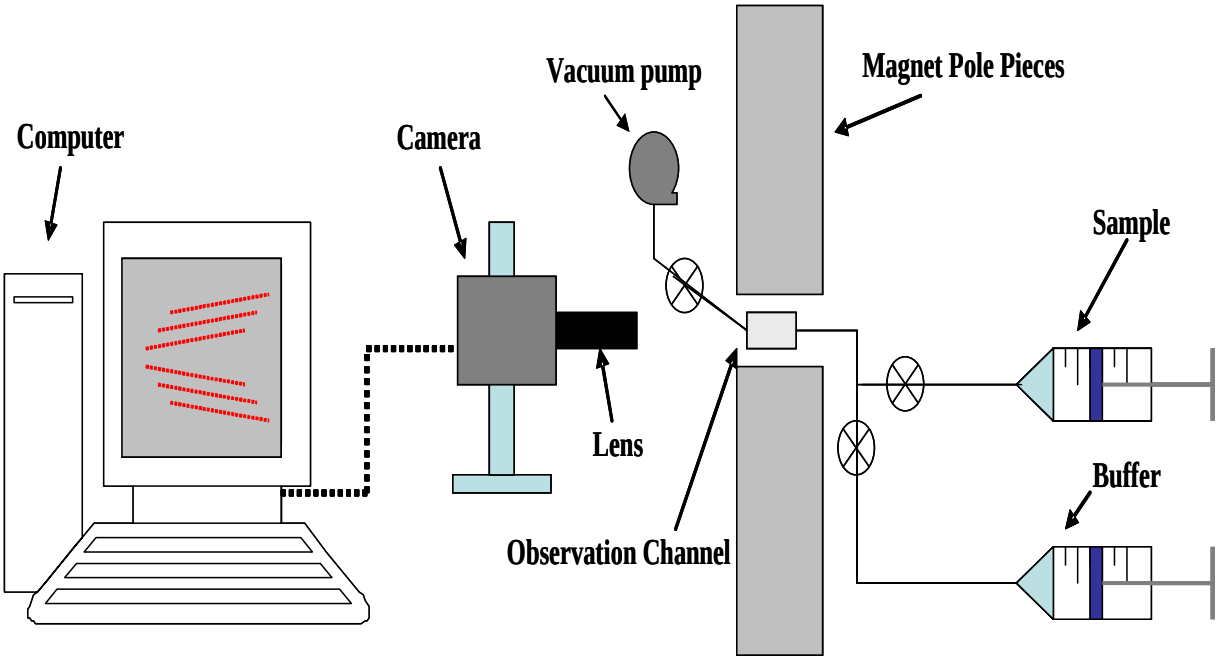

Figure 3.2: A simplified diagrammatic representation of an MPTV system

to identify particle movement by connecting the tracks of each identified particle to its match in a successive frame. Proprietary predictive and adaptive algorithms are employed to improve the accuracy of particle matching across frames and eliminate bad tracks. The track lengths are then converted to a rate of travel in pixels per millisecond, and that rate is converted to a magnetophoretic mobility measurement based on the magnet strength and image pixel size. That value is recorded in a histogram with other tracks delimited by logarithmic bin sizes and plotted in the software.

3.4.8 Experimental

The camera lens was adjusted to visualize the central region of the sample cell at constant magnetic energy gradient using the MPTV translation stage. Particle suspensions were injected into the sample cell using a syringe after priming the cell with buffer using a vacuum pump. Fixed volumes of the particle suspension typically 1ml to 5ml were injected into the field of view to observe the magnetic deflection of the particles. Particle samples were pumped in a direction opposite to the direction in which the magnetic energy gradient operates on the particles then stopped. Particle deflection was observed with no fluid velocity so that particle motion was only due to magnetic and gravitational force. Successive volumes of the suspensions were injected to obtain several series of deflection images at a rate of 30 frames per second. After analyzing the samples in MPTV, the optimized parameters given by software were used to run QMS with magnetic particles. Outlets from QMS were counted for particle concentrations by microscope and compared with MPTV predictions.

3.5 Results and Discussion

Several improvements were made on cell tracking velocimetry to facilitate measurement of the magnetophoretic mobility of much larger particles such as pancreatic islets and to obtain essential data to set the parameters of the QMS to isolate the magnetic fraction (islets) from non-magnetic fraction in QMS. A newly built MPTV was tested with Dynabeads® to evaluate performance. Figure 3.3 shows a histogram of the magnetophoretic mobility of Dynabeads® developed by MPTV. The magnetophoretic mobility was obtained by dividing the MPTV determined particle velocity by the magnitude of the magnetic energy gradient, S_m, 6.275 TA/mm^2. Particles with mobility less than 10^{-16} m^3/TAs are considered as underflows. Figure 3.5 is the tracks developed by MPTV for one set of Dynabeads moving magnetically in the sample cell. Dark spots in the Figure 3.5 are the disturbances on the sample cell wall, for example, were neglected when tracking by thresholding the images. Any of these disturbances measured as tracks were characterized as "underflows" (particles with zero mobility). These are seen in Figure 3.3 as a vertical line at 10^{-16} on mobility axis.

The important development made to the MPTV is the ability to predict the QMS flow parameters required to get the desired isolation based on the mobilities measured using MPTV. Figure 3.4 shows the histograms developed by MPTV for the three outlet fractions from QMS for Dynabeads based on the mobility predictions for the total flow rate in the QMS of 400 ml/min, inlet flow ratio of 0.2 and outlet flow ratio of 0.4. Underflows are neglected while predicting the flow parameters.

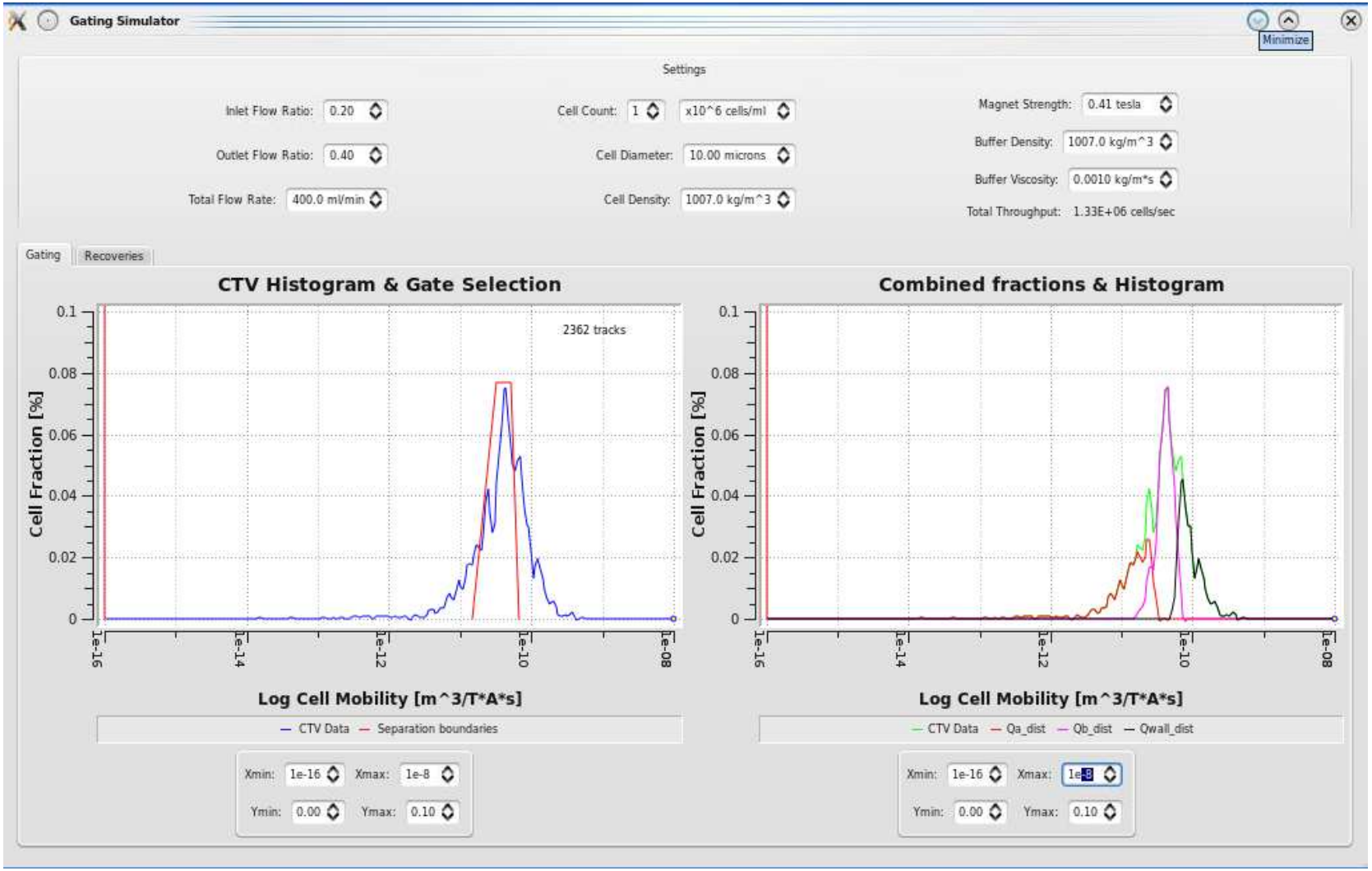

Figure 3.3: Mobility histogram given by MPTV for Dynabeads

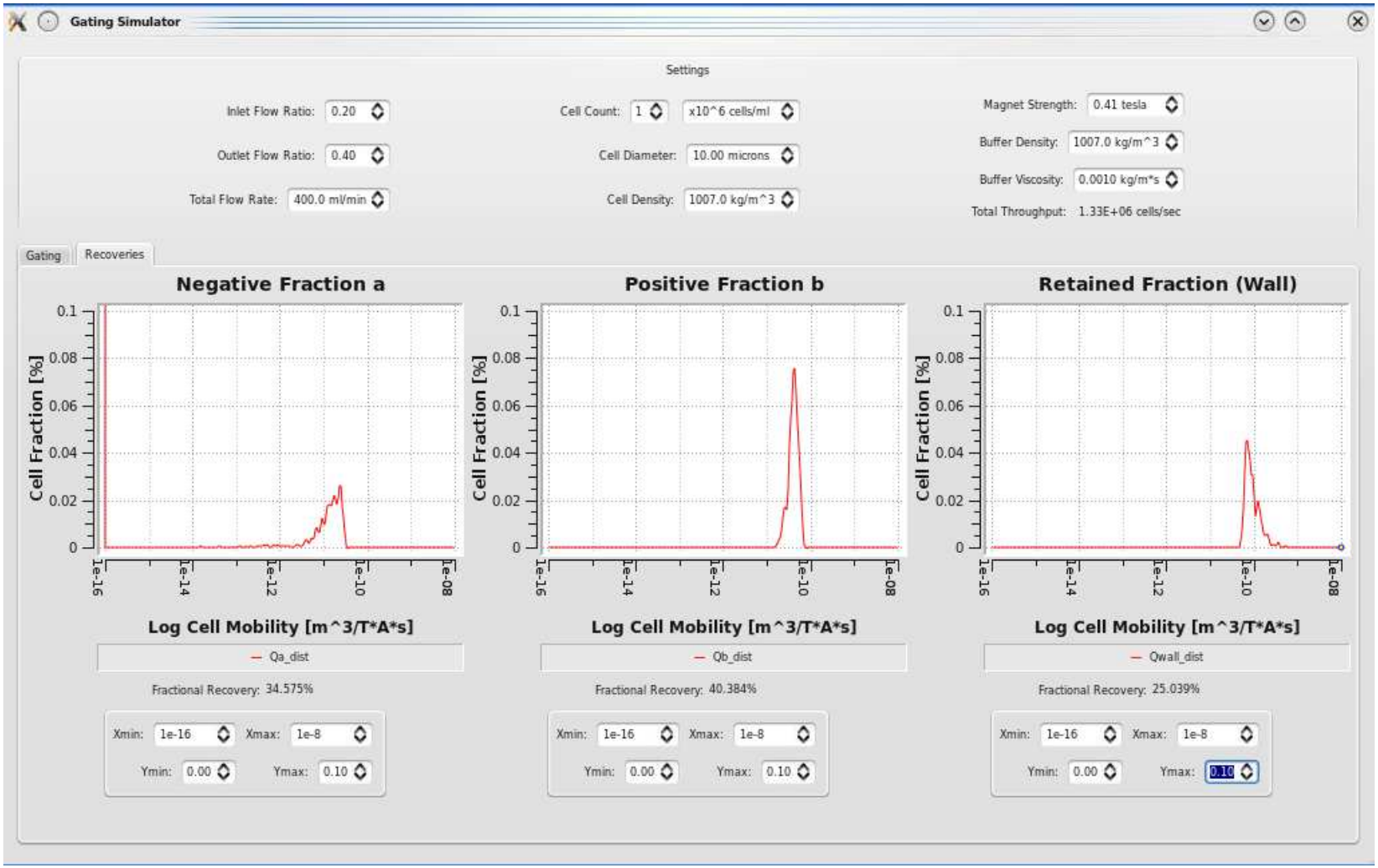

Figure 3.4: Histograms of Dynabeads in each fraction of the QMS output.

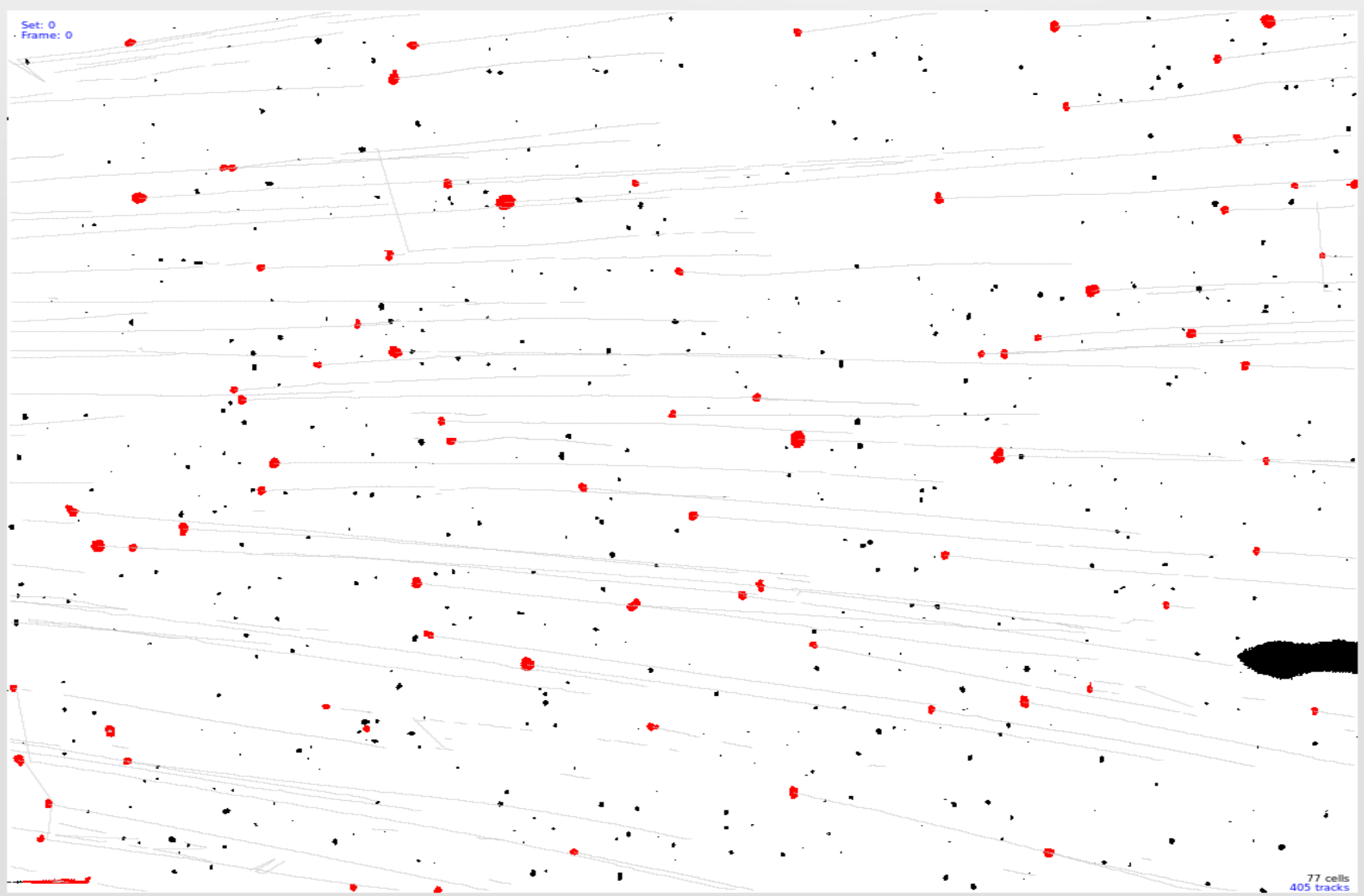

Figure 3.5: Particle tracks developed by MPTV. Red dots are the particles tracked and black spots are disturbance.

The expression of particle magnetization from their motion in a magnetic field is a compound quantity depending on particle size, magnetic velocity and field gradient. Field gradient in the measurement region is assumed to be constant. Size of the three different magnetic particles used in this study is maintained similar in size. So the variation in magnetic mobility is due to the magnetite loading in the particles. Variation in the magnetite concentration changes the velocity of the particle in the magnetic filed, which is measured by the MPTV. Three different magnetic particles with magnetite loading 0.5%, 1% and 6% were used for MPTV studies.

Figure 3.6 shows the histogram of the magnetic micro beads BSI. The x-axis represents the magnetophoretic mobility values of the magnetic bead on a log scale and y-axis represents the fraction of the beads with specific magnetophoretic mobility. Mobilities were measured in a high viscous Ficoll® medium to avoid settling of the micro beads while measuring the velocity due to magnetic field. Histograms are plotted with mobilities calculated for water based on the viscosities. Mobilities are measured for the beads with minimum size of 250 µm and maximum size of 350 µm by omitting the other smaller and bigger beads. Total 126 beads are tracked with 2030 tracks. Beads with mobility less than 10^{-16} are grouped as under flows.

Figure 3.7 and 3.8 shows the mobility histograms for magnetic micro beads BSII and BSIII. Results generated with 147 beads with 2672 tracks for BSII and 186 beads with 3276 tracks for BSIII were plotted. MPTV can analyze large number of particles in small amount of time on a particle-by-particle basis. As the iron oxide concentration varies in beads BSI, BSII and BSIII, which changes the density of the beads, measurements were done with Ficoll® solution with appropriate density to avoid the settling of the particles in the sample cell. The required density of the medium was 1.36 g/cm^3 corresponding to Ficoll® 400 having viscosity of

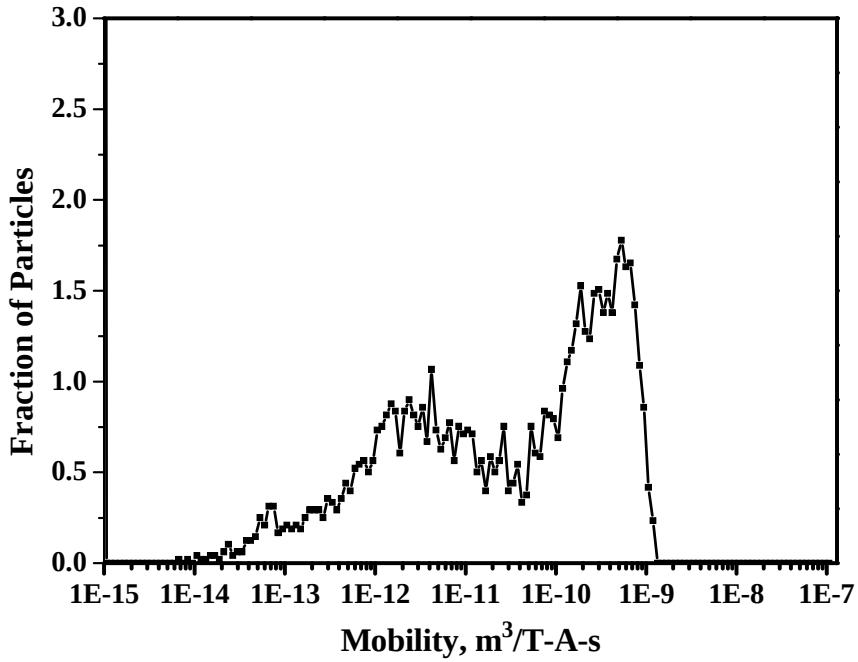

Figure 3.6: Magnetophoretic mobility histogram of BSI magnetic particles.

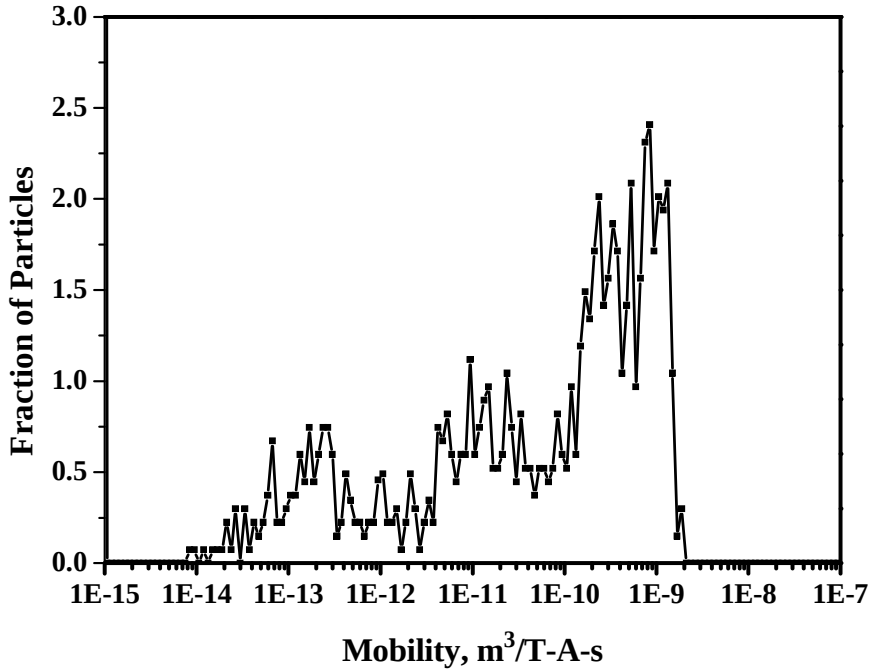

Figure 3.7: Magnetophoretic mobility histogram of BSII magnetic particles.

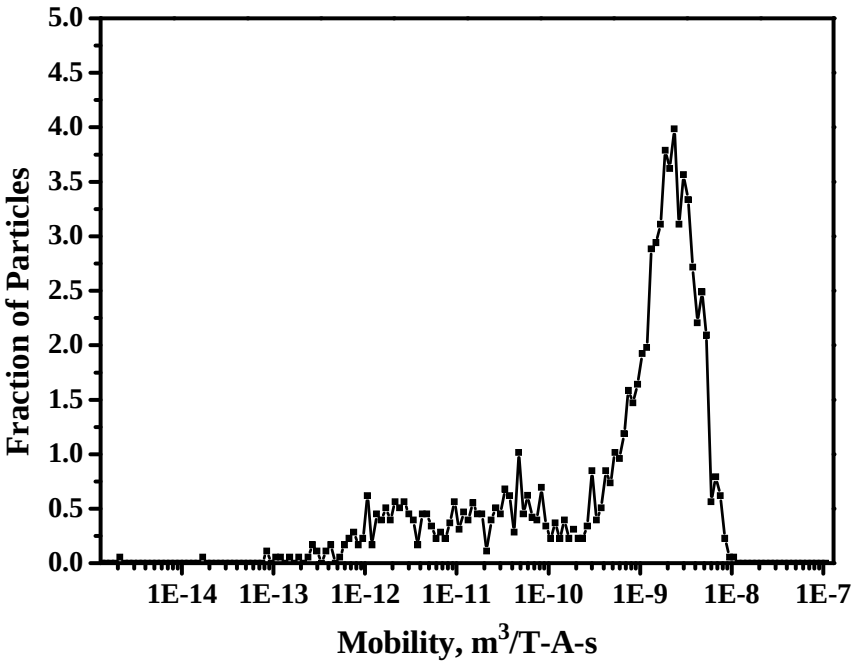

Figure 3.8: Magnetophoretic mobility histogram of BSIII magnetic particles.

10.8 Pa s. Particle velocities were corrected for viscosity when calculating magnetophoretic mobilities. Mobility histograms show the increase in the average and maximum mobility of the beads with the increase in the magnetite concentration from beads BSI to beads BSIII and these histograms indicate that significant differences in magnetophoretic mobility can be detected between magnetic beads.

Magnetophoretic mobility measurements and flow rate parameters prediction made by MPTV software were tested by conducting the experiments in QMS using the pure magnetic beads. Figure 3.8 shows the comparison of the predictions and experimental results for the three outlet fractions from QMS for magnetic particles BSI. The QMS isolation process was controlled by three flow parameters: total flow rate (Q), inlet flow ratio ($R_i=Q_{a'}/Q$), Outlet flow ratio ($R_o=Q_a/Q$). These flow rates were fixed based on the measured magnetophoretic mobility of the magnetic beads. The critical mobilities μ_{m0} and μ_{m2} were selected to maximize the amount of beads in the b fraction. The flow rates predicted were Q = 400 ml/min, R_i = 0.25 and R_o = 0.4 corresponding to critical mobilities for beads BSI of μ_{m0} = $14.79X10^{-12}$ m^3/TAs and μ_{m2} = $1.355X10^{-11}$ m^3/TAs.

Figure 3.9 is the recovery of the particles in all fractions. Total recovery of the magnetic particles during the experimental isolation with QMS was 98%. The loss of some magnetic particles was due to the settling of the particles in the inlet tubes and at the bottom of the flow channel. MPTV predicted ‘a’ fraction recovery was high compared to the experimental isolation as the MPTV predicted ‘a’ fraction also contains some disturbance tracks. Predicted and experimental ‘b’ fraction recovery is very low because the magnet strength of the QMS is high enough to capture most of the magnetic particles on to the wall of the flow channel. The difference in the wall fraction recoveries is due to the difference in the ‘a’ fractions which

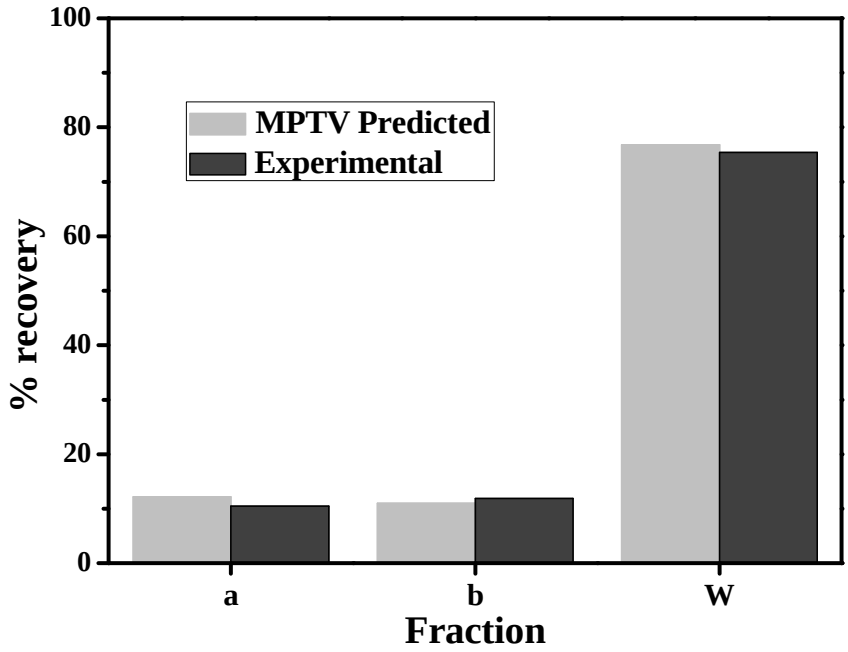

Figure 3.9: Comparison of MPTV predicted fractional recovery of BSI particles in the three outlet fractions of the QMS with experimental results.

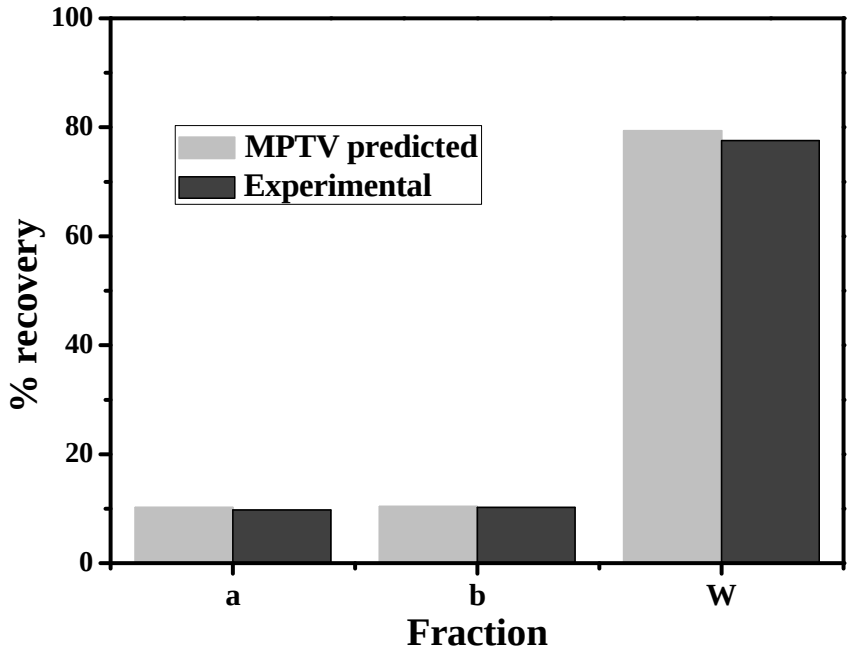

Figure 3.10: Comparison of MPTV predicted fractional recovery of BSII particles in the three outlet fractions of the QMS with experimental results.

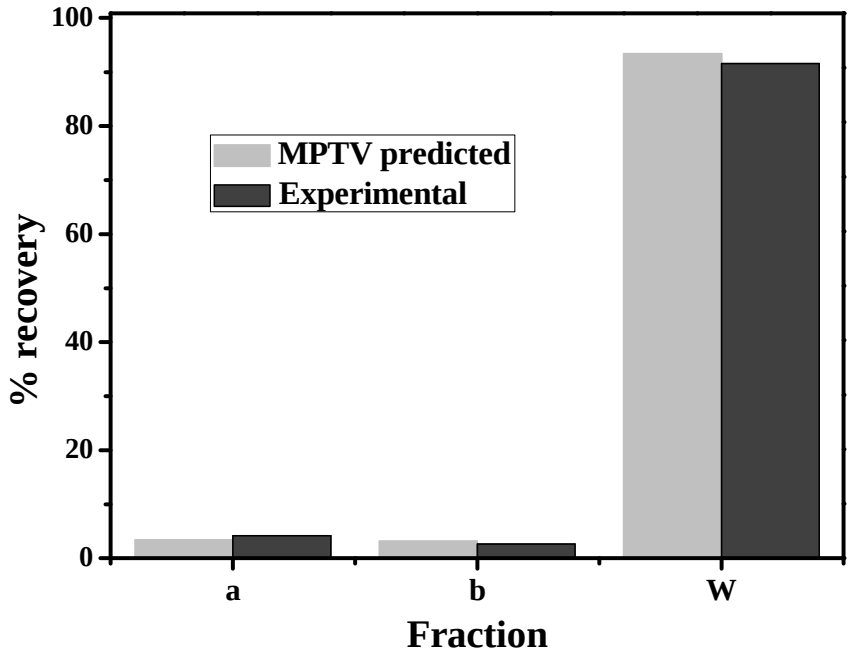

Figure 3.11: Comparison of MPTV predicted fractional recovery of BSI particles in the three outlet fractions of the QMS with experimental results.

affected the total recovery. Figures 3.10 and 3.11 show the experimental outlet fractions compared with MPTV predictions and recoveries for beads BSII and BSIII.

Figure 3.12a shows the histogram of magnetophoretic mobilities of the porcine islets isolated from acinar tissue with QMS (Chapter 4). These are the islets from the b fraction of the QMS operated at a total flow rate of 400 ml/min and inlet ratio of 0.4 and outlet ratio of 0.6. Islets were infused with Dynabeads. After MPTV developed the mobility histogram, QMS flow parameters for the islets isolation were set to Q= 400 ml/min, Qa'/Q = 0.4 and Qa/Q = 0.6 and fractional recovery histograms were generated. Figure 3.12b, 3.12c and 3.12d shows the MPTV predicted fractional recovery of each outlet of QMS. These histograms show that more than 90% of the islets used to measure the mobility exit in the b fraction. Islets that are in the 'a' fraction histogram show the nonspecific crossover in the islet isolation experiments. This also confirmed the efficiency of the MPTV to predict the QMS parameters based on the measured mobilities.

3.6 Conclusions

The purpose of this study was to develop a MPTV to measure the mobility of magnetic particles up to 1000 microns in size and to predict optimized flow parameters based on the magnetophoretic mobilities to isolate magnetic particles from nonmagnetic particles using QMS. The capability of newly developed MPTV in measuring magnetophoretic mobility was confirmed with the measurements of the mobilities of the standard Dynabeads®. MPTV was successfully used to measure the mobility of magnetic particles up to 500 microns in size with different mobilities. MPTV's ability to predict the optimized flow parameters was also tested successfully with magnetic particles and the isolated islets of Langerhans as it is the final application of the MPTV. MPTV can be used online to analyze the mobilities of the

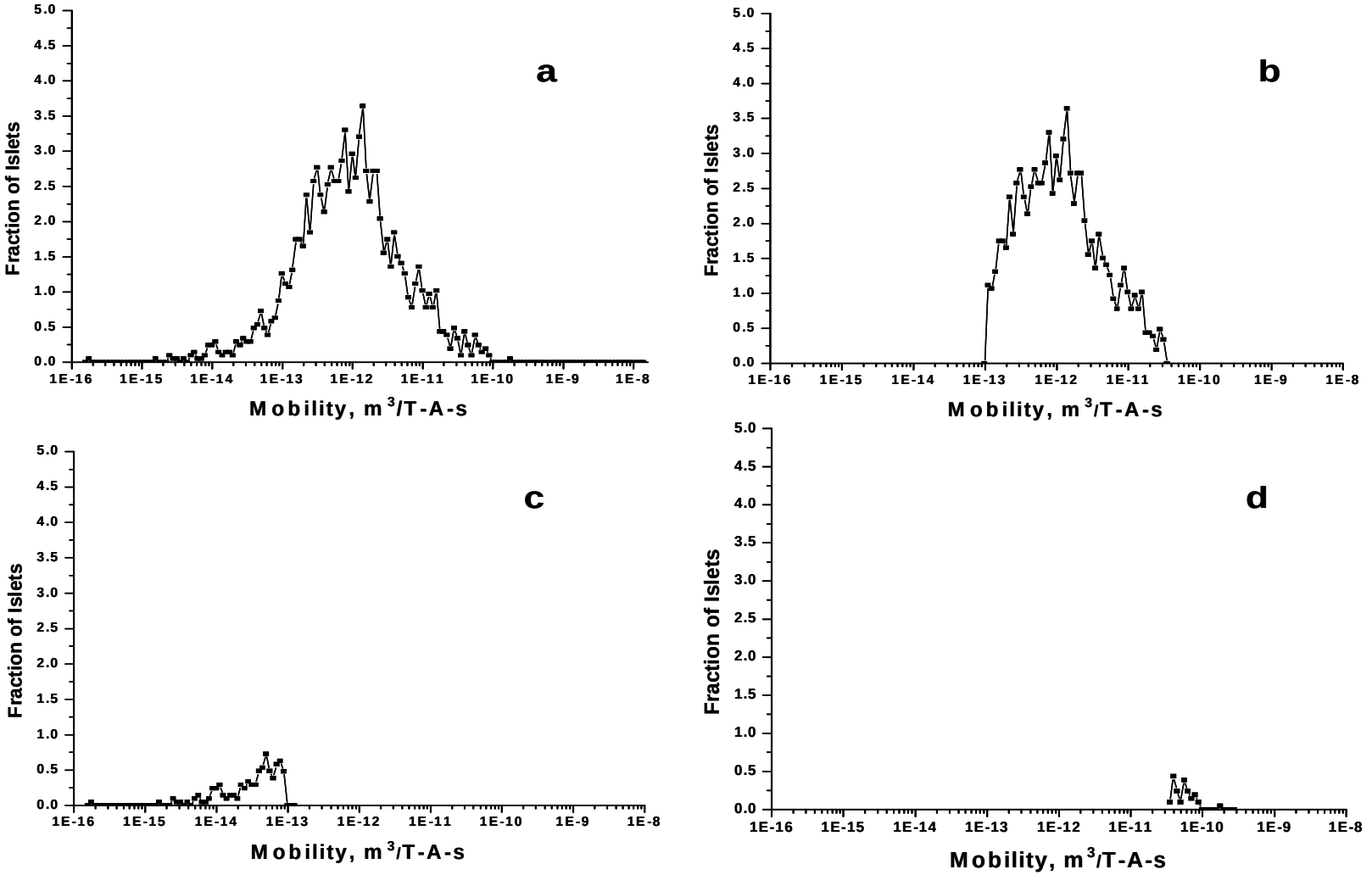

Figure 3.12: a) Magnetophoretic mobility histogram of pancreatic islets isolated with QMS. b) MPTV predicted b fraction c) a fraction d) wall fraction of the islets at a total flow rate of 400ml/min and $R_i = 0.25$ and $R_o = 0.6$.

magnetically infused islets and to predict the flow parameters before sending tissue through magnetic field to isolate using QMS.

3.7 References

Chalmers JJ, Zhao Y, Nakamura M, Melnik K, Lasky L, Moore L, Zborowski M. 1999. An Instrument to Determine the Magnetophoretic Mobility of Labeled, Biological Cells and Paramagnetic Particles. Journal of Magnetism and Magnetic Materials 194:231-241.

Chalmers JJ, Haam S, Zhao Y, McCloskey K, Moore L, Zborowski M, Williams PS. 1999. Quantification of Cellular Properties from External Fields and Resulting Induced Velocity: Cellular Hydrodynamic Diameter. Biotechnology and Bioengineering 64:509-518.

Davis RS. 1993. New method to measure magnetic susceptibility, Measurement Science and Technology 4(2):141-147.

Gill SJ, Malone CJ, Downing M. 1960. Magnetic susceptibility of single small particles. The review of scientific instruments 31(12):1299-1303.

Häfeli UO, Ciocan R, Dailey JP. 2002. Characterization of Magnetic Particles and Microspheres and Their Magnetophoretic Mobility Using a Digital Microscopy Method. European Cells and Materials 3(2):24-27.

Kennedy DJ, Todd P, Logan S, Becker M, Papas KK, Moore LR. 2007. Engineering quadrupole magnetic flow sorting for the isolation of pancreatic islets. Journal of Magnetism and Magnetic Materials 311:388-395.

London NJM, Swift SM, Clayton HA. 1998. Isolation, culture and functional evaluation of islets of Langerhans. Diabetes & Metabolism 23:200-207.

McCloskey KE, Zborowski M, Chalmers JJ. 2001. Measurement of CD2 Expression Levels of IFN-α-Treated Fibrosarcomas Using Cell Tracking Velocimetry. Cytometry 44:137-147.

McCloskey KE, Chalmers JJ, Zborowski M. 2000. Magnetophoretic Mobilities Correlate to Antibody Binding Capacity. Cytometry 40:307-315.

McCloskey KE, Comella K, Chalmers JJ, Margel S, Zborowski M. 2001a. Mobility Measurements of Immunomagnetically Labeled Cells Allow Quantitation of Secondary Antibody Binding Amplification. Biotechnology and Bioengineering 75(6):642-655.

Melnik K, Nakamura M, Comella K, Lasky LC, Zborowski M, Chalmers JJ. 2001. Evaluation of Eluents from Separations of CD34+ Cells from Human Cord Blood Using a Commercial, Immunomagnetic Cell Separation System. Biotechnology 17:907-916.

Moore LR, Milliron S, Williams PS, Chalmers JJ, Margel S, Zborowski M. 2004. Control of Magnetophoretic Mobility by Susceptibility-Modified Solutions as Evaluated by Cell Tracking Velocimetry and Continuous Magnetic Sorting. Analytical Chemistry 76:3899-3907.

Nakamura M, Zborowski M, Lasky LC, Margel S, Chalmers JJ. 2001. Theoretical and Experimental Analysis of the Accuracy and Reproducibility of Cell Tracking Velocimetry. Experiments in Fluids 30:371-380.

Soon-Shiong P, Heintz R, Terasaki P. 1989. Identification of novel blood group reactive monoclonal antibodies cytotoxic to human acinar cells but not islets. Transplantation Proceedings 21(1):2622-2623.

Sridhar Reddy, Lee R Moore, Liping Sun, Maciej Zborowski, J J Chalmers. 1996. Determionation of the magnetic susceptibility of labeled particles by video imaging, Chemical Engineering Science, 51(6):947-956.

Suwa M, Watarai H. 2004. Magnetophoretic Detection of Photo-Induced Spin Transition. Chemistry Community 1656-1657.

Watanabe K, Suwa M, Watarai H. 2004. New Principles of Magnetophoretic Velocity Mass Analysis. Analytical Sciences 20:1483-1485.

Watarai H, Namba M. 2001. Magnetophoretic Behavior of Single Polystyrene Particles in Aqueous Manganese (II) Chloride. Analytical Sciences 17:1233-1236.

Zborowski M, Ostera GR, Moore LR, Milliron S, Chalmers JJ, Schechter AN. 2003. Red Blood Cell Magnetophoresis. Biophysics Journal 84:2638-2645.

Zhang H, Nakamura M, Comella K, Moore L, Zborowski M, Chalmers J. 2002. Characterization/Quantification of the Factors Involved in the Imparting a Magnetophoretic Mobility on Cells and Particles. European Cells and Materials 3(2): 34-36.

4. QMS Isolation of Porcine Islets of Langerhans

4.1 Abstract

Pancreatic islet transplantation offers a viable option to achieve permanent metabolic control in Type 1 diabetes patients. However, large quantities of pure viable donor islet cells are necessary for transplantation. Using currently available islet isolation methods multiple donor organs are required to achieve successful transplantation, and there is a demand for an isolation method with high islet yield and viability. Additionally, with porcine xeno-islet cell transplantation providing much hope, improving the porcine islet isolation process has become a worthwhile endeavor. To achieve isolation with high purity and yield Quadrupole Magnetic Sorting (QMS), a single cell separation method, is being modified for the isolation of pancreatic islets. Islets are infused with magnetic4.6µm Dynabeads® and separated continuously with QMS. Results from 10 porcine pancreas isolations indicated the possibility of infusing islets with magnetic beads and isolating them continuously, thereby reducing the exposure time of islets to digestive enzymes. QMS isolated islets showed good morphology compared to those isolated by the standard COBE centrifugation method. Oxygen consumption rate (OCR) per DNA measurements confirmed the viability of the islets after isolation. The QMS isolation method can save post-isolation culture time and helps to eliminate the mechanical stress due to centrifugation of the islets. Restoration of euglycemia in diabetic nude mice transplantation experiments results confirmed Dynabeads do not affect the functionality of the islets.

Keywords: magnetic flow sorter, pancreatic islets, magnetic particles, diabetes, islets isolation

4.2 Introduction

Whole pancreas transplants or transplants of isolated pancreatic islets can achieve insulin independence in type 1 diabetes (Shapiro et al., 2000; Hering et al., 2005; Frank et al., 2004; Froud et al., 2005). Whole Pancreas transplant includes complex surgery and involves significant morbidity and mortality. Even 20 years after the first successful clinical islet transplantation the goal of donor-to-recipient ratio of 1:1 is still elusive. While significant progress has been made towards achieving this objective, most transplants require two, three, and in some cases even up to four infusions of pancreatic islets from separate donors before insulin independence is realized.

Islets constitute only 1-2% of the pancreas volume, and their isolation and purification are stressful mechanical and enzymatic procedures that can inflict significant damage, which may be further amplified by prolonged times of warm and cold ischemia (London et al., 1994). Current clinical human islet purification protocols rely on a density gradient centrifugation method which depends on the small density differences between islets and exocrine tissue. As the density of the exocrine tissue depends on the age of the donor and progress of enzymatic digestion, over which there is no direct control, purity of islets attainable low and inconsistent. It is generally accepted that there are substantial losses in islet yield and potency during digestion and purification (Hering et al., 2002). During the process of enzymatic digestion and subsequent purification, liberated islets encounter immense stresses caused by, among other factors, hypoxia, sudden and repeated changes in temperature, shear forces, disruption of cell matrix interactions, removal of critical growth factors, high concentrations of reactive oxygen intermediates, proinflammatory cytokines and exposure to hyperosmolar density gradients. Density gradient method also has undesirable effects on islets like exposure to high mechanical stress, toxic chemicals and prolonged exposure to proteolytic enzymes (Samejima et al., 1998;

Pinkse et al., 2004). Additionally, with porcine xeno-islet transplantation providing much hope (Hering et al., 2006), improving the porcine islet isolation process has become a worthwhile endeavor.

Magnetic micro-particles coated with antibodies were used to successfully isolate islets from rat pancreas by targeting exocrine tissue (Davies et al., 1995; Winto-Morbach et al., 1989; Davies et al., 1994; Davies et al., 1997). The major objective in these studies was to enhance secondary purification following isolation and primary purification with standard density gradients and centrifugation. Positive selection of islets is more desirable than negative selection, as positive selection would also allow subsequent magnetic manipulation of islets (Nandigala et al., 1997). These techniques used bar magnets to isolate islets in a batch process. These techniques fail to get high purities as inter-islet binding formed capture nets and retained significant amounts of acinar tissue, and monoclonal antibodies were found to easily shear off of tissue under gentle handling.

Magnetic separation of glomeruli from kidney tissue was achieved by directly infusing the iron oxide particles into renal vasculature (Gauthier et al., 1988). It had been observed that pancreatic islets and renal glomeruli have similar angioarchitechtures. Pinkse et al. (2004) infused unlabeled paramagnetic microbeads directly into the vascularization of rat pancreata prior to enzymatic digestion (Pinkse et al., 2004). Results showed that the microbeads were preferentially captured in the islet vasculature, that the islets were easily purified, and that the purified islets could reverse insulin dependence in rodents. This process was successfully applied to human islets to achieve maximum of 80% yields but only 40% purity. Iron oxide particles were replaced by Dynal® D-450 Dynabeads® to label only islets by taking the advantage of the hypervascularity of islets compared with acinar tissue (Tons et al., 2008).

Quadrupole Magnetic Sorting (QMS) technology developed for stem cell separation was successfully applied to purify porcine islets of Langerhans with high yields but with very low purity (Shenkman et al., 2009). It has been observed that mechanical stress applied in QMS or the magnetic beads present in the islets do not affect islets functionality (Shenkman et al., 2009a). To overcome the limitations of the density gradient method and to develop a technique which makes donor to recipient ratio to 1:1, we redesigned and tested QMS (Kennedy et al., 2007) to isolate porcine islets of langerhans as soon as they are liberated from the pancreatic tissue mass.

4.3 MATERIALS AND METHODS

4.3.1 QMS and separation theory

QMS is a type of split-flow thin channel continuous isolation device (Sun et al., 1998; Tong et al., 2007; Jing et al., 2007; Hoyos et al., 2003). Figure 4.1 shows the design and the mechanism of the QMS for isolating magnetic islets from non-magnetic tissue. Briefly, the system is composed of an annular column with a concentric inlet splitter to separate the islet suspension inlet (a') from the carrier buffer inlet (b') and an outlet splitter to separate the outlet for isolated islets (Positive Fraction, b) from that for nonmagnetic tissue (Negative fraction, a). The column is centered within the bore of a strong Halbach quadrupole magnet and by the effect of magnetic force, islets previously infused with Dynabeads are deflected outward into the positive fraction or onto the wall. Unlabeled tissue is collected in the inner, negative fraction. The magnetic field is provided by four neodymium-iron-boron permanent magnets and four pole pieces with a maximum magnetic field strength of the quadrupole, B_0, of 0.714 T.

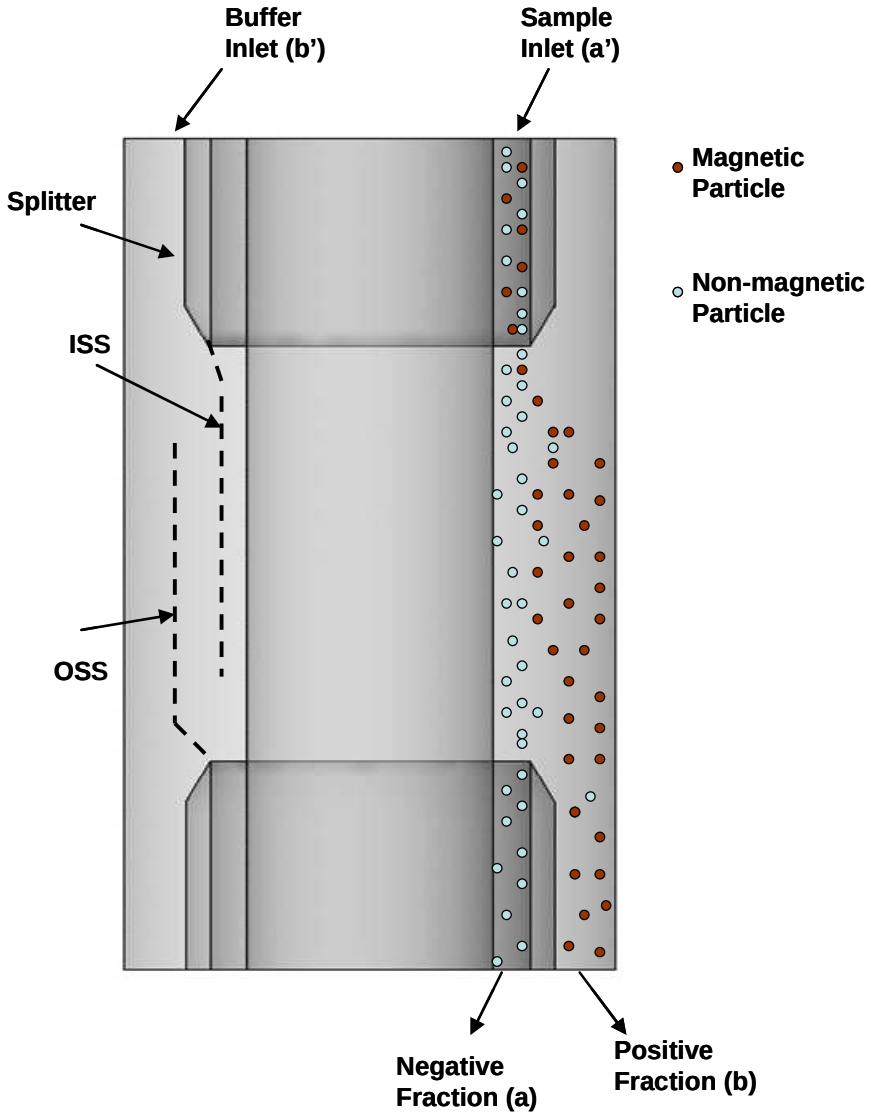

Figure 4.1: Schematic diagram of the quadrupole magnetic cell sorter (QMS) showing separation of magnetic from non-magnetic particles.

The fluid trajectory in the annulus is well documented and is described by the relation:

$$\int_0^z dz = \int_{\delta_1}^{\delta} \frac{v(\delta)}{u_m(\delta)} d\delta \qquad (4.1)$$

Where u_m is the velocity of the magnetic particle in the magnetic field, δ is the radial position, $v(\delta)$ is the velocity profile of fluid flow. As the density of the islets is high enough to sediment in the flow channel, adding the Stokes' sedimentation velocity (v_s) to the velocity relation gives:

$$\int_0^z dz = \int_{\delta_1}^{\delta} \frac{v(\delta) + v_s}{u_m(\delta)} d\delta \qquad (4.2)$$

4.3.2 Magnetophoretic Mobility

The QMS system's ability to isolate magnetic bead-infused islets depends on the magnetphoretic mobility of islets, which indicates the degree to which the islets are infused with Dynabeads. The magnetophoretic mobility, μ_m, can be calculated by measuring the velocity of the magnetic particle in the constant magnetic energy gradient.

$$\mu_m = \frac{v_m}{S_m} \qquad (4.3)$$

v_m is the magnetically induced velocity and S_m is the magnetic energy gradient. The magnetophoretic mobility can be measured using Magnetic Particle Tracking Velocimetry (MPTV). MPTV is the improved model of the Cell tracking velocimeter to measure the mobility of the large magnetized particles such as islets.

4.3.3 Pancreas Procurement and labeling

All procedures involving animals were approved by the Institutional Animal Care and Use Committee (IACUC) and performed at the Schulze Diabetes Institute at the University of

Minnesota. The porcine procurement was performed by standard protocol used at the Schulze Diabetes Institute (Ferrer et al., 2008). Pancreata was harvested from adult Landrace pigs following cardiac death using an *en bloc* dissection technique. The posterior aorta was identified, longitudinally divided and both the celiac trunk (CT) and superior mesenteric artery (SMA) were cannulated. Distal splenic, gastric and hepatic vessels were clamped and 1 L of cold preservation solution (CPS, cold storage/purification stock solution containing 2% Pentastarch, Mediatech, Inc, Herndon, VA) was flushed into both the CT and SMA, simultaneously. During the flush, the main pancreatic duct was identified and cannulated just proximal to its insertion into the duodenum. Approximately 60 mL of CPS was then slowly infused over two minutes by hand-syringe into the main pancreatic duct. Following the flush, the pancreas was excised and divided into the combined connecting and duodenal lobes and splenic lobe, all while taking care to preserve native vasculature. To compare infused versus uninfused islets obtained from the same pancreas, the splenic pancreatic lobe alone was infused with magnetic beads. Paramagnetic Magnetic Particles (4.5 µm diameter, Dynabead M450, Invitrogen, Carlsbad, CA) suspended in 1 L of CPS were then infused into the splenic lobe only, via the CT and SMA by either hanging bag or hand-syringe infusion. Infusion of MP suspension was immediately followed by a 1 L flush with CPS. All lobes were then submerged into CPS and stored at 0-4°C for transportation from the procurement facility to the laboratory. A procedure requiring less than 30 minutes.

4.3.4 MRI

Following complete formalin fixation (≥ 24 hours), pancreata underwent MRI. MRI was performed at 1.5 T with an APOLLO spectrometer (Tecmag Inc., Houston, TX, USA) and a custom-built 16-leg low-pass birdcage resonator (24 cm diameter, 20 cm in length). Images were obtained with a T2*-weighted true three-dimensional gradient echo sequence with one

dimension frequency-encoded and the other two dimensions phase-encoded. A nonselective pulse was used to nutate the nuclei approximately 25 degrees during the scan. Typical acquisition parameters included a 9.6 msec acquisition time, 6.5 msec echo time, 120 msec repetition time, and a 20 cm x 10 cm x 5 cm field of view.

4.3.5 Histopathology

After MRI, biopsies were collected from several regions of the pancreas, embedded in paraffin and sectioned at 4 µm. Sections were examined using hematoxylin and eosin (H/E) and insulin immunohistochemical stains. Sections were evaluated by an experienced histopathologist (Dr. Thomas D.O'Brien) to estimate the fraction of magnetic particle incorporation within islet and acinar tissues.

4.3.6 Pancreas Digestion and Islets Isolation

Tissue samples were collected from pancreas before digestion for histology evaluation for beads. Then the infused pancreas was digested for islets isolation using the Ricordi method (Ricordi et al., 1998). Before performing an actual isolation using QMS, the QMS column was filled with Hanks' balanced salts solution (HBSS, Sigma, St.Louis, MO) with serum solution. Once the digested tissue collection started from the Ricordi chamber, the collection tube from the Ricordi chamber was connected to a reservoir bag, partially filled with HBSS with 10% porcine serum and placed in line between the QMS flow channel a' inlet and the Ricordi chamber. Tissue arrived at the reservoir at a flow rate equal to the QMS inlet flow rate. A reservoir bag is essential to avoid any pressure problems due to differences in the flow rates of QMS inlet and Ricordi chamber collection pumps and also helps to avoid tissue concentration problems. Outlet fractions from QMS were collected and centrifuged to collect samples for analysis. After sending all digested tissue through the QMS, the flow channel was carefully removed and islets attached

to the wall were recovered for counts and quality analysis studies. All tubing and flow channel used are disposable and sterilized. All flow channels were recycled in this research.

4.4 Islet Quality Assessment

4.4.1 Oxygen Consumption Rate (OCR) Assay

OCR was measured on COBE (standard method) and QMS purified islets as described previously (Papas et al., 2007) . Islet samples were rinsed and suspended in Dulbecco's modified Eagle's medium (Mediatech, Herndon, VA) containing 4.5 g/L L-glutamine and supplemented with 100 U/ml penicillin, 100µg/ml streptomycin, 10 mM HEPES without serum. Then each islet suspension was placed into three or more 200-µL titanium chambers. The chambers were sealed and maintained at 37^{o}C. The time-dependent oxygen partial pressures (pO_2) within the chambers were recorded over time using a fluorescent-based fiber optic oxygen sensor (Micro Oxygen Uptake System, FO=SYSZ-P250; Instech Laboratories, Plymouth Meeting, PA). The initial tracings at the highest pO_2 were then fit by a straight line and OCR was calculated from the following equation: $OCR = V_{ch}\alpha(\Delta pO_2)$, where ΔpO_2=Dt is the slope of the line, V_{ch} is the chamber volume, and α is the Bunsen solubility coefficient of oxygen in an aqueous medium at 37^{o}C (1.27 nmol mm Hg^{-1} mL^{-1}).

4.4.2 DNA Quantification

Islet samples analyzed by the OCR assays were subsequently sampled for quantification of DNA content. To measure DNA content, islet samples were diluted in an aqueous solution of 1M ammonium hydroxide and 3.4mM Triton X-100 and sonicated. DNA content was determined using the Quant-iT PicoGreen dsDNA kit (Molecular Probes, Eugene, OR) as per manufacturer's instructions. Fluorescence readings were taken on a SpectraMax M5 microplate reader (Molecular Devices, Sunnyvale, CA)

4.4.3 Nude Mouse Bioassay

Adult mice were rendered diabetic by intraperitoneal streptozotocin injection. Once hyperglycemia was established, 2,000 IEQ of islets from Dynabeads infused and un-infused pancreas were transplanted into the renal subcapsular space of diabetic nude mice and observed for 30 or more days. After 30 days the mice were nephrectomized to ensure that blood glucose returned to diabetic levels, after which the mice where euthanized.

4.5 Results and Discussion

4.5.1 Cross-over studies of QMS

The presence of unlabelled magnetic particles in the positive fraction (b) of the output is called non-specific cross over. Hydrodynamics at the edges of splitters, channel or splitter imperfections, hydrodynamic instabilities and shear-induced diffusion are some phenomena that contribute to non specific crossover (Williams et al., 2003; Williams et al., 2003a; Williams et al., 2008). As the islets count for only 2% of whole pancreas, a small amount of crossover can obviously change the purity of isolated islets. Crossover studies were conducted using only nonmagnetic acinar tissue. Acinar tissue from a pig pancreas, “CTS1”, collected from the negative QMS fraction was centrifuged and re-suspended into 4 liters HBSS buffer and 500ml of sample was used for each run. The effect of different total flow rates, inlet and outlet flow ratios and concentration of tissue in the sample was tested. Peristaltic pumps (Watson-Marlow) were used to pump the sample and carrier liquid through the flow channel and to control positive outlet flow rate. The negative (a) outlet was held open at atmospheric pressure to balance the flow rates. Turbidity sensors connected to positive and negative outlets were used to measure the quantity of tissue in each outlet. From the resulting absorbance data non specific crossover was calculated using the following equation.

$$S_b = \frac{N_b}{N_a + N_b} \qquad (4.4)$$

Where N_b is the amount of tissue in the b outlet and N_a is the amount of tissue in the a outlet. The amount of the tissue in the negative fraction was calculated with the following relation

$$S_a = \frac{N_a}{N_a + N_b}. \qquad (4.5)$$

The total volumetric flow rates used for the crossover experiments are presented in Table 4.1. Experiments were conducted with different inlet and outlet flow rate ratios and to test the effect of the amount of the tissue in the sample at constant total flow rate of 400ml/min. Figure 4.2 shows the relative amount of tissue in the negative and positive fractions at different outlet flow ratios for constant inlet flow ratio of 0.25 at a total flow rate of 400ml/min. It shows the decrease in the crossover with the increase in outlet flow ratio. Increasing the outlet flow ratio increases the transport lamina thickness (Figure 4.1) which helps to reduce the crossover. Figure 4.3 shows the crossover of the acinar tissue at different inlet flow rate ratios at constant outlet flow ratio and constant total flow rate. Crossover also increases with the increase in the inlet flow ratio. Increasing the inlet flow ratio at constant total flow rate moves the inner splitting surface away from the core towards outer wall which moves the outer splitting surface away from the splitter causing more crossover. Figure 4.4 shows the crossover at constant total flow rate, inlet and outlet flow ratios with the change in the amount of the tissue in the sample. Increasing sample concentration results in an increase in the amount of tissue that enters in between the core and ISS and has to cross the OSS to reach the positive fraction. crossover with the increase in the concentration of the tissue in the sample, interactions between tissue fragments plays a role in the crossover.

Table 4.1: Total flow rates used in crossover studies and corresponding ISS and OSS values.

Flow rate Q (ml/min)	R_{in}	R_{out}	Inner Splitting Surface (r_{ISS}, cm)	Outer Splitting Surface (r_{OSS}, cm)
400	0.25	0.4	2.698	2.749
400	0.25	0.5	2.698	2.781
400	0.25	0.6	2.698	2.813
400	0.25	0.7	2.698	2.846
400	0.3	0.6	2.716	2.813
400	0.4	0.6	2.649	2.813
350	0.25	0.6	2.698	2.813

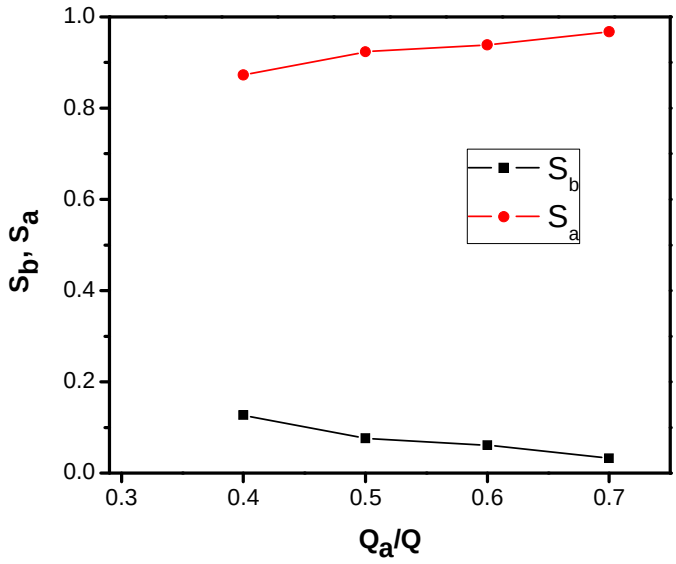

Figure 4.2: Crossover of the acinar tissue at different outlet flow ratios for constant inlet flow ratio and total flow rate. The relative amount of tissue (ordinate) was calculated using equations (4.4) and (4.5). See Table 4.1.

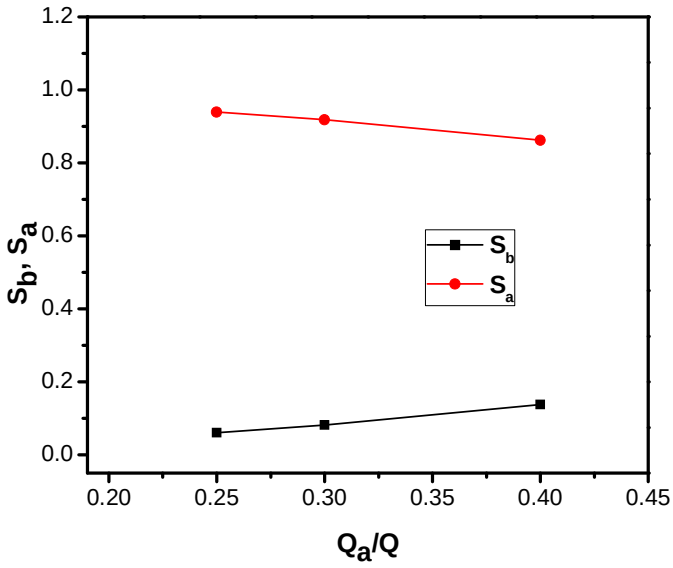

Figure 4.3: Crossover of the acinar tissue at different inlet flow ratios for constant outlet flow ratio and total flow rate.

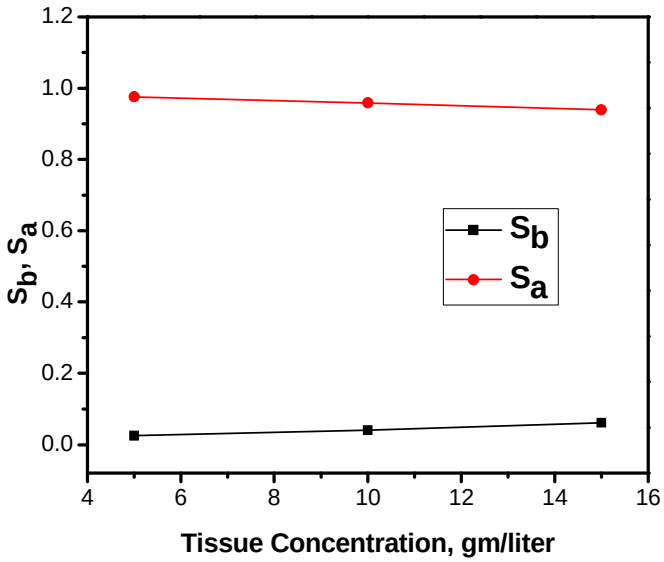

Figure 4.4: Crossover of the acinar tissue at different tissue concentrations at constant inlet flow ratio, outlet flow ratio and total flow rate.

4.5.2 Isolation of Islets

A total of five pig pancreata were infused with Dynabeads and processed through QMS for purification of islets. In the case of the first three pancreata, P808, P810 and P685, only the splenic lobe was infused with the Dynabeads and for the other two pancreata, P686 and P687, the whole pancreas was infused with Dynabeads. In all cases splenic lobe was digested for QMS isolation and the other two (Duodenal and Connecting) lobes were separately digested for standard COBE isolation. After digesting the P808 pancreas, tissue was centrifuged and re-suspended into 1L solution and split into two halves and processed at different flow rates. Tissue from the other four pancreata was send through QMS straight from the Ricordi chamber by maintaining the flow rates of QMS and Ricordi chamber collection pump equal. Total flow rate, inlet flow ratio and outlet flow ratios were changed for each run to study the effect on recovery and purities. Table 4.2 presents the flow rates and flow ratios studied. Even though QMS was designed to collect the magnetic islets in the positive ("b") fraction, Dynabeads infused into the islets made them sufficiently magnetic so that infused islets reached the wall of the flow channel. Islets were collected from the flow channel wall after sending total tissue through the QMS by carefully removing the flow channel from the magnet assembly. Manual islet counts using dithizone staining was used to asses the purity, yield and total IEQ of the islets for QMS and COBE isolated fractions. Table 4.2 shows the results from all isolations. This shows the differences between COBE and QMS isolated islets based on the IE.

Table 4.2: Purity and yields of the islets from all the experiments conducted with four porcine pancreata at the University of Minnesota.

Isolation	Condition	IE / gm (yield)	Total IE based on DNA
P685 Conn/Duo	COBE	1,772	26,760
P685 Splenic	QMS	479	421,942
P686 Conn/Duo	COBE	804	33,625
P686 Splenic	QMS	277	85,274
P687 Conn/Duo	COBE	1,256	60,913
P687 Splenic	QMS	160	226,713

4.5.3 Magnetophoretic Mobility Measurements

Samples from the digested tissue and all three fraction from QMS were run through MPTV to check the magnetophoretic mobilities of the magnetic bead infused islets. These tests helped to confirm the presence of magnetic tissue in the negative fractions or the presence of nonmagnetic tissue in the isolated wall fraction. Figure 4.5 shows the histograms developed by MPTV for tissue sample from Ricordi chamber before sending it through QMS for isolation. Critical mobilities required for islets to reach the positive fraction of the QMS output are m_0 = 2.91 x 10^{-12} m^3/T-A-s (minimum value of mobility required for islets to cross transport lamina) to m1 = 1.257X10^{-11} m^3/T-A-s (maximum value of mobility required for islets to cross transport lamina). Islets with mobility less than m_1 will end up in the negative fraction and the islets with mobility more than m_1 will reach and stick to the wall during isolation. Peaks at magnetophoretic mobility less than $1e^{-12}$ are the result of the sedimentation of tissue in the MPTV cell. The mobility histogram shows small quantities of tissue with mobilities greater than m_1 which is due to pancreas consists of around 98% of unlabeled acinar tissue. Figure 4.6 is the mobility histogram for the negative fraction and confirms the absence of magnetic tissue in the negative outlet fraction. Figure 4.7 is the histogram for the positive fraction and shows islets with small mobility, which is not enough to reach the wall of the flow channel. Figure 4.8 is the histogram for the wall fraction with 65% purity and shows higher mobility values. MPTV can not differentiate the islets and acinar tissue but it helped to confirm the amount of magnetic tissue in the samples from all fractions.

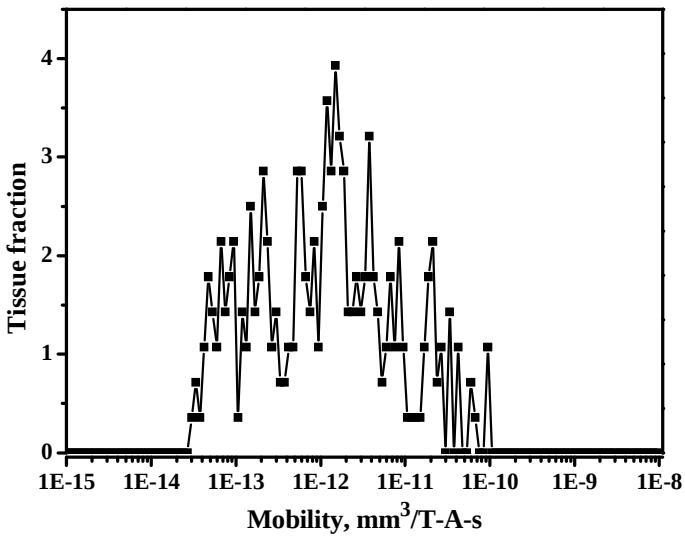

Figure 4.5: Magnetophoretic mobility histogram of digested tissue sample taken before sending it through QMS for isolation.

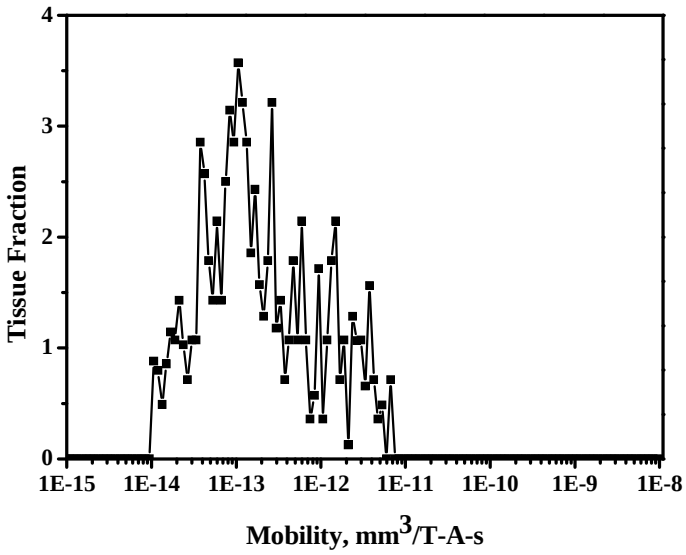

Figure 4.6: Magnetophoretic mobility histogram of digested tissue sample taken from the Negative (a) fraction of a QMS isolation.

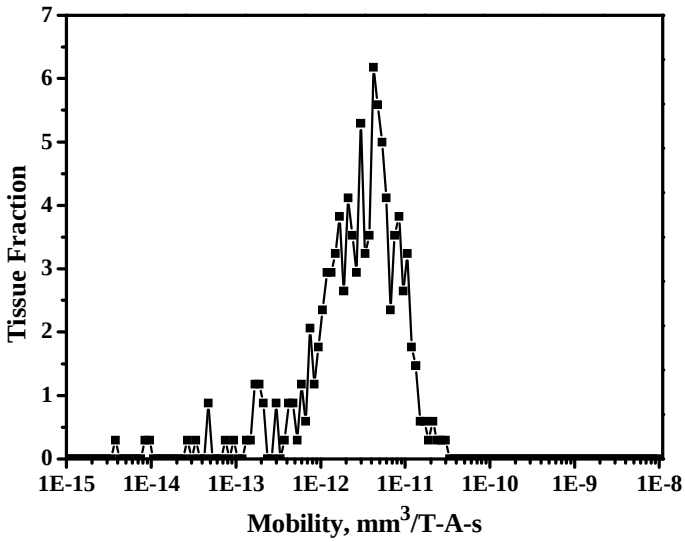

Figure 4.7: Magnetophoretic mobility histogram of digested tissue sample taken from the Positive (b) fraction of a QMS isolation.

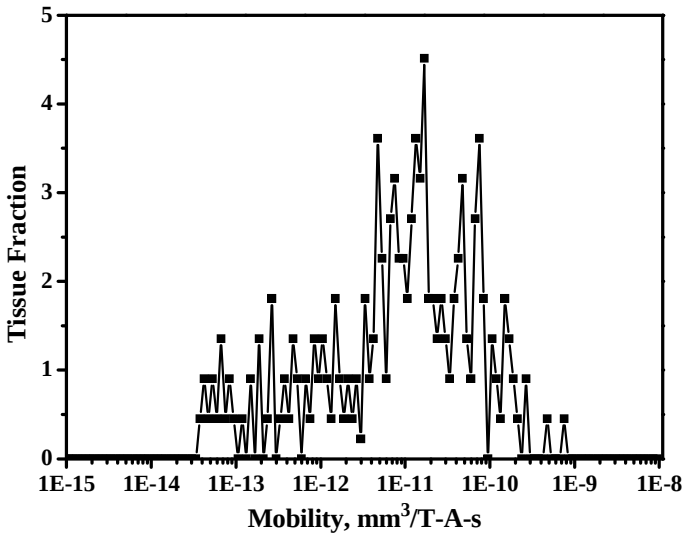

Figure 4.8: Magnetophoretic mobility histogram of digested tissue sample taken from wall fraction of QMS isolation.

4.5.4 Histology of Pancreas

Hanging bag or hand-syringe infusion techniques were used to infuse the beads into the pancreas with varying concentration of magnetic particles. T2*-weighted MRI illustrated a uniform distribution of hypointense regions, indicating the presence of magnetic particles throughout the experimental splenic lobe in all organs (Figure 4.9). Histologic analysis confirms that magnetic particles were found predominantly within islet microvasculature, with few present in surrounding acinar tissue as distinguished by hematoxylin and eosin (H/E) staining (Figure 4.10). Hand-syringe infusion technique achieved good infusion of magnetic particles into the islets. Further details are given in a separate publication (ref. Rizzari paper).

4.5.5 Quality assessment of Islets

Quality assessment studies were conducted on QMS and COBE isolated islets. Purity and yield of the islets from P808 isolation was too low to allow quality tests, so quality assessment was done for the other four isolations. Figure 4.11 shows the pictures of the islets taken immediately after isolation using QMS and COBE method. Islets isolated with COBE method appear irregular in shape and fragile, whereas the islets isolated using QMS appear very solid wit smooth surfaces. Pressure applied to the islets and prolonged exposure to the digestion enzymes during the COBE separation damage the small islets causing them to fragment into small tissue while the smooth (low-shear) flow of islets through the QMS flow channel helps islets to maintain the solid structure and minimizes the time islets are exposed to digestion enzymes.

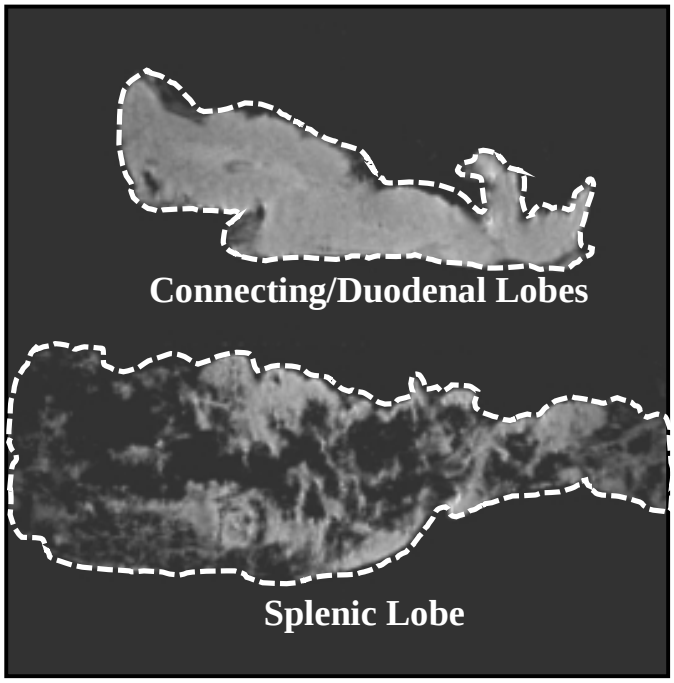

Figure 4.9: MRI of the control connecting/duodenal lobes (above) and the experimental splenic lobe (below), in which infused magnetic beads resulted in well-distributed hypointense regions.

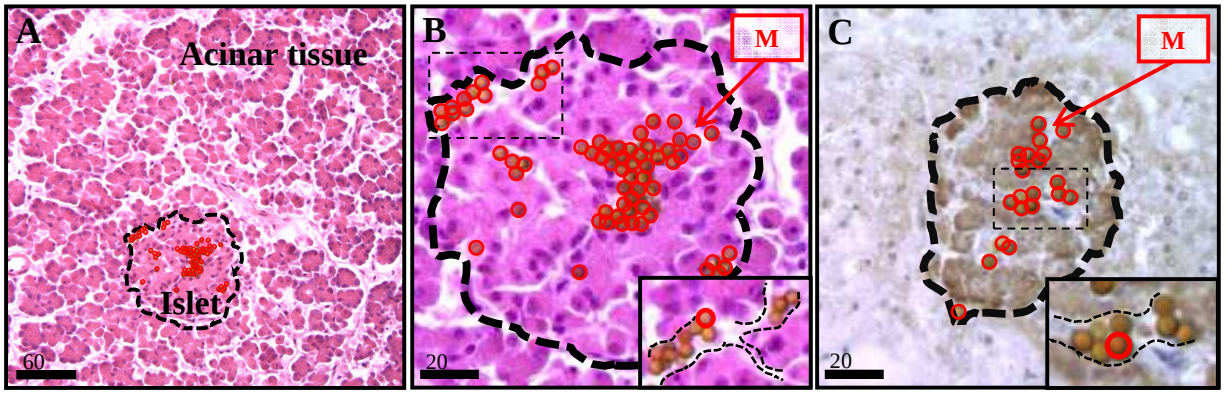

Figure 4.10: Representative low and high magnification micrographs of an islet located in the experimental splenic lobe (distal region), illustrating minimal accumulation of magnetic particles in the acinar tissue (Fig. 4.10A, H/E) and significant accumulation within the islet (Fig. 4.10B, H/E) and magnetic particles within capillaries of an islet located in the proximal splenic lobe, near the site of infusion at the celiac trunk (Fig. 4.10C, insulin stain).

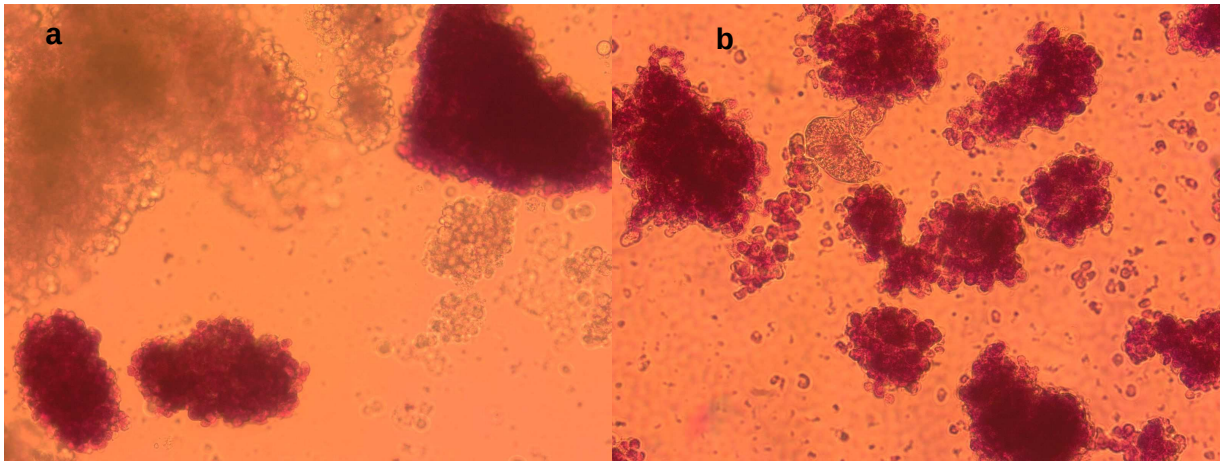

Figure 4.11: Pictures of the dithizone-stained islets taken under microscope at 20X magnification a) islets isolated with QMS b) islets isolated with COBE.

Figure 4.12 shows the OCR per DNA (nmol min^{-1} mg^{-1} DNA) for COBE and QMS isolated islets. These results for day 0 clearly show the difference between QMS and COBE isolated islets. OCR per DNA for COBE isolated islets on day 0 was less than the standard required value of 150 nmol min-1 mg-1 DNA to transplant into the mouse for in vivo testing whereas the QMS isolated islets have high enough OCR to transplant. COBE and QMS isolated islets were cultured for 7 days and checked for OCR and the resulting increased OCR values for COBE and QMS isolated islets both exceeded the required standard values. Figure 4.13 shows the average values of the OCR/DNA for COBE and QMS isolated islets at day 0 and day 7. QMS isolation can reduce or eliminate culture time and helps to eliminate the mechanical stress due to centrifugation on the islets.

Islets were evaluated to check their ability to reverse diabetes in mice. These studies help to study the effect of the presence of Dynabeads on the islets' functionality. Immunodeficient diabetic mice were transplanted with 2000IEQ of islets from COBE and QMS isolation from the same pancreas. Histological evaluation confirmed no inflammatory reaction in the murine kidneys due to the presence of the Dynabeads and diabetes reversal was achieved in the mice with Dynabead infused islets.

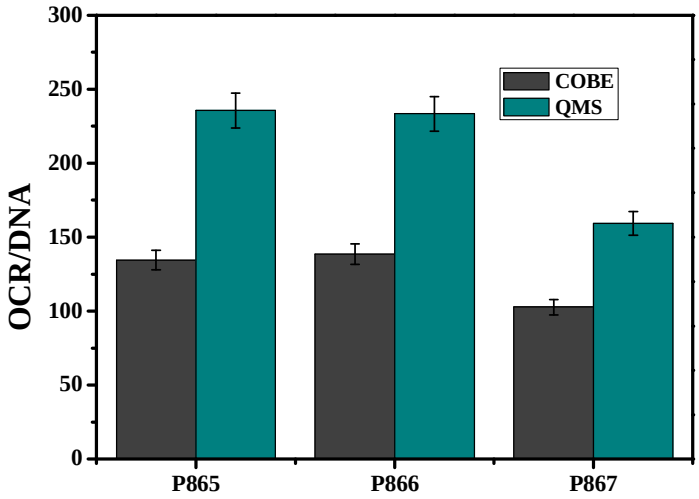

Figure 4.12: Stimulation index for OCR measurements from control and infused islets from three separate isolations.

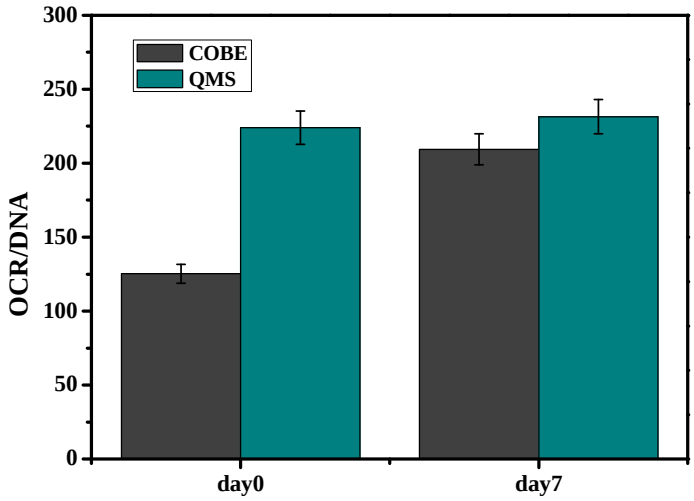

Figure 4.13: Stimulation index for average OCR measurements from control and infused islets from three separate isolations at day0 and day7.

Based on the MPTV tests and visual observations it is confirmed that the infusion of the Dynabeads into the islets was not 100% successful. Even though Dynabeads were selected based on their size and the vascular structure differences between islets and acinar tissue, not all islets were infused with beads, and some of the acinar tissue also received magnetic beads. Obtaining homogeneity of bead infusion is important to isolate islets using QMS, and more studies are ongoing at University of Minnesota to further the understanding of the anatomy of porcine pancreata, improvement of procurement, flushing and homogeneous perfusion of the organ through the vasculature for optimal bead infusion, effect of pressure of infusion, different bead concentration and also considering the option of other beads with less magnetophoretic mobility and optimal size.

When digested tissue was first centrifuged and suspended in buffer prior to running through QMS during the P808 isolation, the tissue formed large clumps and clogged the QMS inlet port and reduced the purity of islets produced by a great percentage. By sending the tissue straight from the Ricordi chamber to QMS these problems were eliminated, and the time islets were exposed to digestion enzymes was greatly reduced thereby avoiding over digestion and fragmentation problems. When islets stick to the wall of the QMS flow channel they are exposed to fresh buffer with serum and not the digestion fluid. Even though the QMS flow channel was designed to collect the bead infused islets in the positive fraction, the higher magnetophoretic mobilities of the Dynabeads forced us to collect the infused islets on the wall of the flow channel and collect them after sending all tissue through QMS. Some acinar tissue sedimented at the bottom of the flow channel and it reduced the purity of the islets collected from wall. Some small modifications in the flow channel design can also increase the purity of the islets.

4.6 Conclusions

QMS successfully isolated the Dynabead infused islets immediately after islets were liberated from the pancreas in a continuous process. Visual observations through microscope and quality assessment of the isolated islets confirmed the advantage of the QMS isolation over the standard COBE method. Achieving the homogeneous infusion of the magnetic beads into the islets and by implementing the small changes in the flow channel design it is possible to make the QMS a successful instrument to isolate superior quality porcine or human islets in less time than required by the available standard methods.

4.7 References

Davies JE, James RF, London NJ, Robertson GS. 1995. Optimization of the magnetic field used for immunomagnetic islet purification. Transplantation 59(5):767.

Davies JE, Robertson GS, Swift S, Chamberlin J, Bell PR, James RF, London NJ. 1994. Transplatation Proceedings 26(2):649-650.

Davies JE, chamberlain JC, Swift S, James RF, London NJ, Robertson GS. 1997. The use of immunomagnetic separation for secondary purification of pancreatic islets. A comparison of different magnetic fields in the rat. Adv Exp Med Biol 426:435-440.

Ferrer J, Scott WE, 3rd, Weegman BP, Suszynski TM, Sutherland DE, Hering BJ. 2008. Pig pancreas anatomy: implications for pancreas procurement, preservation, and islet isolation. Transplantation 86(11):1503-1510.

Frank A, Deng S, Huang X, Velidedeoglu E, Bae YS, Liu C, Abt P, Stephenson R, Mohiuddin M, Thambipillai T, Markmann E, Palanjian M, Sellers M, Naji A, Barker CF, Markmann JF. 2004. Transplantation for type I diabetes: comparison of vascularized whole organ pancreas with isolated pancreatic islets. Ann Surg. 240:631.

Froud T, Ricordi C, Baidal DA, Hafiz MM, Ponte G, Cure P, Pileggi A, Poggioli R, Ichii H, Khan A, Ferreira JV, Pugliese A, Esquenazi VV, Kenyon NS, Alejandro R. 2005. Islet transplantation in type 1 diabetes mellitus using cultured islets and steroid-free immunosupression: Miami experience. Am J Transplant. 5:2037.

Gauthier VJAMM. 1988. A method for isolation of mouse glomeruli for quantitation of immune deposits. Kidney Int. 33:897.

Hering BJ, Kandaswamy R, Ansite JD, Eckman PM, Nakano M, Sawada T, Matsumoto I, Ihm SH, Zhang HJ, Parkey J, Hunter DW, Sutherland DE. 2005. Single donor, marginal-dose islet transplantation in patients with type 1 diabetes. JAMA 293:830.

Hering BJ, Matsumoto I, Sawada T, Nakano M, Sakai T, Kandaswamy R, Sutherland DER. 2002. Impact of two-layer pancreas preservation on islet isolation and transplantation Transplantation 74:1813-1816.

Hering BJ, Wijkstrom M, Graham ML, Hårdstedt M, Aasheim TC, Jie T, Ansite JD, Nakano M, Cheng J, Li W, Moran K, Christians U, Finnegan C, Mills CD, Sutherland DE, Bansal-Pakala P, Murtaugh MP, Kirchhof N, Schuurman HJ. 2006. Prolonged diabetes reversal after intraportal xenotransplantation of wild-type porcine islets in immunosuppressed nonhuman primates. Nat Med 12 (3):301-303.

Hoyos PS, Decker K, Nakamura M, Chalmers JJ, Moore LR, Zborowski M. 2003. Splitter imperfections in annular split-flow thin separation channels: experimental study of nonspecific crossover. Anal Chem 75:6687.

Jing Y, Chalmers JJ, Zborowski M. 2007. Blood progenitor cell separation from clinical leukapheresis product by magnetic nanoparticle binding and magnetophoresis. Biotechnol Bioeng 96(6):1139.

Kennedy DJ, Todd P, Logan S, Becker M, Papas KK, Moore LR. 2007. Engineering quadrupole magnetic flow sorting for the isolation of pancreatic islets. Journal of Magnetism and Magnetic Materials 311:388-395.

London NJ, Robertson GS, Chadwick DR, Johnson PR, James RF, Bell PR. 1994.Human pancreatic islet isolation and transplantation. Clin transplant 8(5):421-459.

Mccloskey KE, Moore LR, Hoyos M, Rodriguez A, Chalmers JJ, Zborowski M. 2003. Magnetophoretic cell sorting is a function of antibody binding capacity. Biotechnol Prog 19:899.

Nandigala P, Chen TH, Yang C, Hsu WH, Heath C. 1997. Immunomagnetic isolation of islets from rat pancreas. Biotechnol Prog. 13:844-848.

Papas KK, Colton CK, Nelson RA, Rozak PR, Avgoustiniatos ES, Scott WE, Wildey GM, Pisania A, Weir GC, Hering BJ. 2007. Human islet oxygen consumption rate and DNA measurements predict diabetes reversal in nude mice. Am J Transplant 2007;7(3):707-713.

Pinkse G, Steenvoorde E, Hogendoorn S, Noteborn M, Terpstra OT, Bruijn JA, De Heer E. 2004. Stable transplantation results of magnetically retracted islets: a novel method. Diabetologia 47:55.

Ricordi C, Lacy PE, Finke EH, Olack BJ, Scharp DW. 1998. Automated method for isolation of human pancreatic islets. Diabetes 37:413.

Samejima T, Yamaguchi K, Iwata H, Morkawa N, Ikada Y. 1998. Gelatin density gradient for isolation of islets of Langerhans. Cell Transplant 7(1):37- 45.

Shapiro AM, Lakey JR, Ryan EA, Korbutt GS, Toth E, Warnock GL, Kneteman NM, Rajotte RV. 2000. Islet transplantation in seven patients with type 1 diabetes mellitus using a glucocorticoid-free immunosuppressive regimen. N Engl J Med 343(4):289-290.

Shenkman RM, Chalmers JJ, Hering BJ, Kirchhof N and Papas KK. 2009. Quadrupole Magnetic Sorting of Porcine Islets of langerhans, Tissue Engineering: Part C 15(2):147-156.

Shenkman RM, Godoy-Silva R, Papas KK and Chalmers JJ. 2009a. Effects of Energy Dissipation Rate on Islets of Langerhans: Implications for isolation and Transplantation, Biotechnol Bioeng 103(2):413-423.

Sun L, Zborowski M, Moore LR, Chalmers JJ. 1998. Continuous, Flow-Through Immunomagnetic Cell Separation in a Quadrupole Field. Cytometry 33:469.

Tong X, Xiong Y, Zborowski M, Farag SS and Chalmers JJ. 2007. A Novel High Throughput Immunomagnetic Cell Sorting System for Potential Clinical Scale Depletion of T Cells for Allogeneic Stem Cell Transplantation. Exp Hematol 35(10):1613.

Töns HAM, Baranski AG, Terpstra OT, Bouwman E. 2008. Isolation of the Islets of Langerhans from the human pancreas with magnetic rectraction. Transplant Proc. 40:413.

Williams PS, Zborowski M, Chalmers JJ. 1999. Flow Rate optimization for the Quadrupole Magnetic Cell Sorter. Anal Chem 71:3799.

Williams PS, Moore LR, Chalmers JJ, Zborowski M. 2003. Splitter Imperfections in Annular Split-Flow Thin Separation Channels: Effect on Nonspecific Crossover. Anal Chem 75:1365-1373.

Williams PS, Decker K, Nakamura M, Chalmers JJ, Moore LR, Zborowski M. 2003a. Splitter Imperfections in Annular Split-Flow Thin Separation Channels: Experimental Study of Nonspecific Crossover. Anal Chem 75:6687-6695.

Williams PS, Hoyos M, Kurowski P, Salhi D, Moore LR, Zborowski M. 2008. Characterization of Nonspecific Crossover in Split-Flow Thin Channel fractionation. Anal Chem 80:7105-7115.

Winoto-Morbach, Ulrichs K, Hering BJ, Leyhausen G, Muller-Ruchholz W. 1989. Methods in Islet Transplantation Research. Hormone and Metabolic Research supplement 25:51-54.

5. Summary and Future Work

The dissertation has successfully demonstrated that Quadrupole Magnetic Flow Sorter can be used for isolation of pancreatic islets from exocrine tissue using magnetic beads infusion into islets. Differences in the vascular structure of islets from acinar tissue can be used for successful infusion of Dynabeads® only into islets. QMS isolated islets are better in quality because of the less stress applied by QMS and the reduction of the exposure time of the islets to the digestive enzymes. CFD simulations can be used to test the performance of the QMS flow channel and can be used as a tool to improve the efficiency of the flow channel to achieve good isolation with high purity. MPTV developed to quantify the magnetophoretic mobility of the labeled tissue can be used as a tool to optimize the parameters of the QMS to isolate labeled islets from exocrine tissue.

CFD simulations of flow pattern performed on the new design of QMS flow channel confirm circumferentially uniform flow development around the annular channel. Quantitative agreement between experimental measurements of nonspecific crossover and prediction based on CFD modeling of the fluid flow was shown. For all flow conditions, crossover predicted by CFD simulations was found to be slightly lower than experimentally observed results. This difference may be due to the contribution of crossover from other factors such as particle lift and particle interactions. Diffusion was not considered in the CFD modeling. The good agreement between experimental and CFD predicted results allowed the performance of simulations with different channel prototype models to develop a design to minimize nonspecific crossover.

The capability of newly developed MPTV in measuring magnetophoretic mobility was confirmed with the measurements of the mobility of the standard Dynabeads. MPTV was successfully used to measure the mobility of magnetic particles up to 500 microns in size with different mobilities. MPTV's ability to predict the optimized flow parameters was also tested successfully with magnetic particles and the isolated islets of Langerhans as it is the final application of the MPTV.

The present research has opened up several avenues for continuing the fundamental and development research works on magnetic islet isolations. Following research area may be further explored to support the future islet transplantation studies.

1. Computational Fluid Dynamics study of the flow of the magnetic particles in the Quadrupole Magnetic Sorter flow channel using magnetic models in the FLUENT, which along with nonspecific crossover studies helps to design the magnet and flow channel assembly for QMS to achieve the best isolation purity with the collection of acinar tissue in the negative fraction and pure islets in positive fraction. Flow channel can be modified to avoid the clogging and settling of the tissue in the flow channel.
2. Development of the MPTV further to track only the moving particles in the flow channel by omitting the disturbances on the flow channel and make it possible to connect the MPTV online to the flow process of the Ricordi digestion process to get the QMS parameters for successful isolation of islets.
3. Further study of the magnetic beads infusion process into the islets to achieve uniform and enough beads infusion in the whole pancreas.

Appendix A: QMS Operation

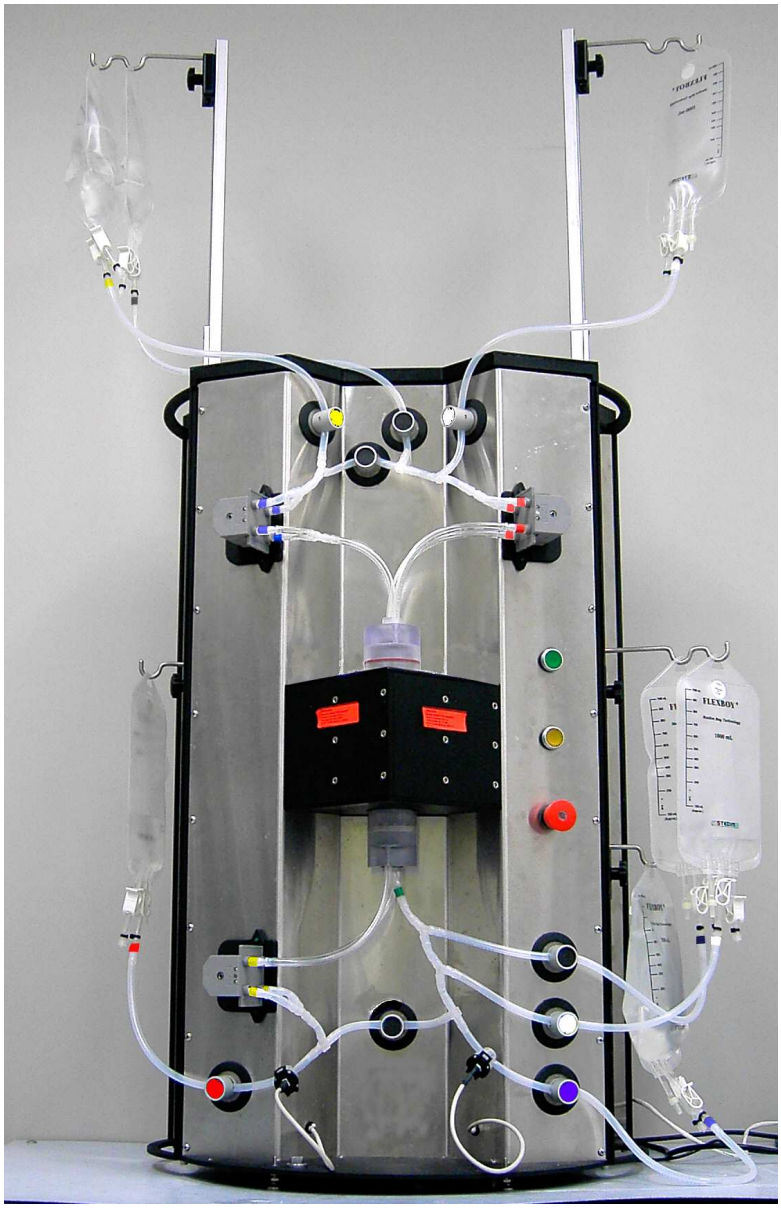

Figure A.1: Photograph of the QMS setup with fluid bags.

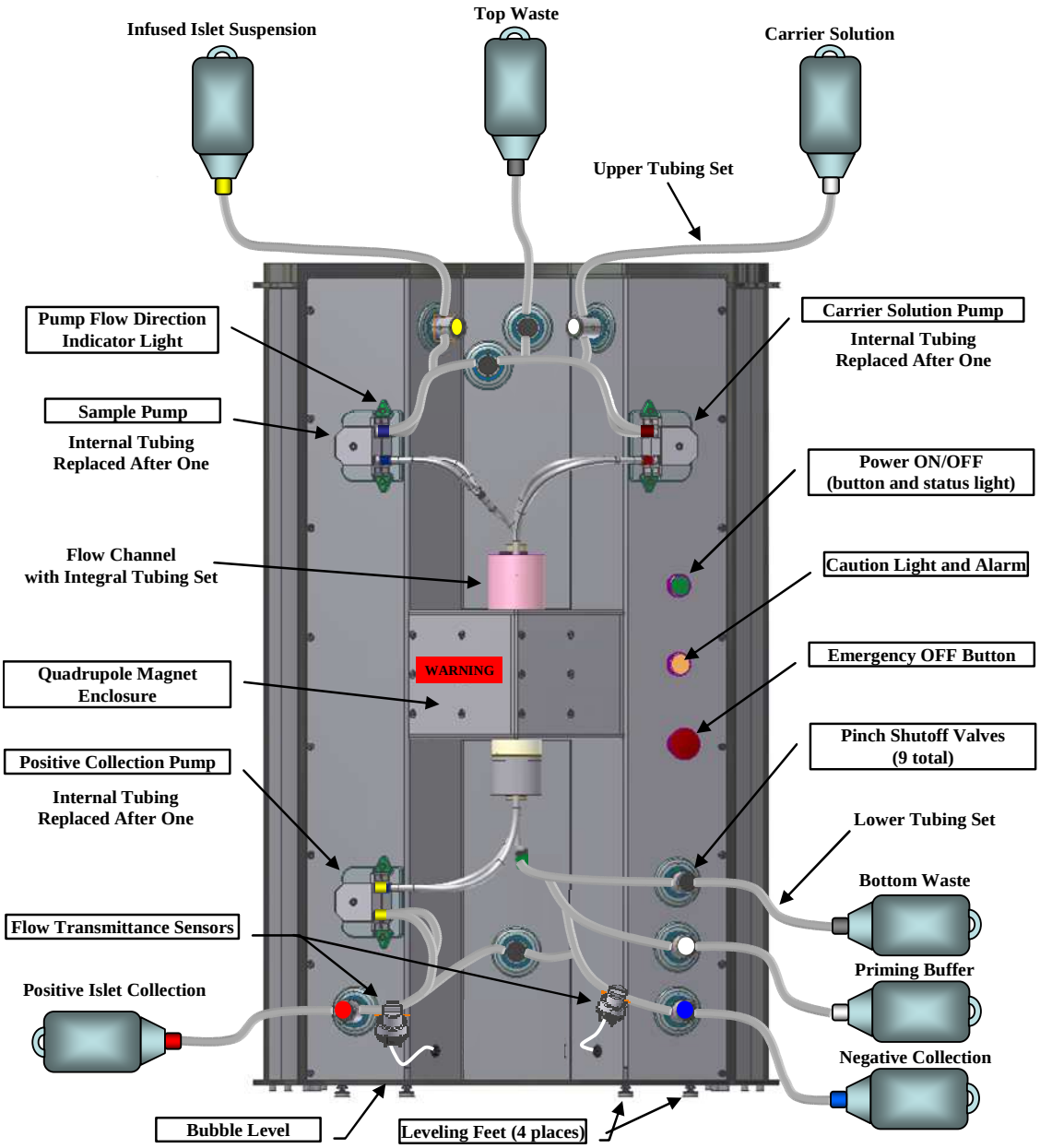

Figure A.2: Components of the QMS. Boxed labels are permanent QMS components, unboxed labels are consumable items replaced after one use

Figure A.3: Screnshot of the QMS software used to control the QMS operation.

Figure A.4: QMS set up for pancreas isolation at University of Minnesota laboratory.

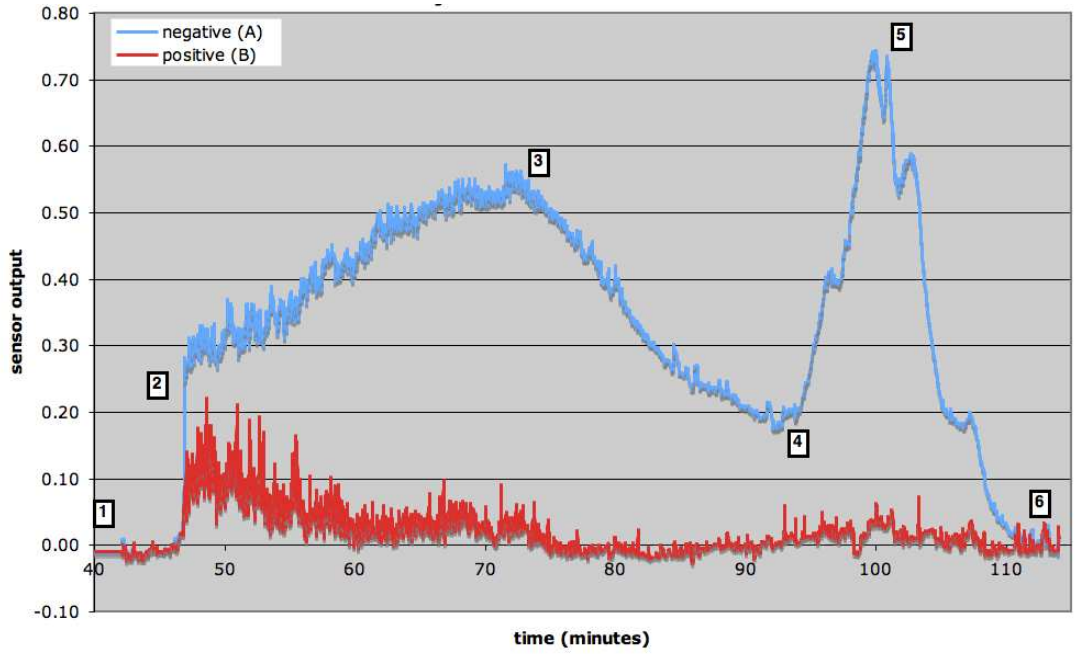

Figure A.5: Absorbance detector traces for P810 isolation run. The QMS was turned on at time t=0 minutes. The turbidity sensor data logging was activated at t=42 minutes [1]. The digestion process was switched to recovery mode and the QMS began operations, with tissue leaving the flow channel at t=48 minutes [2]. The tissue concentration with the Ricordi chamber upright peaked at approximately t=72 minutes [3]. The Ricordi chamber was inverted to maximize the recovery at t=92 minutes [4]. The tissue exiting the inverted Ricordi chamber peaked at t=102 minutes [5]. The isolation was terminated at approximately t=114 minutes [6].

Date	Exp no	Q	Qa'/Q	Qa/Q	Condition
2/26/2009	VC-02-1	224	0.25	0.25	flow Channel outside the magnet, no bead infusion
2/26/2009	VC-02-1A	224	0.25	0.25	flow Channel outside the magnet, no bead infusion
2/26/2009	VC-02-2	224	0.25	0.35	flow Channel outside the magnet, no bead infusion
2/26/2009	VC-02-2A	224	0.25	0.35	flow Channel outside the magnet, no bead infusion
2/26/2009	VC-02-3	224	0.25	0.45	flow Channel outside the magnet, no bead infusion
2/26/2009	VC-02-3A	224	0.25	0.45	flow Channel outside the magnet, no bead infusion
4/24/2009	VC-04-1	400	0.25	0.5	Flow channel in the magnet, no bead infusion
4/24/2009	VC-04-2	400	0.25	0.6	Flow channel in the magnet, no bead infusion
4/24/2009	VC-04-3	400	0.25	0.7	Flow channel in the magnet, no bead infusion
4/24/2009	VC-04-4	400	0.25	0.7	Flow channel in the magnet, no bead infusion
6/11/2009	VC-06-1	400	0.25	0.7	2ml dynabeads infused into pancreas
1/5/2010	P808 - T1	400	0.25	0.5	4ml of dynabeads in splenic lobe
1/5/2010	P808 - T2	400	0.25	0.7	splenic lobe tissue resuspended into 1L
1/5/2010	P808 - C1	400	0.25	0.5	Control lobes(duodenal and connectiong lobe without beads)
1/5/2010	P808 - C2	400	0.25	0.7	only for cross over studies, tissue obtained from cobe
1/7/2010	P810	400	0.25	0.7	4ml of dynabeads in splenic lobe
					Tissue was send to QMS staright from Ricordi chamber
5/25/2010	P865	400	0.25	0.6	4ml dynabeads infused into splenic
5/26/2010	P866	400	0.4	0.6	4ml dynabeads infused into pancreas
5/27/2010	P867	400	0.43	0.6	4ml dynabeads infused into pancreas
6/7/2010	CTS-1	400	0.43	0.6	4ml dynabeads infused into whole pancreas
6/9/2010	CTS-2	400	0.3	0.6	4ml dynabeads infused into whole pancreas

Table A.1: Summery of the Porcine isolation experiments.

A.1 QMS Operation Procedure

1. Install pump tubing, tubing set and flow channel.
2. Connect fluid and empty bags to the tube set.
3. Prime the flow channel and tubes.
4. Calibrate the pumps.
5. Set the flow rates using QMS islets software.
6. Start turbidity sensors to get the absorbance data.
7. Use the QMS software to run QMS in auto mode.
8. Collect the positive and negative fractions.
9. Collect wall fraction by removing flow channel from magnet.
10. Drain the tubing and clean.

Appendix B: MPTV Operation

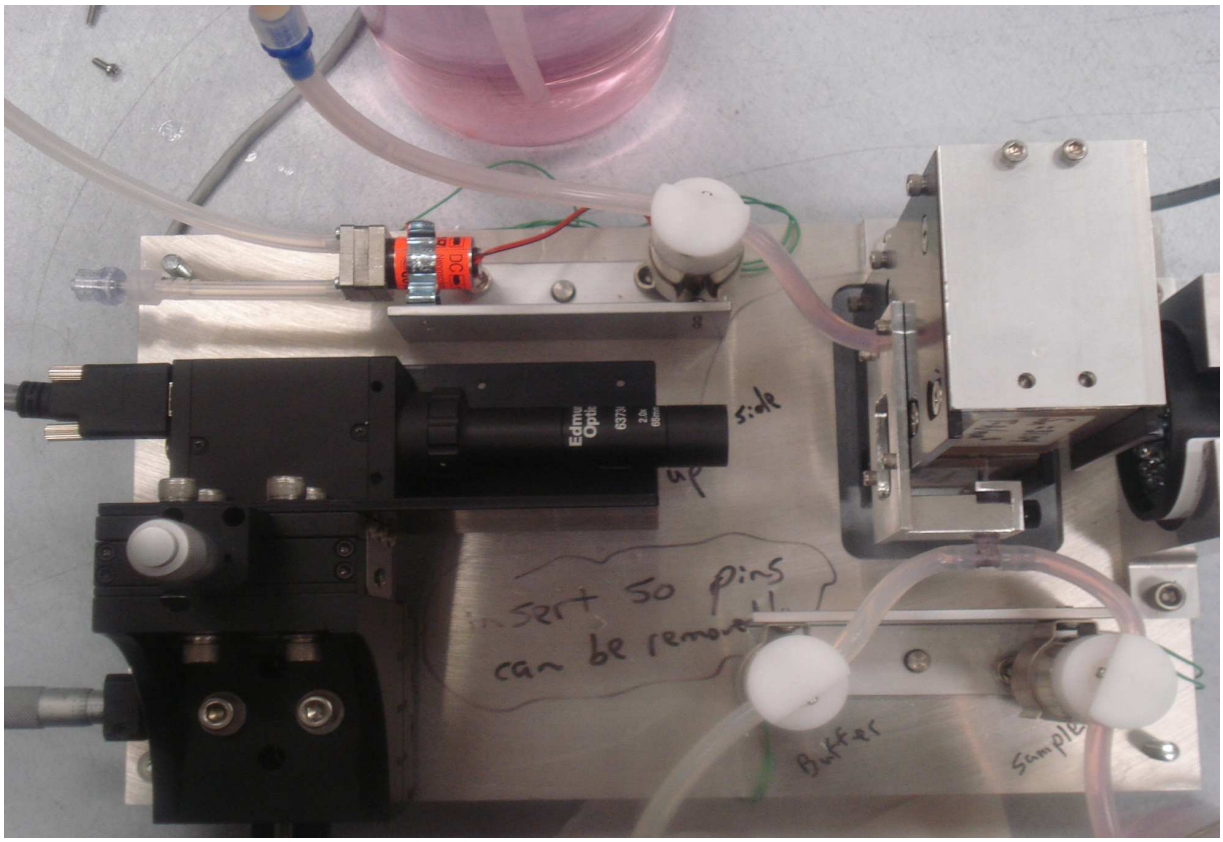

Figure B.1: Photograph of the MPTV assembly.

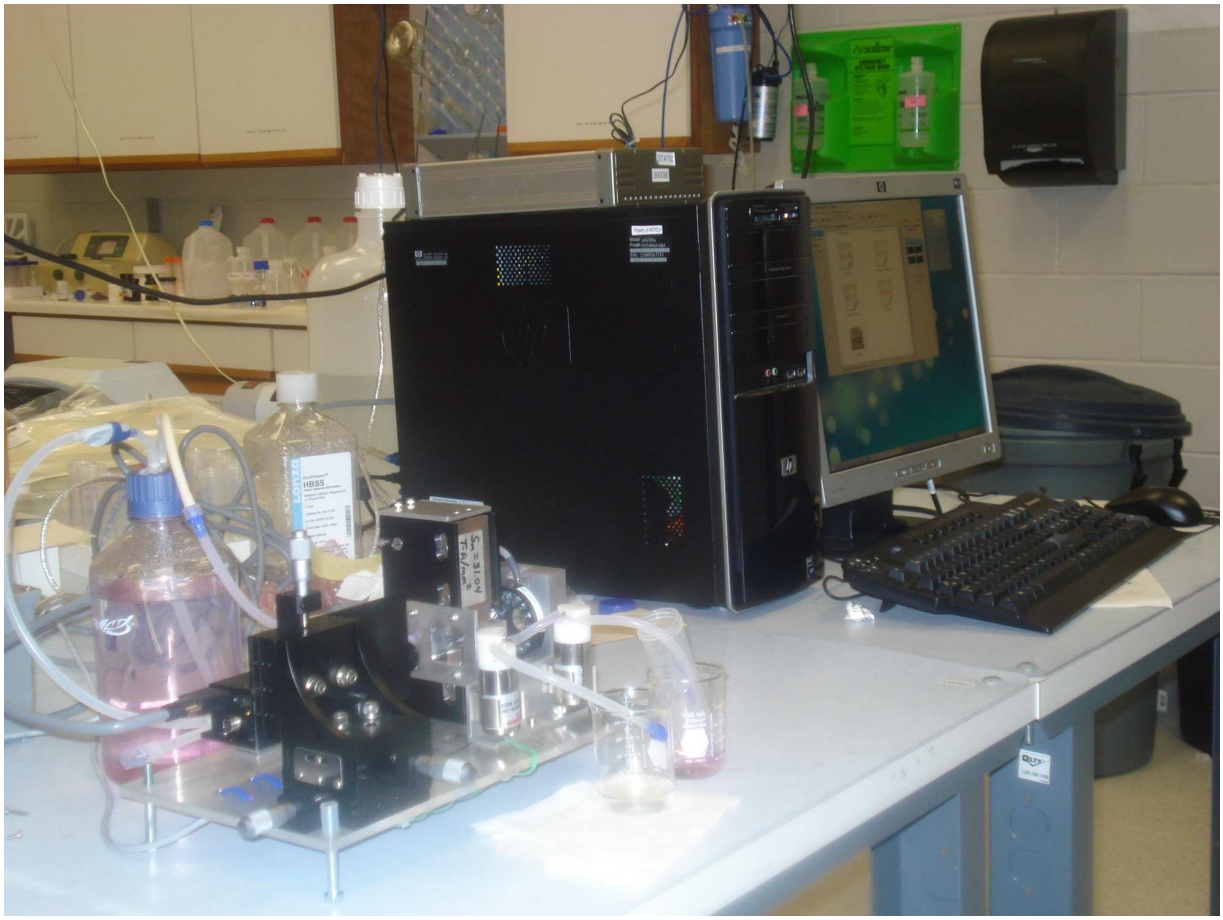

Figure B.2: Photograph of the MPTV set up.

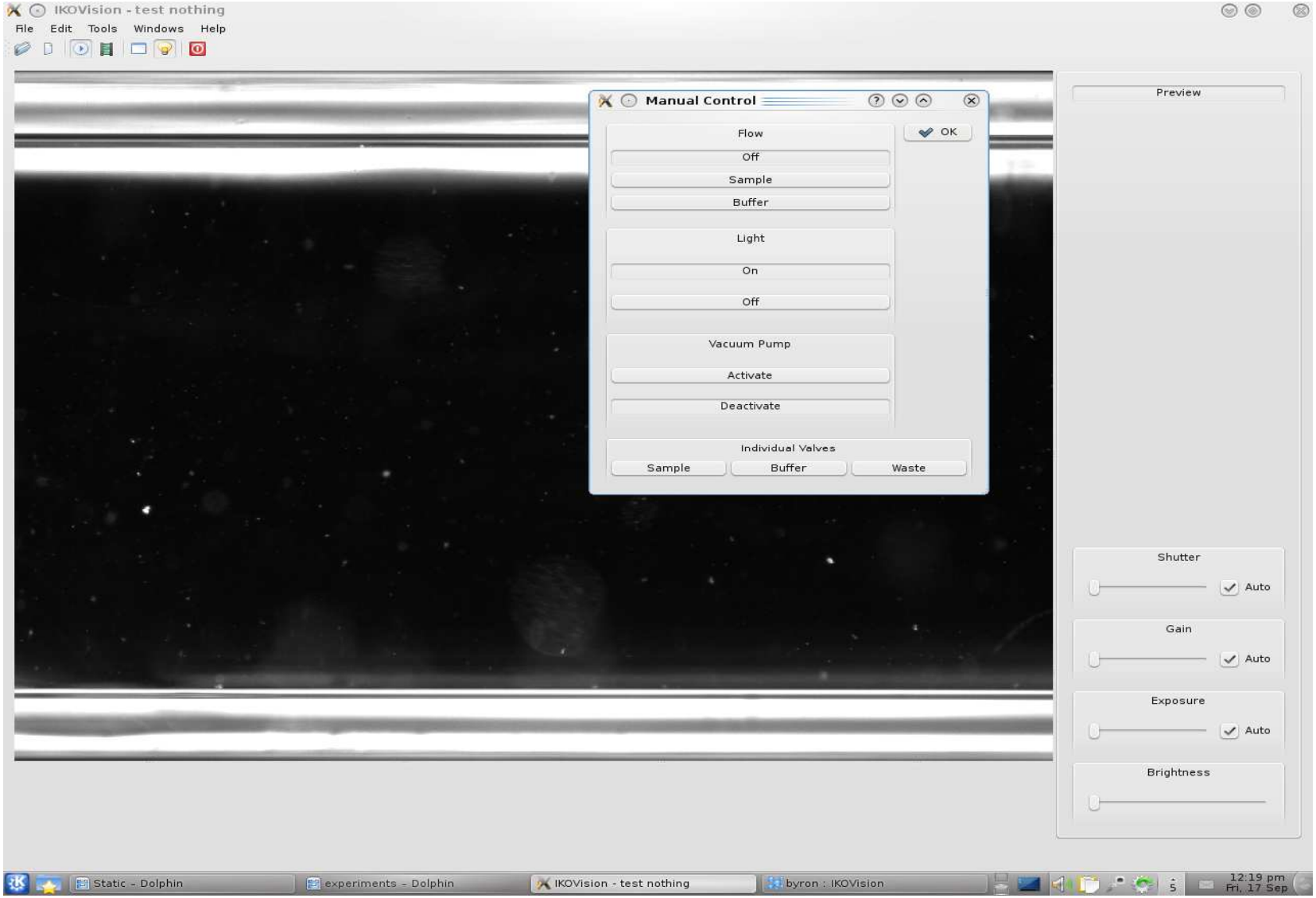

Figure B.3: Screeshot of the IKOVISION used to run the MPTV.

Appendix C: Fluent Simulations

C.1 Fluent Simulation Procedure

- Start the program from the command line by typing “fluent 3ddp”.
- Open the .msh file with the pull-down menus File → Read → Case.
- Save the loaded .msh file as a .cas file by the pull-down menus: File → Write → Case.
- Under Grid → Scale make sure that the domain extents in meters are correct. If not specify that the grid was created in inches.
- Under Define → Materials define the “Fluid Material” as liquid water by loading it from the database or finding it in the pull-down menu.
- Under Define → Boundary Conditions set Fluid to liquid water, Outlet to zero gauge pressure, and Inlet to the appropriate Velocity Magnitude (calculated from the volumetric flow rate and cross-sectional area at the channel inlet). In this case 00 ml/min gave a velocity magnitude of 0.42 m/s.
- Under Define → Injections create “Surface” inert injections released from the channel Inlet.
- Under Define → Units use the SI default.
- Accept the default Define → Solver options.
- Under Injection → Define Inert material properties.
- Under Define → Models → Viscous make sure the regime is Laminar.

- Under Define → Models → Discrete Model.
- Under Solve → Monitors → Residual set the Convergence Criterion to at least 1E-6 and the Iteration Storage to at least several thousand. Make sure the Residual Monitor appears on the screen.
- Under Solve → Initialize set the X velocity to the same value as the calculated inlet X-Velocity Magnitude.
- Under Solver → Controls → Solution use the SIMPLE Pressure-Velocity Coupling, Standard Pressure Discretization, and Second Order Upwind Momentum Discretization. The Under-Relaxation Factors (except Momentum) can be left at the default values.
- Start the solution from Solver → Iterate with at least several thousand iterations and reporting after every ten.
- A simulation can be expected to run for several hours. If after several hours the Residuals remain flat you may halt the iteration and reduce the Momentum Relaxation Factor from the Solver → Controls → Solution menu then restart the iteration. The Momentum Relaxation Factor may have to be reduced several times.
- When the residuals have converged, run the Discrete model using display particle trajectories and select summery.
- Save the data from the File → Write → Case and Data menu.
- The results may be seen from the many option in the Display pull-down menu.

```
Loading "C:\Fluent.Inc\fluent6.3.26\lib\fl_s1119.dmp"
Done.


> Reading "C:\DP\104445AA2BDPSURNC\104445AA2BDPSURNC.cas"...
 1677872 tetrahedral cells, zone  2, binary.
  432346 triangular wall faces, zone  3, binary.
     164 triangular outflow faces, zone  4, binary.
     164 triangular outflow faces, zone  5, binary.
     164 triangular velocity-inlet faces, zone  6, binary.
     164 triangular velocity-inlet faces, zone  7, binary.
     164 triangular outflow faces, zone  8, binary.
     164 triangular velocity-inlet faces, zone  9, binary.
 3139079 triangular interior faces, zone 11, binary.
  389993 nodes, binary.
  389993 node flags, binary.

Building...
     grid,
     materials,
     interface,
     domains,
        mixture
     zones,
        default-interior
        a_prime
        negative
        b1_prime
        b2_prime
        positive1
        positive2
        wall
        qms
Material cultispheres:
  New property "Thermal Conductivity" has been added.
  Selecting constant method for "Thermal Conductivity" -- data required.

     shell conduction zones,
Done.
Reading "C:\DP\104445AA2BDPSURNC\104445AA2BDPSURNC.dat"...
Done.
number tracked = 164, escaped = 77, aborted = 0, trapped = 0, evaporated = 0, incomplete = 87

 Fate                  Number          Elapsed Time (s)                          Injection, Index
                                          Min        Max        Avg    Std Dev                  Min                  Max
 ----                  ------  ---------- ---------- ---------- ---------- -------------------- --------------------
 Incomplete                87  1.574e+001 4.652e+002 4.154e+001 5.043e+001    cultispheres   13    cultispheres  112
 Escaped - Zone 4           3  2.904e+001 3.282e+001 3.057e+001 1.624e+000    cultispheres  118    cultispheres    7
 Escaped - Zone 5           4  2.812e+001 3.206e+001 2.991e+001 1.447e+000    cultispheres   98    cultispheres   25
 Escaped - Zone 8          70  2.951e+001 3.497e+001 3.169e+001 1.072e+000    cultispheres  128    cultispheres   23

                  (*)- Mass Transfer Summary -(*)

 Fate                       Mass Flow (kg/s)
                          Initial      Final     Change
 ----                     ---------- ---------- ----------
 Incomplete               1.327e-005 1.327e-005 0.000e+000
 Escaped - Zone 4         3.852e-007 3.852e-007 0.000e+000
 Escaped - Zone 5         5.921e-007 5.921e-007 0.000e+000
 Escaped - Zone 8         1.075e-005 1.075e-005 0.000e+000
```

Figure C.1: Summery of the particle flow simulation.

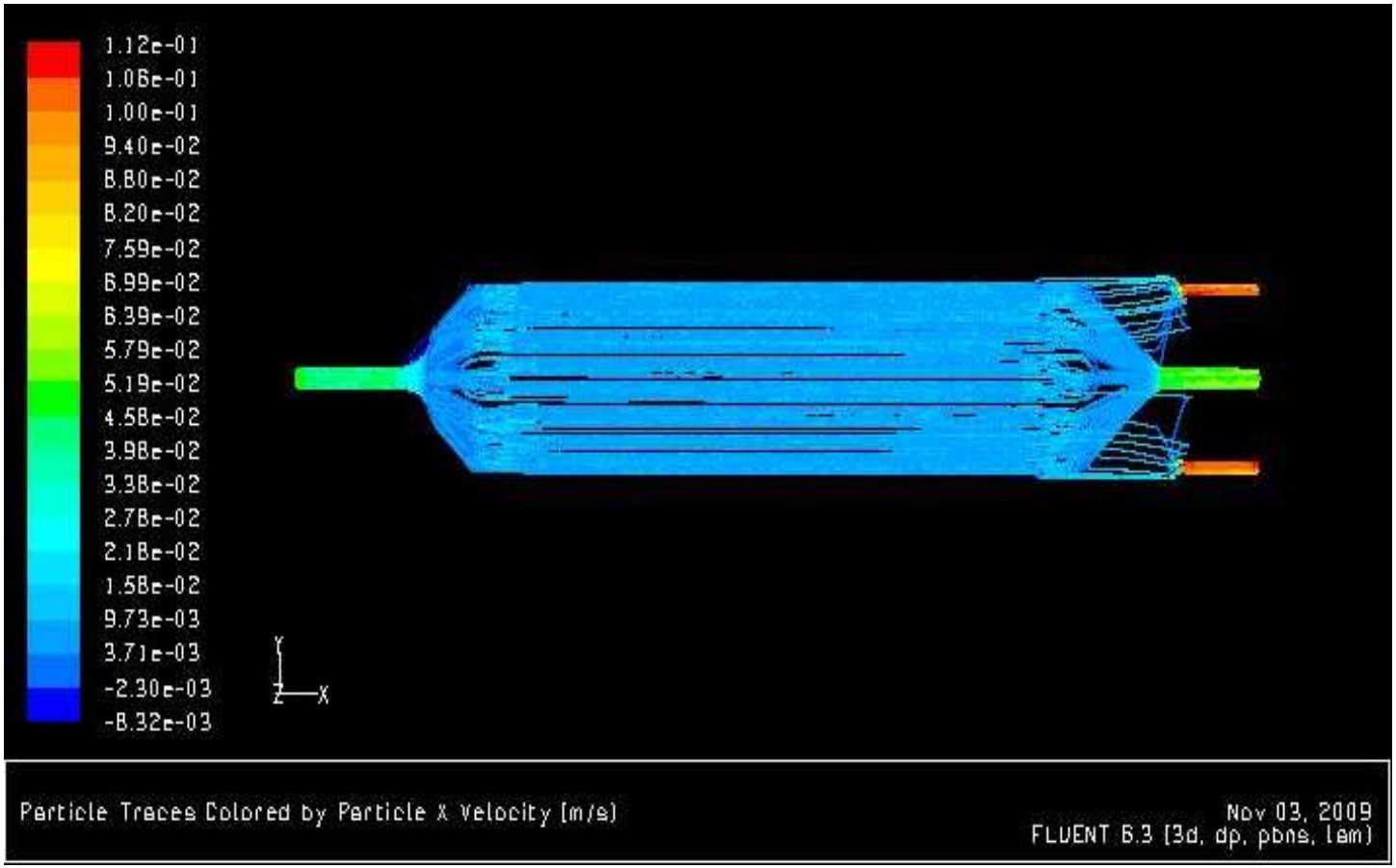

Figure C.2: Particles trajectories calculated in Fluent simulations.